Amygdala Mechanisms of Fear Suppression

By

Alon Amir

A Dissertation submitted to the

Graduate School-Newark

Rutgers, The State University of New Jersey

in partial fulfillment of the requirements

for the degree of

Doctor of Philosophy

Graduate Program in Behavioral and Neural Sciences

written under the direction of

Denis Pare

and approved by

_____

_____

_____

_____

_____

Newark, New Jersey

October, 2015

Abstract of the Dissertation

Amygdala Mechanisms of Fear Suppression

By Alon Amir

Dissertation Director:
Prof. Denis Pare

The amygdala plays a critical role in mediating fear responses to a cue (CS) that was previously associated with danger (US) or to species-specific stimuli such as predators. However, for proper behavioral functioning, these defensive behavioral tendencies must, at times, be suppressed. For example, animals have to suppress fear responses elicited by the CS when the CS is presented repeatedly in the absence of the US, a process called extinction of conditioned fear responses. In addition, animals have evolved defensive strategies that minimize the likelihood of encounters with predators. However, in order to attain food, these defensive strategies must be suppressed.

Intercalated (ITC) amygdala neurons are thought to play a critical role in the extinction of conditioned fear. However, we lack criteria to identify ITC cells in vivo and as a result, it has been impossible to test key predictions of ITC extinction models. Among these, it was predicted that ITC cells are strongly excited by infralimbic inputs, explaining why infralimbic inhibition interferes with extinction. In the first chapter, I found ITC cells are strongly responsive to infralimbic stimuli and their unique responses to infralimbic inputs constitute a reliable criterion to identify them in behaving animals.

In addition, the amygdala regulates innate fear in a foraging task. In this task, rats had to leave a safe nest to retrieve food positioned at various distances from a robot predator. Intra-amygdala infusions of drugs that reduced or enhanced the activity of amygdala neurons respectively led to increases or decreases in risk-taking. While these findings indicate that the amygdala regulates innate fear responses, how it does so is unclear. To address this question, I recorded neurons in the basolateral nucleus while rats engaged in the foraging task. I found that the vast majority of projection cells became silent upon initiation of foraging. Last, by comparing the activity of BL cells during the foraging task with tasks that did not include explicit threats or rewards, we found that BL activity is best understood as reflecting a continuous evaluative process where internal states, reward availability, and threat determine whether rats will engage in a situation.

Acknowledgements

First, I express my deepest gratitude to Denis Pare, my thesis advisor for his outstanding mentorship. Denis' scientific knowledge, insight, enthusiastic and dedication have inspired me throughout my studies, and will remain with me as inspiration for the years to come. I also would like to thank the members of my thesis committee, James Tepper, Bart Krekelberg, Tibor Koós and Gregory Quirk for their time, effort, guidance and valuable input.

I would like to thank all former and current members of the Denis' lab for their friendship, help, support and stimulating discussions throughout my PhD. I would like to especially thank a number of lab mates with whom I have collaborated with over the years. First, I would like to thank Taiju Amano for his contributions to the in vitro electrophysiology study. In addition, I would like to thank Cagri Temucin Unal for teaching me in vitro electrophysiology. I would like to thank Seung-Chan Lee, Drew Headly and Darrell Haufler for their contribution to the in vivo studies. Moreover, I would like to thank Jagdish Patel for teaching me building and implanting silicon probes in rodents. I would like to thank Shuzo Sakata for teaching me Juxtacellular labeling.

I would like to thanks to Alfonso Renart, Liad Hollender, Jaime de la Rocha, Paul Chadderton, and Artur Luczak for their support and friendship during the early stage of my PhD. I would like to thank all my friends and colleagues at the Center For Molecular and Behavioral Neuroscience for their support and

friendship throughout my PhD, with special thanks to Temucin, Bengi and Manas Unal and to Jagdish Patel for being there for me in all the good and bad times. You made my life in the USA much nicer and easier. Last, I want to thank my parents and family and to Alice Segal, who supported me throughout these years.

Preface

The study presented in chapters 3 was a collaborative effort between myself and Taiju Amao. This work was published (Amir et al., 2011). The studies presented in chapters 4 and 5 were a collaborative effort between myself, Seung-Chan Lee, Drew Headly and Mohammad Herzallah. This work is currently under preparation for publication.

Table of Contents

List of Figures

List of Abbreviations

AB	accessory nucleus of the amygdala
aCSF	artificial cerebrospinal fluid
Ast	amygdalostriatal transition area
BL	basal nucleus of the amygdala
BLA	basolateral complex of the amygdala
BNST	bed nucleus of stria terminalis
BOLD	blood oxygen level dependent
BS	brain stem
CB	calbindin
CCK	cholecystokinin
Ce	central nuclear group of the amygdala
CeL	central lateral nucleus of the amygdala
CeM	central medial nucleus of the amygdala
CRH	cotricotropin releasing hormone
CRs	conditioned fear responses
CS	conditioned stimuli

D1R	dopamine type 1 receptor
FRs	firing rates
IL	Infralimbic cortex
ISI	inter-trial interval
ITC	Intercalated
ITCd	dorsal intercalated clusters
ITCl	lateral clusters located along the external capsule
ITCm	medial clusters located along the internal capsule
ITCv	ventral intercalated clusters
ITN	interneuron
LA	lateral nucleus of the amygdala
LFP	local field potential
LTP	long-term potentiation
MEA	medial amygdala nucleus
MGm	medial geniculate body
μOR	μ-opioid receptor
mPFC	medial prefrontal cortex

nAc	nucleus accumbens
PAG	periaqueductal gray
PB	phosphate buffer
PBS	phosphate buffer saline
PIN	posterior internuclear nuclei
PKC-δ	protein kinase C-δ
PL	prelimbic cortex
PNs	projection cells
PV	calcium binding protein parvalbumin
QW	quiet waking
SO	spontaneously occurring slow oscillation
SOM	somatostatin
SWS	slow-wave sleep
US	unconditioned stimuli
VIP	vasoactive intestinal peptide

CHAPTER 1:

INTRODUCTION

Fear, including its endocrine, autonomic, cognitive and behavioral correlates is elicited by unconditioned stimuli (US) such as electrical shocks or predators or by conditioned stimuli (CS) that were previously associated with adverse outcomes. Fear responses elicited by CSs are called conditioned fear responses (CRs). Fear responses enable animals to predict and avoid or appropriately respond to danger in the wild, thereby promoting survival and eventually increasing reproductive success. Therefore, the neural circuits that mediate fear responses have been retained by natural selection. As such, these neural circuits are expected to be conserved across species, including humans. Indeed, while the majority of studies on the neural circuits mediating fear responses have been conducted in rodents, it has been confirmed that the same neural circuits are present in primates, including humans (Buchel et al., 1998; LaBar et al., 1998; Kalin et al., 2004; Phelps et al., 2004; Phelps and LeDoux, 2005).

In search for the neural circuits that mediate fear responses, early studies focused on the role of the medial temporal lobe (Papez, 1937; Kluver and Bucy, 1937). When the medial temporal lobe (including the amygdala) of monkeys was lesioned bilaterally, monkeys showed reduced fear responses. Afterwards, it was found that the impairment was due to the amygdala (Weiskrantz, 1956). Later, many studies demonstrated the important role of the amygdala in fear learning and expression.

In animals, fear is studied using observable defensive behaviors such as freezing or flight responses. Unfortunately, subjective feelings of fear cannot be

measured and may not exist in animals and therefore cannot be studied. However, in humans, it has been shown that subjective or conscious feelings of fear and non-conscious implicit fear responses can be dissociated. Indeed, unconditioned or conditioned fear stimuli presented to healthy humans could elicit fear responses without the subjects' awareness of the presented stimuli or their feeling fear (Lazarus and McCleary, 1951; Ohman and Soares, 1994; Anderson and Phelps, 2002; Olsson and Phelps, 2004; Bornemann et al., 2012). In addition, humans with focal amygdala damage exhibit impaired fear responses to a CS previously associated with a US. However, these subjects form an explicit memory of the association between the CS and the US. In contrast, humans with hippocampal damage cannot recall the CS/US association. However, they exhibit normal fear responses to the CS (Bechara et al., 1995; Feinstein, 2013). In sum, fear responses and their neural substrates are different from the neural circuits generating subjective feelings of fear, and from those allowing humans to form explicit memories of the feared stimuli. Therefore, fear responses should be viewed as parts of a generalized defensive system that help animals appropriately respond to threats.

The subsequent sections of this chapter will discuss current knowledge on the neural circuits that mediate implicit fear learning and responses. First, I will provide an overview of their anatomical and physiological organization. Second, I will summarize the role of these structures, including their involvement in fear learning, expression, extinction, and suppression. Below, note that for simplicity, I will use the term fear when in fact referring to defensive behaviors.

1.1 Anatomical and physiological organization of the amygdala

The amygdala is a key structure for fear learning and expression (Davis and Whalen, 2001; LeDoux, 2000). The amygdala is a heterogeneous collection of twelve or so nuclei located in the medial temporal lobe. I will focus throughout this introduction on amygdala nuclei involved in the acquisition, expression and extinction of conditioned fear responses. These nuclei can be divided into two main groups: the first is the basolateral complex (BLA) which is a cortex-like structure that consists of the lateral, basal and accessory nuclei (LA, BL and AB, respectively); the second group is the central nuclear group (Ce) which is a striatal-like structure that consists of the central lateral and central medial nuclei (CeL and CeM, respectively) (McDonald, 1998). In addition, the amygdala also contains cell clusters called the intercalated (ITC) cell masses (Sah et al., 2003). ITC neurons, a population of GABAergic cells, tend to aggregate in small densely packed clusters located in the main fiber bundles that surround the BLA laterally (external capsule) and medially (intermediate capsule) (Nitecka and Ben-Ari, 1987; Pare and Smith, 1993b).

Intrinsic connections and physiological properties

I will provide a short overview of the morphology, intrinsic connectivity and electrophysiological properties of BLA, Ce and ITC cells.

BLA:

The neural makeup of the BLA is similar to that of the cerebral cortex, except for the fact that BLA cells are randomly oriented (McDonald, 1992; Washburn and Moises, 1992; Pare et al., 1995b; Faber el al., 2001; Sah et al., 2003). As in the cortex, most BLA cells (~80%) are glutamatergic projection cells (Kamal and Tombol, 1975; McDonald, 1992; Pape and Pare, 2010). Typical BLA glutamatergic projection cells exhibit multipolar dendritic trees covered with spines and axons that contribute collaterals within the vicinity of the cell before projecting outside the nucleus (Kamal and Tombol, 1975; McDonald, 1992; Pape and Pare, 2010). The majority of these cells exhibit regular spiking properties, with marked differences between cells with respect to the amount of spike frequency adaptation. This is due to variations in the expression of voltage and calcium dependent potassium conductances (Washburn and Moises, 1992; Rainnie et al., 1993; Pare el al., 1995b; Lang and Pare, 1998; Pape el al., 1998; Faber et al., 2001; Faber and Sah, 2002; Faber and Sah, 2003). There is no clear difference in the morphology of principal cells between the different BLA nuclei, except that cells in LA generally have a smaller soma diameter (10-15 μm) compared to cells in BL and AB (15-20 μm) (Sah et al., 2003).

The second group of cells (~20%) consists of local GABAergic interneurons. As in the cortex, interneurons in the BLA have non-spiny or sparsely spiny dendrites with local axons and they express a wide variety of markers (Kamal and Tombol, 1975; McDonald, 1992). About half of the BLA interneurons express the calcium binding protein parvalbumin (PV). The second

biggest class of interneurons is the somatostatin positive (SOM) cell group. Other local interneurons are: (1) small cells expressing vasoactive intestinal peptide (VIP) and cholecystokinin (CCK), (2) large CCK cells and (3) cells expressing 5-HT-3A receptors (Kemppainen and Pitkänen, 2000; McDonald and Betette, 2001; McDonald and Mascagni, 2001; McDonald and Mascagni, 2002). Calbindin (CB) is usually coexpressed with PV, SOM and large CCK interneurons (Pitkänen and Amaral, 1993).

As in the cortex, PV interneurons target the soma, initial axon segment, and proximal dendrites of BLA projection cells (Smith et al., 2000). In contrast, SOM cells target the distal dendrites of BLA projection cells (Muller et al., 2007). Moreover, PV interneurons receive excitatory inputs from local BLA projection cells but very few from the cortex, and therefore are involved in feedback inhibition (Smith et al., 2000). In contrast, SOM cells receive excitatory inputs from the cortex and therefore participate in feedforward inhibition (Pitkänen and Amaral, 1993; McDonald and Betette, 2001; Unal et al., 2014).

In terms of electrophysiological properties, most BLA interneurons are characterized by fast spiking patterns with narrow spike width and little or no spike frequency adaptation (Spampanato et al., 2011). Lastly, similar to cortical interneurons, many types of electrophysiological responses have been described, even among neurochemically homogenous interneurons (Rainnie et al., 2006; Woodruff and Sah, 2007; Jasnow et al., 2009).

Ce:

CeL and CeM each contain one main cell type (Cassell et al., 1986; Kamal and Tombol, 1975; McDonald, 1982; Pape and Pare, 2010). In CeL, the main cell type shows similar morphological and physiological properties as medium spiny striatal neurons. These cells have multiple dendrites densely covered with spines, and their axons make local collaterals before leaving the nucleus. In contrast, CeM cells have a larger soma, lower spine density, and dendrites that branch more sparingly (McDonald, 1982; Martina et al., 1999; Schiess et al., 1999). Cells in CeL and CeM express a variety of peptides, such as protein kinase C-δ (PKC-δ), enkephalin, neurotensin and cotricotropin releasing hormone (CRH) (Day et al., 1999; Sah et al., 2003; Haubensak et al., 2010). It has been shown that cells expressing different peptides mediate different components of defensive responses. For example, in CeL, it has been shown that PKC-δ^+ positive cells have an anxiolytic effect, whereas PKC-δ^- negative cells are anxiogenic (Haubensak et al., 2010). I will return to the PKC-δ pathway later in my introduction. CeM and CeL, additionally, contain a low number of local circuit aspiny GABAergic cells (Pape and Pare, 2010).

In terms of physiological properties, most cells in CeL and CeM express a regular spiking firing pattern with some degree of spike frequency adaptation and hyperpolarization activated cation current (Dumont et al., 2002; Lopez de Armentia and Sah, 2004). A low proportion of Ce cells additionally express T-type calcium channels that are responsible for low threshold bursts of action potentials (Dumont et al., 2002).

ITC:

As I mentioned earlier, ITC neurons tend to aggregate in small densely packed clusters. These clusters are located in the external capsule lateral to the BLA as well as in the intermediate capsule that separates the BLA from Ce, effectively forming a sheet of GABAergic neurons around the BLA. The clusters located along the external capsule will be termed ITCl (lateral) and the medially located ones ITCm (medial) (Nitecka and Ben-Ari, 1987; Pare and Smith, 1993b).

There are two classes of ITC neurons. The first class, which comprises the majority of ITC cells, is characterized by a small soma (8-19 μm, diameter), a flattened dendritic tree, and moderate to high density of dendritic spines (Millhouse, 1986). This class of cells expresses μ-opioid (μOR) and dopamine type 1 receptors (D1R) (Jacobsen et al., 2006). The second class, which comprises a minority of ITC cells, is characterized by a large soma (>40 μm, diameter) and aspiny dendrites (Millhouse, 1986; Jacobsen et al., 2006; Busti et al., 2011). In addition, these large ITC cells express metabotropic glutamate receptors 1α and form a sheet of cells surrounding the small packed ITC cell clusters (Busti et al., 2011). The functions of these large ITC cells are unknown and will not discussed further.

In terms of electrophysiological properties, the small ITC cells have a high input resistance (500-900 MΩ) compared to cells in neighboring nuclei (Garacitano et al., 2007; Marowsky et al., 2005; Royer et al., 2000a). ITC cells exhibit little spike frequency adaptation and can sustain high firing rates (Garacitano et al., 2007; Marowsky et al., 2005; Royer et al., 2000a).

Tracing and cell labeling studies performed in guinea pigs revealed that ITC cells located in the intermediate capsule project toward other more medially located ITC cell clusters (Figure 1.1; Royer et al., 2000b). In addition, ITC cells inhibit other ITC cells located in the same cluster (Garacitano et al., 2007).

Extrinsic connections

The amygdala has direct connections with diverse brain structures including the cortex, hippocampus, thalamus, striatum, hypothalamus, basal forbrain, and brainstem nuclei (Pitkanen et al., 2000; Sah et al., 2003). As a result, the amygdala is in a position to receive complex sensory and internal information and influence a wide variety of processes.

Afferent connections:

The amygdala receives information about all sensory modalities: gustatory, visceral, auditory, visual, olfactory, and somatosensory (Sah et al., 2003). I will describe how auditory, visual, somatosensory and polymodal inputs reach the amygdala since these connections are playing a role in the behavioral tasks used in this thesis.

Auditory and visual inputs to the amygdala originate from association cortices but not primary cortical areas. The LA is the main recipient of these inputs (LeDoux et al., 1991). LA receives additional auditory information from a subcortical area, specifically the thalamic medial geniculate nucleus. Visual

information from high order visual cortices and from the posterior thalamus terminates in LA, BL and CeL (McDonald, 1998; Shi and Davis, 2001).

Cortical somatosensory information reaches the amygdala mainly from the parietal insular cortex (Shi and Cassell, 1998a). In similar fashion to the auditory and visual modality, the primary somatosensory cortex sends only sparse projections to the amygdala (Shi and Cassell, 1998a). Cortical somatosensory projections terminate in the LA, BL and CeL (Shi and Cassell, 1998a, Shi and Cassell, 1998b). Subcortical somatosensory information originates from the following structures: (1) the parabrachial nucleus, (2) the medial portion of the medial geniculate, and (3) the posterior internuclear nuclei (PIN), which all terminate in LA, BL, AB and CeM (Bernard et al., 1993; Linke et al., 2000). Inputs that originate from the PIN also relay nociceptive information (Bernard et al., 1989; Bordi and LeDoux, 1994; LeDoux et al., 1987).

Polymodal inputs from the prefrontal cortex, entorhinal cortex, perirhinal cortex and hippocampus end in all nuclei of the amygdala. However, the BLA receives the majority of these inputs (Sah et al., 2003). The prefrontal cortex receives convergent information related to all sensory modalities. In addition, it plays an important role in behavior control and reward processing (McDonald, 1998; Sah et al., 2003). The perirhinal cortex, entorihinal cortex and hippocampus participate in declarative memory, and relay spatial information about the environment to the amygdala (Milner et al., 1998).

Input to ITC cells have received less attention than afferents to BLA and Ce nuclei. One of the main reasons is that the retrograde tracing methods that

are used widely to study connectivity between brain structures cannot be applied to such small structures as ITC cell clusters. However, as I mentioned earlier, ITC cells express D1R and indeed receive dopaminergic input from the midbrain dopaminergic system (Marowsky et al., 2005; Marcellino et al., 2012). In addition, the ITCm cells receive dense inputs from the medial prefrontal cortex (McDonald, 1998; Pinard et al., 2012; Cho et al., 2013). These inputs play a major rule in the acquisition and extinction of conditioning fear.

Efferent connections:

Amygdala nuclei project to a diverse array of cortical and subcortical structures. In contrast to amygdala afferent connections discussed above, there is a clear segregation of the targeted areas depending on the amygdala nucleus contributing the projection. Indeed, the BLA sends projections to the striatum and to the cortex, but does not send projections to the brainstem (Krettek and price, 1977a; Krettek and price, 1977b; Krettek and price, 1978b). In contrast to the BLA, Ce sends dense projections to the brainstem, but not to the cortex and the striatum.

The following high order cortical areas receive inputs from the BLA: the medial prefrontal cortex (mPFC), insula, hippocampus and rhinal cortices. The BLA sends only light projections to primary cortical areas (Pape and Pare, 2010). In addition, BLA projections to the striatum are strongest to nucleus accumbens, although some parts of the caudate nucleus also receive a significant BLA inputs (McDonald, 1991a; McDonald, 1991b). In addition, the BLA and high order

cortical areas are reciprocally connected (Pape and Pare, 2010). Lastly, all BLA efferents originate from principal glutamatergic neurons (Sah et al., 2003).

The CeM sends projections to the hypothalamus and different nuclei in the midbrain, pons and medulla (Sah el al., 2003). These subcortical structures are responsible for mediating fear responses such as freezing, potentiated startle, release of stress hormones, as well as changes in blood pressure and heart rate (Davis et al., 1994; LeDoux, 2000). Indeed, Ce stimulation elicits autonomic responses by directly activating neurons in brainstem autonomic system and by indirectly activating hypothalamic neurons that in turn modulate the brainstem autonomic system (Kapp et al., 1982; LeDoux et al., 1988). CeM sends projections to three main brainstem areas: (1) the periaqueductal gray (PAG) that mediates freezing, startling, analgesia and cardiovascular changes (Behbehani, 1995; Rizvi et al., 1991); (2) the nucleus of solitary tract-vagal system; (3) the parabrachial nucleus that modulates pain (Gauriau and Bernard, 2002; Moga et al., 1990). CeM and CeL send projections to the dorsolateral and caudolateral areas of the hypothalamus, areas involved in mediating autonomic responses (Petrovich et al., 2001). Furthermore, the Ce makes reciprocal connections with the bed nucleus of stria terminalis (BNST) and their brainstem target areas overlap extensively (Dong et al., 2000; Dong and Swanson, 2004; Dong and Swanson, 2006). For instance, both Ce and BNST send strong projections to neuromodulatory systems: the basal forebrain cholinergic system, noradrenergic locus coeruleus, dopaminergic substantia nigra and ventral tegmental area, as well as to the serotonergic dorsal raphe nucleus (Davis and Whalen, 2001). By

means of these projections to modulatory systems, the amygdala is in a position to influence the excitability and synaptic plasticity of much of the brain (Hasselmo and Giocomo, 2006; Pape and Pare, 2010).

The ITC cells are local amygdala interneurons and their projections are mainly confined to the amygdala. One exception is that ITCm cells located in the dorsal cluster send projections to the amygdalostriatal transition area (Busti et al., 2011). In addition, in many biocytin-filled ITC cells obtained in slices, some axonal collaterals extend beyond the boundaries of the amygdala. However, where these axons end is unknown (Busti et al., 2011).

Internuclear connections

Connections between amygdala nuclei are extensive and organized in a specific direction (Pitkanen et al., 1997). Within BLA, LA sends dense glutamatergic projections ventrally, toward the basal nuclei, BL and AB. In contrast, the basal nuclei send only sparse projections back to LA (Pare et al., 1995a; Savander et al., 1995). Additionally, all BLA nuclei project to Ce, but Ce does not project back to BLA. More specifically, LA projects to CeL, but not to CeM, whereas the basal nuclei project to both, CeL and CeM (Krettek and Price, 1978a; Pare et al., 1995a; Savander et al., 1997; Smith and Pare, 1994).

In addition to the direct excitatory connections from BLA to Ce, indirect inhibitory connections from BLA through ITCm to Ce also exist (Pare et al., 2004). Tracing and cell labeling studies performed in guinea pigs revealed that ITCm cells along the intermediate capsule project to the adjacent sector of Ce.

Specifically, ITCm clusters located adjacent to CeL project to CeL, while clusters located adjacent to CeM project to CeM (Figure 1.1) (Pare and Smith, 1993a; Royer et al., 1999). Furthermore, as I mentioned earlier, ITCm clusters project toward other more medially located ITCm cell clusters but not laterally (Figure 1.1). Related to this, Royer and Pare (2000b) showed that ITC neurons receive glutamatergic inputs from the adjacent region of the BLA (Figure 1.1) (Royer et al., 2000b). Thus, the results in guinea pigs indicate that there is a lateromedial correspondence between the position of ITC cells, where they derive glutamatergic inputs from BLA and where they project in Ce. One of my aims is to find out whether ITC connectivity in rats is the same as the ITC connectivity in guinea pigs. In contrast to ITCm, ITCl cells located along the external capsule send axonal projections toward the BLA (Marowsky et al., 2005).

Within Ce, CeL sends dense GABAergic projections toward CeM, but CeM does not project back to CeL. Instead most projections that originate from CeM target downstream hypothalamus and brainstem structures mediating fear responses. Figure 1.2 summarizes the internuclear connections between the different amygdala nuclei (Pape and Pare, 2010).

In conclusion, the internuclear connectivity of the amygdala, starting from the BLA and ending in CeM suggests that the BLA is the input station of the amygdala where the sensory information related to the CS and US converge, whereas CeM is the output station of the amygdala where projections to downstream structures mediating fear responses originate.

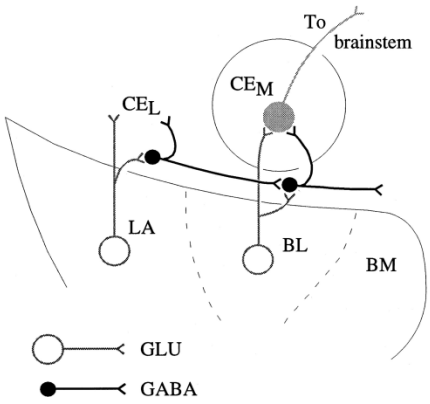

Figure1.1 Summary of internuclear amygdala connections in Guinea pig; focusing on the ITC (adapted from Royer et al., 2000b).

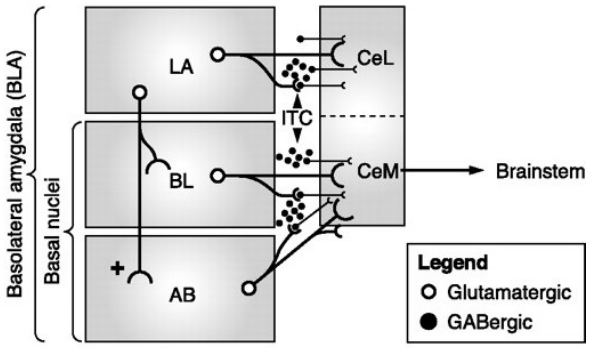

Figure 1.2 Summary of main internuclear amygdala connections in rat (adapted from Pape and Pare, 2010).

1.2 Amygdala roles in fear acquisition, expression and extinction

In this section, I will provide a summary of the role of the amygdala in the acquisition and expression of conditioned fear responses, and then summarize

the amygdala's role in fear extinction. Lastly, I will provide a summary of the role of the amygdala in innate fear.

Fear learning:

Learned fear represents an advantageous evolutionary adaptation because the ability to learn and appropriately respond to a stimulus that predicts a threat, or was previously associated with a threat, is key to survival. Classical fear conditioning is a laboratory model for studying the acquisition and expression of learned fear responses. In this model, repeated presentations of a stimulus such as a tone (conditioned stimulus, CS) paired with an aversive stimulus such as a footshock (unconditioned stimulus, US) leads to the formation of a CS-US association such that later presentation of the CS alone elicits conditioned fear responses. This experimental model has been very useful in identifying key brain structures involved in fear learning. It has been found that the amygdaloid complex is necessary for the acquisition and expression of conditioned fear responses (LeDoux, 2000).

Since most of the available data regarding fear conditioning were obtained using an auditory cue as a CS, and by using foot shock as a US, my discussion on the acquisition, expression, and extinction of learned fear in the amygdala will focus on these sensory modalities.

As I mentioned earlier, the LA receives auditory information (CS) from the medial geniculate body (MGm) and posterior intralaminar nucleus (PIN) of the thalamus as well as from the auditory cortex (LeDoux, 2000). In addition, LA

receives nociceptive information (US) through the PIN (LeDoux, 2000). In turn, LA neurons project to BL, AB and CeL, which send projections to CeM. CeM, a major output station of the amygdala, sends projections to brain areas that mediate components of fear responses (LeDoux et al., 1988; Davis and Shi, 1999).

The LA, which receives both CS and US information, is thought to be the site where the CS-US association is formed. Indeed, it was found that LA neurons show associative plasticity during fear conditioning, namely that the responses of LA cells to the CS increase after US-CS parings (Quirk et al., 1995; Collins and Pare, 2000). Moreover, an ex vivo study demonstrated that fear conditioning was associated with long-term potentiation (LTP) of thalamic and cortical synapses conveying CS information to LA neurons (McKernan and Shinnick-Gallagher, 1997; Tsvetkov et al., 2002). Also, Tsvetkov et al. (2002) showed that LTP of thalamic inputs induced by fear conditioning occludes electrically-induced LTP in LA (Tsvetkov et al., 2002). These results suggest that formation of the CS-US association depends on the potantiation of thalamic and/or cortical synapses to LA neurons. In agreement with this, lesion or temporary inactivation of LA during fear conditioning blocks the acquisition of conditioned fear responses (LeDoux et al., 1990; Wilensky et al., 1999; Maren et al., 2001). In addition, acquisition of fear memory is NMDA-dependent since administration of NMDA antagonists in LA during fear conditioning blocks fear learning (Fanselow et al., 1994). Lastly, LA neurons increase their firing rate to a presentation of CS after conditioning, and the activity of LA neurons is correlated

with fear behavior (Quirk et al., 1995). Altogether, these results suggest that LA plays a critical role in the formation of the tone-shock association.

In order for the CS to induce fear responses, the CS information that is present in LA must be transferred to brainstem-projecting CeM cells. However, LA does not project to CeM. Instead, CS information from LA reaches CeM indirectly, via the basal nuclei, via the CeL, and via the ITC cell clusters. Indeed, lesion studies suggest that CS information can be transferred using multiple pathways. Lesions of the basal nuclei before conditioning do not interfere with the acquisition of conditioned fear responses (Amorapanth et al., 2000; Nader et al., 2001; Holahan and White, 2002). However, post-conditioning lesions do (Anglada-Figueroa and Quirk, 2005). These results suggest that, in the intact brain, the basal nuclei participate in fear learning. However, when the basal nuclei are damaged, CS information can be transferred to CeM cells using other pathways. In agreement with the role of the basal nuclei in fear learning, many BL and AB neurons increase their responses to the CS as a result of fear conditioning (Herry et al., 2008; Amano et al., 2011).

As I mentioned above, pre-training lesions of the basal nuclei have no effect on the acquisition and expression of conditioned fear responses. Therefore, CS information reaches CeM output cells via a parallel route, namely through the CeL. Indeed, temporary inactivation of, or inhibition of protein synthesis in Ce block fear acquisition, suggesting that Ce is critically involved in the acquisition of conditioned fear responses (Goosens and Maren, 2003; Wilensky et al., 2006). However, in these studies, both CeM and CeL were

affected. A more recent study relying on selective inactivation of CeM or CeL revealed a different role of these nuclei regarding the acquisition and expression of conditioned fear responses (Ciocchi et al., 2010). As expected from connectivity studies, CeM but not CeL is required for the expression of conditioned fear responses (Ciocchi et al., 2010). In agreement with that, optogenetic activation of CeM by itself induces strong unconditioned freezing (Ciocchi et al., 2010). In contrast, inactivation of CeL but not CeM during the acquisition phase results in a memory deficit a day later. In sum, CeL is required for fear acquisition whereas CeM is required for fear expression (Ciocchi et al., 2010).

In agreement with the above, CeM neurons exhibit one type of response to the CS: an increase in firing rate to CS presentation that positively correlated with freezing (Ciocchi et al., 2010; Duvarci et al., 2011). In contrast, CeL neurons exhibit two types of responses: CeL-On cells that are excited during the CS, and CeL-Off cells that are inhibited during CS presentations (Ciocchi et al., 2010; Duvarci et al., 2011). It was further shown that CeL-Off cells express PKC-δ^+ and CeL-On cells do not (PKC-δ^-) (Ciocchi et al., 2010; Haubensak et al., 2010). These findings suggest that CeM projection cells are under tonic inhibition from CeL-Off cells. After fear conditioning, CS presentation excites CeL-On cells which in turn inhibit CeL-Off cells, and indirectly disinhibit CeM projecting cells.

This hypothesis is supported by a more recent study. Li et al. (2013) found that fear learning results in the potentiation of LA synapses onto SOM+ positive CeL neurons, while those onto SOM- negative CeL neurons are weakened (Li et

al., 2013). It was further found that SOM+ neurons inhibit SOM- neurons, and that SOM- but not SOM+ neurons inhibit CeM projection neurons (Li et al., 2013). Therefore, after conditioning, SOM+ neurons are excited by LA input, while SOM- neurons are inhibited by SOM+ neurons. This results in disinhibition of CeM projection cells (Li et al., 2013). Furthermore, the acquisition of conditioned fear responses is abolished when the potentiation of LA synapses onto SOM+ cells is blocked (Li et al., 2013). This result is consistent with the study cited above (Ciocchi et al., 2010) that CeL inactivation causes a deficit of learned fear. As expected, the vast majority of SOM+ neurons correspond to PKC-δ^-, CeL-On neurons, while most SOM- neurons correspond to PKC-δ^+, CeL-Off neurons (Li et al., 2013).

Lastly, CS information reaches CeM via the ITC cells clusters. As I mentioned earlier, in guinea pigs, ITCm clusters located ventral to CeL receive LA inputs, and project to more medially-located ITCm clusters. The more medially-located ITCm clusters inhibit CeM projection cells. The current hypothesis is that activation of LA neurons by the CS excites laterally-located ITCm clusters located dorsal to LA, which results in inhibition of more medially-located ITCm clusters, and eventually disinhibit CeM projection cells (Pare et al., 2004). A study in mice supports this hypothesis (Busti et al., 2011). However, one must take into account the differing orientation of the amygdala in these species. In the rat and mouse amygdala, Ce is medial to BL, whereas in guinea pigs, Ce is dorsal to BL. Thus, the dorsoventral axis of the rat and mouse amygdala corresponds to the lateromedial axis of the guinea pig amygdala. As a

result, the laterally-located ITCm cluster in guinea pigs corresponds to the ITCm dorsal cluster (ITCd) in rats and mice. Whereas, the medially-located ITCm cluster in guinea pigs corresponds to the ITCm ventral cluster (ITCv) in rats and mice (Figure 1.1 and Figure 1.2). Thus, fear conditioning is associated with an increased expression of the Zif268 protein (a marker for neural activity) in the dorsal ITCm cluster (ITCd) but not in the ventral cluster (ITCv) (Busti et al., 2011). Further investigation is required to test these predictions.

Fear extinction learning:

In fear extinction, rats are repeatedly exposed with the feared object (CS) in the absence of negative consequences (US). This results in a reduction of fear responses to the CS. Three behavioral properties suggest that fear extinction depends on a new type of learning and does not simply result from erasure of the original CS-US association. First, whereas the original memory can last the lifetime of a rat (McAllister et al., 1986), expression of fear extinction decays with time, a phenomenon termed spontaneous recovery (Quirk, 2002). Second, expression of conditioned fear responses is context independent, meaning that they are expressed irrespective of the context where the CS is presented. In contrast, the expression of extinction is context dependent, meaning that testing in a context different than where extinction training took place results in a much weaker expression of extinction, a phenomenon termed renewal (Bouton and Bolles, 1979). Last, expression of fear extinction is abolished after unsignaled presentation of the US, a phenomenon termed reinstatement (Rescorla and

Heth, 1975). These three behavioral observations do not support the idea that fear extinction results from erasing the original CS-US association but from the formation of a new context-dependent inhibitory memory that competes with the original fear memory. Below, I will review the neural circuits involved in the extinction of conditioned fear responses.

Studies suggests that a distributed neural network including the amygdala, hippocampus, and mPFC participate in the acquisition and expression of fear extinction (Pape and Pare, 2010; Milad and Quirk, 2002). I will mainly focus on the role of the amygdala in fear extinction.

Many studies indicate that synaptic plasticity in the BLA is required for acquisition of fear extinction. For example, intra-BLA infusion of NMDA receptor antagonists and ERK/MAPK inhibitors prevent the acquisition of fear extinction (Lu et al., 2001; Herry et al., 2006; Kim et al., 2007; Sotres-Bayon et al., 2007). In agreement with these observations, many BL neurons that show no responses to the CS during fear learning become CS responsive after extinction training. These cells are called extinction neurons (Herry et al., 2008; Amano et al., 2011). In contrast, another group of cells in the BL develop CS responses as a result of fear conditioning, but lose their responses after extinction training. These cells are called fear neurons (Herry et al., 2008; Amano et al., 2011). The last group of BL cells responds similarly to the fear neurons, but continues to be CS responsive after extinction learning. These cells are called extinction-resistant neurons (Herry et al., 2008; Amano et al., 2011). Duvarci and Pare (2014) suggest that extinction-resistant neurons might account for the maintenance of

the original CS-US association after extinction. Not only do fear and extinction neurons exhibit contrasting responses to CS presentation, but they are also part of distinct neural networks (Herry et al., 2008; Senn et al., 2014). For example, extinction neurons project to the infralimbic (IL) subdivision of the mPFC, a key structure participating in extinction learning (Sotres-Bayon and Quirk, 2010), whereas fear neurons project to prelimbic (PL) subdivision of the mPFC, a key structure participating in fear learning (Sotres-Bayon and Quirk, 2010; Senn et al., 2014). In sum, the existence of fear and extinction cells within the basal nucleus suggests that fear and extinction memory coexist in the amygdala.

In contrast to BL neurons, CeM cells do not exhibit activity similar to extinction-resistance or extinction BL neurons. Instead, CeM neurons that were responsive to the CS after fear learning gradually lose their CS responsiveness during extinction learning, similar to fear neurons in the BL. Moreover, this decrease in firing rate is accompanied by a parallel decrease of fear responses elicited by the CS (Duvarci et al., 2011). The fact that CeM neurons lose their CS responsiveness during extinction training, while many BL neurons maintain it (extinction-resistance neurons), suggests that an inhibitory circuit prevents the activation of CeM neurons by BL neurons. Indeed, many studies suggest that ITCm cells prevent CeM cells from being activated following extinction.

Supporting this idea, ITCm cells receive inputs from a sub-region of the mPFC, the infralimbic region. Using anterograde tract-tracing and electron microscopic techniques, it was shown that ITCm neurons are the recipients of dense inputs from infralimbic cortex (McDonald et al., 1999; Pinto and Sesack,

2008), a structure critical for the consolidation of extinction memory (Milad et al., 2004; Quirk and Mueller, 2008; Laurent and Westbrook, 2009). These results suggest that the infralimbic cortex may mediate extinction learning via the activation of ITCm cells.

In keeping with this idea, selective lesions of ITCm cells caused an extinction deficit that was negatively correlated to the number of surviving ITC cells (Likhtik et al., 2008). Also, an ex vivo study revealed that extinction training causes a potentiation of BL input to ITCv cells, an effect dependent on infralimbic activity for its induction, and on postsynaptic mechanisms for its expression (Amano et al., 2010). In agreement with this finding, pharmacological inhibition of BL inputs to ITCm cells using neuropeptide S interfered with extinction (Jungling et al., 2008). Lastly, extinction is associated with increased expression of the immediate early genes Zif268 and c-fos in ITCv, but not ITCd (Busti et al., 2011; Knapska and Maren, 2009). Thus, these results suggest that, following extinction, CS-related BL and infralimbic inputs trigger, via ITCv cells, feed-forward inhibition in CeM neurons, leading to a reduction in conditioned fear responses.

***Innate fear suppression*:**

Before reviewing the amygdala's role in innate fear suppression, I will review evidence that the amygdala is critically involved in innate fear responses. Indeed, in addition to its role in conditioned fear, the amygdala is also involved in the generation of innate fear responses elicited by species-specific stimuli such

as predators. Kluver and Bucy showed that after bilateral temporal lobectomy, monkeys showed a marked suppression of fear in response to stimuli like snakes (Kluver and Bucy, 1937). It was subsequently shown that amygdala lesions are responsible for this effect (Weiskrantz, 1956). More recently, it was reported that macaque monkeys with ibotenic lesions of the amygdala retrieved a reward placed near a rubber snake more quickly than unlesioned monkeys (Amaral, 2002). Moreover, lesioned monkeys did not hesitate to handle the rubber snake (Amaral, 2002). Similarly, amygdala lesioned rats were seen to approach sedated cats (Blanchard and Blanchard, 1972).

Consistent with the lesion data, rats exposed to a live cat exhibit an increase in c-Fos expression in the medial amygdala nucleus (MEA), LA and posterior AB (Martinez et al., 2011). Furthermore, lesions of the MEA abolished defensive responses, while lesions of the LA, posterior AB, and Ce reduced defensive responses such as freezing during cat exposure (Martinez et al., 2011). Similarly, rats exposed to ferret odor showed elevated c-Fos in the BLA, Ce and MEA (Butler et al., 2011).

The amygdala regulates other types of innate fear responses such as avoidance of open and elevated spaces. Surprisingly however, mice spent more time in the open arms of an elevated plus maze, and in the center in an open field, when BLA inputs to CeL were excited or BLA inputs to the ventral hippocampus were inhibited (Tye et al., 2011; Felix-Ortiz et al., 2013). Conversely, mice avoided the open arm and the center of an open field when BLA inputs to CeL were inhibited or BLA inputs to the ventral hippocampus were

excited (Tye et al., 2011; Felix-Ortiz et al., 2013). These results suggest that different populations of cells within the BLA increase or decrease innate fear responses.

Although, the above results may seem paradoxical, suppression of innate fear responses can be advantageous, even necessary. Often, survival requires reconciling opposite behavioral tendencies. For instance, rodents have acquired defensive behavioral strategies (Blanchard and Blanchard, 1990) that minimize the likelihood of encounters with predators (e.g. staying in small enclosed spaces) and maximize the chance of survival if such encounters occur (e.g. freezing). Yet, in order to attain food, these defensive behavioral tendencies must be suppressed or overcome. Consistent with the large body of evidence implicating the amygdala in the control defensive behaviors (Blanchard and Blanchard, 1972; LeDoux, 2000), evidence obtained by Choi and Kim shows that the amygdala regulates risk-taking in a foraging task (Choi and Kim, 2010). In this specific task, rats were confronted with a mechanical predator-like figure (called Robogator) programmed to surge forward when a rat approached. Rats had to leave a safe nest-like area to retrieve food pellets positioned at various distances from the Robogator. In this task, intra-amygdala infusions of drugs that presumably reduced (muscimol) or enhanced (picrotoxin) the firing rates of amygdala neurons respectively led to increases or decreases in risk-taking (Choi and Kim, 2010). In a similar task that requires suppression of innate fear, human subjects who fear snakes had to bring snakes closer to them. In each trial, the subjects choose whether to move the snake closer or further away while being

scanned using a functional magnetic resonance imaging scanner. Consistent with Choi and Kim's results, when subjects overcame fear by choosing to bring the snake closer, the blood oxygen level dependent (BOLD) signal was attenuated in the amygdala (Nili et al., 2010). In conclusion, inhibition of the amygdala in rats using muscimol causes them to overcome fear; while suppression of amygdala activity in human subjects is associated with successfully overcoming fear.

We used a similar behavioral task to the one introduced by Choi and Kim (2010) to study innate fear suppression. In our study rats faced two opposite behavioral tendencies: avoidance of the robogator and approach of food pellets.

1.3 Overview of the experiments presented in this thesis

In the above introduction I summarized the anatomical and physiological organization of the amygdala. Then, I reviewed the evidence implicating the amygdala in the extinction of conditioned fear responses and in the suppression of innate fear. I will now explain the experiments I performed to further our understanding of these two functions.

***Connectivity and infralimbic control of ITC cells*:**

As I mentioned earlier, it was suggested by Royer and Pare (2002) that, based on the connectivity of ITCm cells and their ability to control the output station of the amygdala, ITCm clusters are in a perfect position to gate BL inputs that relay information about the CS to CeM neurons (Royer and Pare, 2002).

Thus, ITCm are thought to play a critical role in the extinction of conditioned fear responses. Currently, several factors hinder progress in understanding how ITCm cells regulate fear. First, although extinction is usually studied in rats and mice, most studies on ITCm cells including their connectivity have been performed in guinea pigs and cats. Thus, it is currently unclear whether the connectivity of ITCm cells is similar in these various species. Second, we lack criteria to identify ITCm cells on the basis of their discharge pattern. As a result, we cannot test key predictions of ITCm extinction models. Among these, it was predicted that in light of the heavy projections they receive from the infralimbic (IL), ITCm cells should be ortodromically activated by IL stimulation. Thus, the experiments discussed in Chapter 3 address these questions as follows. First, we will examine whether the internuclear connectivity of ITCm cells in rats are consistent with the findings obtained in cats and guinea pigs. Second, we will test whether ITCm cells are ortodromically responsive to IL inputs. We will also examine whether their responses are distinct from that of other types of amygdala neurons.

***Regulation of innate fear by the amygdala*:**

The experiments described in chapter 4 examine the role of the amygdala in the regulation of innate fear. Previously, Choi and Kim (2010) obtained evidence that the amygdala regulates risky foraging decision in the presence of a predator. In particular, they found that local inactivation of the amygdala seemed to abolish the rats' cautious behavior. My experiment will investigate how the

amygdala regulates risky foraging decision. Are amygdala neurons suddenly inhibited when rats initiate foraging? Or do they continue to signal threat? The latter possibility implies a form of quantitative competition between neuronal systems that signal threat vs. drive food seeking. The former implies a qualitative system-level shift in the balance of activity between competing neuronal systems. To address these questions, we recorded BL neurons with multishank silicon probes in rats engaged in the foraging task.

As I mentioned earlier, in the foraging task, rats are faced with two opposite behavioral tendencies: avoidance of the robogator versus approach of the food. However, the semi-naturalistic character of this task complicates analysis of the factors that drive neuronal activity. Are predator risk, reward availability, both, or neither required? Also, this task features uncontrolled behavioral variables such as the rats' movements and speed. Therefore in chapter 5, to shed light on the factors determining BL activity, we studied the activity of BL cells in two additional tasks that did not include explicit threats or rewards.

CHAPTER 2

MATERIALS AND METHODS

2.1 Materials and methods for chapter 3

Experiments were performed in Sprague-Dawley rats, in accordance with the National Institutes of Health Guide for the Care and Use of Laboratory Animals and with the approval of the Institutional Animal Care and Use Committee of Rutgers University (Newark, NJ).

The experiments described in chapter 3 relied on two different approaches. To study the connections of ITCm cells with each other and other amygdala nuclei, coronal slices of the amygdala were prepared and ITCm cells were labeled with neurobiotin during whole-cell patch recordings in brain slices kept in vitro. To study the firing pattern and infralimbic (IL) responsiveness of ITCm cells, we performed juxtacellular recording of ITCm cells in urethane-anesthetized rats. We describe these two approaches in turn below.

Whole-cell patch recording of ITCm cells in vitro

Slice preparation

These experiments were performed using coronal brain slices obtained from 30 Sprague-Dawley rats (100-150 g). The rats were anesthetized with

ketamine, pentobarbital, and xylazine (respectively 80 mg/kg, 60 mg/kg, and 12 mg/kg, i.p.). After abolition of all reflexes, they were perfused through the heart with a cold (4°C) modified artificial cerebrospinal fluid (aCSF) that contained (in mM): 126 choline chloride, 2.5 KCl, 1.25 NaH_2PO_4, 1 $MgCl_2$, 2 $CaCl_2$, 26 $NaHCO_3$, and 10 glucose. The brains were then extracted and cut in 400 µm-thick slices with a vibrating microtome while submerged in the same solution as for the transcardial perfusion. After cutting, slices were transferred to an incubating chamber where they were allowed to recover for at least one hour at 20°C in a control aCSF with the same composition as that used above with the exception that NaCl was substituted for choline chloride (pH 7.3, 300 mOsm). The slices were then transferred one at a time to a recording chamber perfused with the same solution (7 ml/min). Before the recordings began, the temperature of the chamber was gradually increased to 32°C.

Electrophysiology

Under visual guidance with differential interference contrast and infrared video-microscopy, we obtained whole-cell patch recordings of ITCm neurons using pipettes (7-10 MΩ) pulled from borosilicate glass capillaries and filled with a solution containing (in mM): 130 K-gluconate, 10 N-2-hydroxyethylpiperazine-N'-2-ethanesulfonic acid, 10 KCl, 2 MgCl2, 2 ATP-Mg, and 0.2 GTP-tris (hydroxy-methyl) aminomethane (pH 7.2, 280 mOsm) and 0.5% neurobiotin. The liquid junction potential was 10 mV with this solution and the membrane potential was corrected accordingly. Current-clamp recordings were obtained with an

Axoclamp 2B amplifier and digitized at 10 kHz with a Digidata 1200 interface (Axon Instruments, Foster City, CA).

To characterize the electroresponsive properties of recorded cells, graded series of depolarizing and hyperpolarizing current pulses (20 pA, 500 ms in duration) were applied from rest and other pre-pulse potentials. The input resistance (R_{in}) of the cells was estimated in the linear portion of current-voltage plots.

No special current injection protocol had to be used to label ITC cells with neurobiotin. It diffused into the cells as we studied their electroresponsive properties. At the conclusion of the recordings, the slices were removed from the chamber and fixed for 1 to 3 days in 0.1 M phosphate buffer saline (pH 7.4) containing 4% paraformaldehyde. Slices were then embedded in agar (3%) and sectioned on a vibrating microtome at a thickness of 100 μm. Neurobiotin-filled cells were visualized by incubating the sections in the avidin-biotin-horseradish peroxidase solution (ABC Elite Kit, Vector Labs) and processed to reveal the horseradish peroxidase staining (Horikawa and Armstrong 1988).

Juxtacellular recording of ITC cells in vivo

Surgery

A total of 150 Sprague-Dawley rats (250-350 g) were anesthetized with urethane (1.8 g/kg) and administered atropine sulfate (0.05 mg/kg, i.m.) to reduce salivation. Throughout the experiment, body temperature was kept at 37°C with a heating pad. After placing the rats in a stereotaxic frame and

shaving their scalp, we made numerous, evenly spaced, small injections of the analgesic bupivacaine (0.125% solution, s.c.) around the sites to be incised. Ten minutes later, the scalp was incised above the amygdala, IL cortex, and upper brainstem and small openings were drilled into the skull. Then, after opening the dura mater, pairs of stimulating electrodes were stereotaxically inserted in the IL cortex and just dorsal to the substantia nigra, where Ce axons en route to the brainstem form a compact bundle (Hopkins and Holstege, 1978), all in the same hemisphere. These stimulating electrodes were used to antidromically activate BL cells projecting to the IL cortex and Ce cells projecting to the brainstem, respectively (Krettek and Price, 1977b; Hopkins and Holstege, 1978; McDonald, 1991b). In a subset of experiments, IL stimulating electrodes were inserted ipsi- and contralaterally to the recording site in the amygdala. It should be noted that because CeL neurons send strong projections to the parabrachial nucleus (Petrovich and Swanson, 1997) and their axons initially course through the same region as CeM axons en route to their brainstem targets (Hopkins and Holstege, 1978), the brainstem stimuli we delivered, just dorsal to the substantia nigra, could elicit antidromic responses in both CeL and CeM cells.

Recording, stimulation, and labeling with neurobiotin

Juxtacellular ITCm recordings were obtained with pipettes (0.5 μm tip; 20-30 MΩ) pulled from borosilicate glass capillaries and filled with a solution containing 1M NaCl plus 1.5% neurobiotin. The pipettes were aimed to Ce with a slight (18°) mediolateral angle and gradually lowered with a micromanipulator.

Every 25 µm, electrical stimuli were delivered at a low frequency (0.3 Hz) to the brainstem and IL cortex, alternating between the two sites. Although we used a range of stimulation intensities (0.2-1.5 mA, 100 µs), the results section in chapter 3 reports the response patterns obtained with the same stimulation intensity at the two stimulated sites (1 mA). Each time a responsive cell was encountered, we recorded its spontaneous activity for ≥ 3min and their responsiveness to IL and brainstem stimuli. The term spike burst in chapter 3 refers to a cluster of spikes with relatively stereotyped features (comprised of two or more spikes occurring at a frequency ≥ 150 Hz).

Extracellular data was amplified 1000 times with Multiclamp700B, (Molecular Devices, Sunnyvale, CA) using a bandwidth of 0.1 to 6 kHz. The data was sampled at 20 kHz, stored on a hard drive, and analyzed off-line with custom-made programs written in Matlab (Natick, MA) and Igor (Wavemetrics, Lake Oswego, OR). Analyses of spike shapes were performed in Matlab.

Because Ce and BL neurons have differential projections to the brainstem and IL cortex (Krettek and Price, 1977b; Hopkins and Holstege, 1978; McDonald, 1991b), at some point during a proportion of electrode tracks, we observed an abrupt transition in the stimulating sites effective in backfiring recorded neurons (from brainstem to IL stimuli). The region located between the last Ce cell antidromically responsive to brainstem stimuli and the first BL cell backfired from the IL cortex therefore corresponded to the Ce-BL border where ITCm cells are known to be located. Thus, we then moved the electrode back to the position of the last antidromically responsive Ce cell and, without withdrawing the pipette

from the brain, moved the pipette 20-40 µm laterally or medially. After a delay of 20 min, the pipette was moved ventrally again and the first juxtacellularly-recorded neuron that was spontaneously active and/or orthodormically responsive to stimulation of any of our stimulation sites (IL, brainstem) was labeled with neurobition. This was achieved by applying positive current pulses (100 ms) at 5 Hz for 1-5 minutes via the recording pipette. The current amplitude was adjusted to the minimum required to make the cell discharge at each current injection cycle. During this period, if prior to current injection the cell was responsive to IL stimulation, electrical stimuli were delivered at the same site every 30 sec to make sure the firing properties of the cell remained constant. We attempted to label only one cell per experiment.

After labeling, the rats were given an overdose of pentobarbital (80 mg/kg), perfused with 150 ml of saline (0.9%) followed by 150 ml of a fixative containing paraformaldehyde (4%) and glutaraldehyde (0.5%) in 0.1 M phosphate buffer (pH 7.4). The brain was then removed from the skull and sectioned at 100 µm on a vibrating microtome.

Neurobiotin revelation

Slices from in vitro recordings were embedded in agar (3%) and re-sectioned at 100 µm. Following this, the same approach was used to reveal neurobiotin-labeled neurons recorded in vitro and in vivo. Sections were washed several times in phosphate buffer (PB, 0.1 M, pH 7.4) and then transferred to a H_2O_2 solution (0.5%) in PB for 15 min. After numerous washes in PB, sections

were incubated for 12 h at 20^{o}C in a solution containing 0.5% triton, 1% solutions A and B of an ABC kit (Vector, Burlingame, CA) in PB. The next day, they were washed in PB (5 x 10 min). Neurobiotin was visualized by incubating the sections in a 0.1 M PB solution that contained diaminobenzidine tetrahydrochloride (0.05%, Sigma), 2.5mM nickel ammonium sulfate (Fisher) and H_2O_2 (0.003%) for 5-10 min. Then, the sections were washed in PB (5 X 10 min), mounted on gelatin-coated slides, and air-dried. The sections were then counterstained with cresyl violet and coverslipped with permount for later reconstruction.

All visible processes of the labeled neurons were observed in a microscope using a 40X objective and photographed. Typically, their processes extended over several sections. To align the sections, we layered the photographs in Photoshop (Adobe Systems Incorporated, CA) and used blood vessels or other obvious landmarks present in the various sections to align them. The layers were then collapsed and the entire neuron drawn. Below, note that in order for a neuron to be considered as projecting to a particular nucleus, it had to meet two conditions. First, it had to contribute an axon to this nucleus. Second, the axonal segment seen in this nucleus had to bear axonal varicosities.

Processing for μ-opioid receptor (μOR) immunohistochemistry

The transcardial perfusion was as for the in vivo experiments described above with the exception that the fixative also contained picric acid (0.2%) but no glutaraldehyde. After extraction of the brain, overnight post-fixation, and cutting (all steps done as for the in vivo experiments described above), half the sections

(100 µm) were stained with cresyl violet and the other half processed to reveal µOR immunoreactivity. The µOR antibody was obtained from DiaSorin, Inc. (Stillwater, MN). This antibody was previously characterized for specificity and cross-reactivity (Kalyuzhny et al., 1996; Wilson et al., 2002). For instance, absorption of the µOR antibody with its antigen (35 mg/ml) abolished all immunostaining. Furthermore, in our experiments, omission of the antibody from the following protocol abolished all differentiated staining. The sections were washed in phosphate buffer saline (PBS; 4 X 5 min) and then incubated in H_2O_2 (0.5%) in PBS for 15 min, washed in PBS (4 X 5 min), pre-incubated in a blocking solution (10% normal goat serum, 1% BSA, Triton-X100, 0.3%), and incubated overnight in the primary antibody solution containing a µOR antibody from ImmunoStar (Hudson, WI; 1:4000), 1% normal goat serum, 1% BSA, and Triton-X100 (0.3%) in PBS. Then, sections were incubated in the secondary antibody solution (Jackson, West Grove, PA, 1:200), followed by the avidin-biotin-complex (Vector, Burlingame, CA). After several washes in PBS, the immunoreactivity was then revealed by incubating the sections in a 0.1 M PB solution that contained diaminobenzidine tetrahydrochloride (0.05%, Sigma), 2.5 mM nickel ammonium sulfate (Fisher) and H_2O_2 (0.003%) for 5-10 min. Then, the sections were washed in PB (5 X 10 min), mounted on gelatin-coated slides, and air-dried. We then compared the position of ITCm cell clusters on adjacent sections processed to reveal µOR or stained with cresyl violet.

Histological identification of ITCm cell clusters

Below, we considered that a neurobiotin-labeled neuron was an ITCm cell when counterstaining with cresyl violet revealed that it was located in a densely packed cluster of darkly stained neurons at the BL-Ce border. This approach was selected on the basis of earlier work and additional tests, as described below. Previously, it was reported that in amygdala sections processed to reveal GABA immunoreactivity or counterstained with cresyl violet, ITCm cells are conspicuous because they occur as densely packed and darkly stained clusters of small neurons (Pare and Smith, 1993a; Pare and Smith, 1993b; Pare and Smith, 1994). Moreover, in adjacent sections of the rat amygdala, a close correspondence was found between the positions of the ITCm cell clusters labeled with these two methods (see Figure 1 in Pape and Pare, 2010).

Since earlier work had revealed that ITC cell clusters exhibit high levels of μOR, (Wilson et al., 2002; Jacobsen et al., 2006), we further tested whether the ITC cell clusters identified with cresyl violet corresponded to patches of dense μ-OR immunoreactivity. As shown in chapter 3, a close correspondence was found between the position of ITC cell clusters in adjacent sections stained with cresyl violet or processed to reveal μ-OR immunoreactivity. However, pilot tests revealed that the intensity of the μOR immunoreaction was so high that it interfered with visualization of neurobiotin-labeled neurons. In order to prevent the μOR staining from interfering with the visualization of the neurobiotin-labeled cells, the revelation time had to be reduced. However, we found that at a lower intensity, the μOR staining became no more useful than the cresyl violet to

identify ITC cell clusters yet required much more processing. Given that counter-staining with cresyl violet yielded highly reproducible results, we opted for this approach to identify ITC cell clusters for both in vitro and in vivo experiments.

2.2 Materials and methods for chapter 4 and 5

Procedures were approved by the Institutional Animal Care and Use Committee of Rutgers University, in compliance with the Guide for the Care and Use of Laboratory Animals (DHHS). We used male Sprague-Dawley rats (310-360g, Charles River Laboratories, New Field, NJ). We used 6 rats for the foraging task described in chapter 4 and 2 additional rats for the open field task described in chapter 5. Three of the rats that were used in the foraging task were also used for the shuttle task described in chapter 5. Prior to the experiments, all rats were habituated to the animal facility and handling for one week.

Surgery

Rats were anesthetized with a mixture of isoflurane and O_2, and administered atropine sulfate (0.05 mg/kg, i.m.) to aid breathing. In aseptic conditions, rats were mounted in a stereotaxic apparatus with non-puncture ear bars. A local anaesthetic (bupivacaine, sc) was injected in the scalp. Fifteen minutes later, the scalp was incised and a craniotomy was performed above the amygdala. Then, silicon probes (Neuronexus, City, State) were stereotaxically aimed at the BL. Four shanks silicon probes were used for 3 rats described in chapter 4 (foraging task), while 8 shanks silicon probes were used for 3 rats

described in chapters 4,5 (foraging task and shuttle task) and 2 rats described in chapter 5 (open field task). Inter-shank distance was 200 μm. Each shank consisted of 8 recording leads (de-insulated area of 144 μm^2) separated by ~20 μm dorsoventrally. In a subset of three rats in chapter 4, a craniotomy was also performed above nucleus accumbens (nAc) and mPFC. Then, pairs of tungsten stimulating electrodes (inter-tip spacing of 1-1.7 mm) were stereotaxically inserted in these two structures. Rats were allowed two to three weeks to recover from the surgery.

Behavioral protocol

After recovery from the surgery, rats were housed individually with ad libitum access to water. To ensure proper motivation in the foraging task, daily access to food was restricted in time so that the rats' bodyweight was maintained at about 90% of age-matched subjects with continuous access to food.

Foraging task

Foraging apparatus. The foraging apparatus was a long rectangular alley (245 cm in length by 60 cm in width) with high walls (60 cm) but no ceiling. It was divided into two compartments by a door (height, 50 cm; width, 10 cm). At one end of the apparatus was a small (length 30 cm), dimly lit (10 Lux) nesting area with a water bottle. The rest of the apparatus was a much longer (215 cm) and brighter (200 Lux) foraging arena. An overhead digital videocamera (frame rate 29.97/sec) recorded the rats' behavior in the two compartments.

Mechanical predator. (Robogator): On a proportion of trials in the foraging task, a mechanical predator (length, 34 cm; width, 17 cm; height, 14 cm) on wheels was positioned at the end of the foraging arena, facing the nesting arena. This Robogator (Mindstorms, LEGO systems) was equipped with a sensor that detected the rats' approach and triggered a sudden forward movement (80 cm at 60 cm/sec) and repeated opening and closing of the jaws (9 times) followed, after 2 sec, by return to its original position.

Habituation to nesting area (Days 0-1). Rats were first habituated to the nesting area for 2 daily consecutive sessions of 7 hours. During this period, they could consume up to 6 g of food (sweet cereal pellets). However, the gateway to the foraging arena remained shut at all times.

Foraging in the absence of Robogator (Days 2-3). On the following day, in the absence of the Robogator, rats were given the opportunity to retrieve sweetened food pellets (80-100 mg) in the foraging arena. No food was available in the nesting area in this case. Sixty trials were conducted, each beginning with a period of 30 min in the nesting area with the gateway shut. This was repeated the next day. A single food pellet was placed at various distances from the door. The gateway was then opened. After a period of hesitation at the doorway, rats retrieved the food pellet and returned to the nesting area to consume it. Upon reentry in the nesting arena, the gateway was closed. The distance between the nesting area and food pellet was gradually increased in steps of 25 cm (from 25 to150 cm), after three successful trials at each distance. Later on, the distance was varied randomly from trial to trial.

Foraging in the presence of Robogator (Days 4-5). On the following day, rats were again given the opportunity to retrieve food pellets in the foraging arena. However, 60% of trials were conducted with the Robogator present. Blocks of trials with (n = 10-20) or without (n = 10-15) the Robogator were conducted, for a total of 100-120 trials.

Analysis of behavior

The rats' behavior was recorded by an overhead videocamera at a frame rate of 29.97 Hz. To analyze the rats' behavior, we used two approaches. First, a matlab script was written to determine the position of the rats based on the shifting distribution of light intensity across frames. This also allowed us to determine the rat's velocity. In the thesis, speed is expressed in pixels/sec. With our camera and distance to the apparatus, 315 pixels correspond to one meter. However, while this approach could reliably track the rat's position and speed, it did not have sufficient resolution to identify the exact video frame when they started waiting at the door threshold (defined as when the rat's snout extended beyond the door into the foraging arena), when he initiated foraging (defined as the last frame of immobility prior to completely moving out of the nest), retrieval of food pellet, and retreat into the nest. These task events were identified by a trained observer who performed a frame-by-frame analysis of the video file. The observer also noted whether rats failed or succeeded each trial.

Shuttle task

In this task, rats ran back and forth between two nest-like compartments (50 cm long by 20 cm wide) through a central compartment (50 cm long) to retrieve food pallets at the end of the other nest. The walls were 45 cm high. The apparatus was made of black Plexiglas and dimly illuminated (10 Lux). The nests and corridor were separated by retractable doors. Rats received extensive habituation to the apparatus with the doors open. During the recordings, rats were positioned in one of the nests and a food pellet in the other. After opening the doors, rats immediately ran to the other nest to consume the food. While rats consumed the food, the door was closed. The inter-trial interval was ≥ 1min. Analysis of behavior was as described for the foraging task.

Open field

The open field was rectangular (60 cm wide by 180 cm long with walls 60 cm high) and made of black Plexiglas. Ambient light levels were very low (7 Lux). Prior to the recordings, rats received extensive habituation to the apparatus. Analysis of behavior was as described for the foraging task.

Unit recording, clustering, and analysis

BLA unit recordings were performed during all phases of the behavioral protocol described above with the exception of habituation. In rats that had been implanted with stimulating electrodes, at the end of each behavioral session,

electrical stimuli (300-600 μA, 0.1 ms) were delivered at 1 Hz to determine whether recorded cells could be antidromically invaded from one or more of the stimulated sites. Then, the silicon probes were lowered 30 μm, ≥ 8 hours ahead of the next recording session, to ensure mechanical stability.

The signals were sampled at 25 kHz and stored on a hard drive. The data was first high-pass filtered using a median-based filter, then thresholded to extract spikes. We then ran PCA on the spikes and the first three components were clustered using KlustaKwik (http://klustakwik.sourceforge.net/). Spike clusters were then refined manually using Klusters (Hazan et al., 2006). The reliability of cluster separation was verified by inspecting auto- and cross-correlograms. Units with unstable spike shapes during a given recording session were excluded.

To determine spike duration, we first selected the channel where, for a given cell, action potentials had the largest peak to trough amplitude. We then measured the spikes-duration as the time between spike through and peak (see Bartho et al., 2004). Antidromic action potentials were identified as such when they had a fixed latency (≤ 0.1 ms jitter) and collided with spontaneously occurring spikes.

Statistical analyses

All grouped data are reported as average ± SEM. When firing rates (FRs) are expressed logarithmically, we used natural logarithms. All statistical tests were two-sided. No subjects were excluded. Before using parametric tests, we

verified that the assumptions of the test (e.g. normality of distribution) were met. Whenever possible, in every instance where we used a parametric test, we also ran a non-parametric test as a precaution. We obtain congruent results in all cases.

When analyzing the evolution of the food retrieval interval over time, we used a mixed effect ANOVA with subject as a random effect. When analyzing time to food retrieval, we did not use trials (≥ 300/rat) but averages of trials obtained in each rat (n = 6) for all statistical comparisons (paired t-tests). While this approach reduces statistical power, using trials as the unit of analysis would have caused an excessive risk of Type 1 error (Aarts et al., 2014). When analyzing percent successful trials, behavior was analyzed with two-way ANOVAs followed by Tukey-Kramer tests.

In the foraging task, to determine whether neurons showed significant task-related variations in firing rates, we computed Kruskal-Wallis one-way ANOVAs during four distinct periods: (1) in the nest with the door closed ("baseline"), (2) during the waiting period at the door threshold ("waiting"), (3) during foraging, and (4) during escape (when rats turned around and ran toward the nest).

For within cell comparisons of unit activity as a function of trial types, we performed Wilcoxon signed-rank tests across the firing rates of all available cells in the two compared conditions. To assess significance of correlations between firing rates and speed of movement, we computed Spearman's r and used a significance threshold of 0.05. Finally, when comparing proportions of cells in two

or more conditions we used the Fisher exact test or Chi-Square test, as appropriate.

States of vigilance were distinguished using spectral analyses of LFPs and behavioral observations. Spontaneous LFP activity was segmented in five second windows and frequency distributions of LFP power in different frequency bands computed. Active waking could be distinguished from all other states because it was associated with a broadband increase in the power of high frequencies (200-240 Hz), reflecting electromyographic activity. After eliminating active waking, we could easily distinguish slow-wave sleep from quiet waking because total power at frequencies <20 Hz was distributed bimodally between the two states: epochs of high power at low frequencies corresponded to periods of slow-wave sleep.

Histology

At the end of the experiments, the animals were deeply anesthetized. On each shank, one of the recording sites was marked with a small electrolytic lesion (10 μA between a channel and the animals' tail for 10 sec). One day later, rats were perfused-fixed through the heart, their brains extracted, cut on a vibrating microtome and the sections counterstained with cresyl violet.

CHAPTER 3

CONNECTIVITY AND INFRALIMBIC CONTROL OF ITC CELLS

3.1 Introduction

Systematic desensitization, the approach clinicians often depend on to treat anxiety disorders, has much in common with the procedure used to extinguish conditioned fear in the laboratory. In both cases, the feared object or situation (CS) is presented repeatedly in the absence of danger (US). These similarities, coupled to the realization that human anxiety disorders are associated with an extinction deficit (Blechert et al., 2007; Milad et al., 2008), have led to an explosion of interest for the mechanisms underlying extinction (Myers and Davis, 2007; Quirk and Mueller, 2008).

Although extinction likely engages multiple parallel mechanisms, accumulating data suggest that ITCm amygdala neurons play a critical role in extinction (Nitecka and Ben-Ari, 1987; Pare and Smith, 1993a; McDonald and Augustine, 1993). Indeed, as I reviewed earlier, selective lesions (Likhtik et al., 2008) and pharmacological inhibition of basolateral (BL) inputs to ITC cells that are located in the fiber bundle between the BL and Ce (the ITCm cells) interfere with extinction (Jungling et al., 2008). Moreover, an ex vivo study revealed that

extinction causes a potentiation of BL inputs to ITCm cells, an effect dependent on IL activity (Amano et al., 2010). Thus, these results suggest that following extinction, CS-related BL inputs trigger, via ITCm cells, more feedforward inhibition in the CeM, leading to a reduction in conditioned fear.

Currently, several factors prevent progress in our understanding of how ITCm cells regulate fear learning and extinction. First, although experimental studies on extinction are typically performed in rats and mice, the majority of studies on ITCm cells were performed in guinea pigs and cats (Pare and Smith, 1993a; Pare and Smith, 1993b; Collins and Pare, 1999; Royer et al., 1999). As a result, it is currently unclear whether critical aspects of ITCm connectivity also characterize commonly used rodent species. For instance, whereas studies in cats and guinea pigs suggested that ITCm cells contribute a strong projection to Ce (Pape and Pare, 2010), the only available study in rats questioned the existence of this projection (Shammah-Lagnado et al., 1999).

Second, we lack criteria to identify ITCm cells on the basis of their discharge pattern and as a result, it has been impossible to test key predictions of ITCm extinction models (Pare et al., 2004). Among these, it was predicted that ITCm cells are strongly excited by IL inputs, explaining why IL inhibition interferes with the acquisition of extinction (Sierra-Mercado et al., 2006) and prevents the potentiation of BL inputs to ITCm cells (Amano et al., 2010).

Thus, this chapter was undertaken to address these critical gaps in our knowledge focusing on (1) the connections formed by ITCm cells in the

amygdala, (2) the identification of ITCm cells on the basis of their extracellularly recorded activity, and characterizing the impact of IL inputs on rat ITCm neurons.

3.2 Results

Nomenclature used to describe ITC cell clusters at the BL-Ce border

As previously reported (Millhouse, 1986), ITC cell clusters are found along the external capsule as well as in and around the fiber bundle located between the BL and Ce. This thesis focuses on the latter groups of ITC cells, the ITCm cells. For simplicity, I will refer to ITCm as ITC. In sections counterstained with cresyl violet (Figure 3.1A) or processed to reveal μOR immunoreactivity (Figure 3.1B), several ITC cell clusters can be seen at the BL-Ce border. Dorsally, there is a rather wide cluster close the dorsolateral edge of the central lateral nucleus (CeL). Below, we will use the abbreviation ITCd to refer to this dorsal cluster (Figure 3.1). More ventrally, one can usually see one or more thinner and elongated ITC clusters immediately lateral or ventrolateral to CeM. Below, we will use the abbreviation ITCv to designate these more ventral clusters (Figure 3.1). Finally, ventral to CeM, especially at rostral levels of the amygdala, one can see a large ITC cluster. Its size varies depending on the rostrocaudal level, but it can be as wide as 1 mm. Below, we will use the abbreviation ITCmain to refer to this cluster (Figure 3.1). Besides of its larger size and position, ITCmain can be easily distinguished from ITCv.

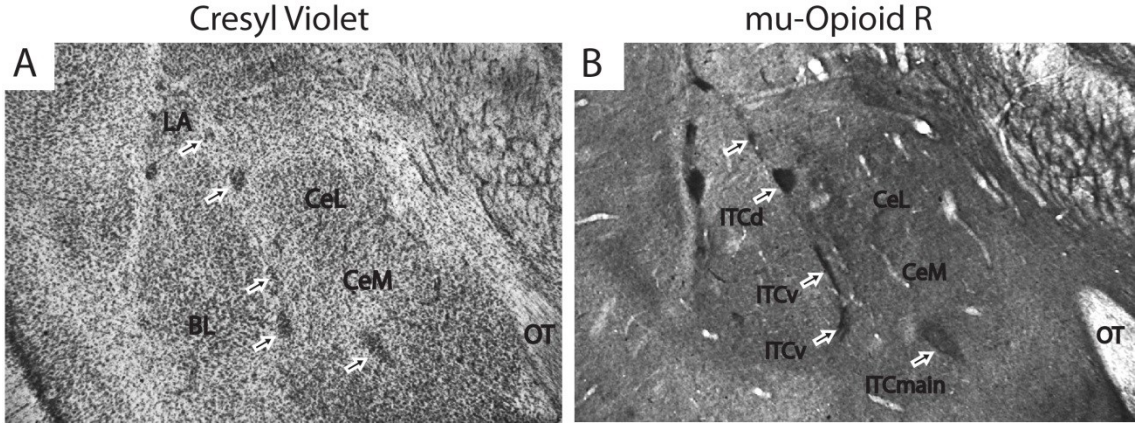

Figure 3.1 Identification of ITC cell clusters. Adjacent coronal sections of the rat amygdala (100 µm thickness). (**A**) Counterstaining with cresyl violet. (**B**) Distribution of immunoreactivity for µ-opioid receptors. Note that darkly stained clusters of cells on the Nissl sections (arrows in A) correspond to patches of dense immunolabeling for µ-opioid receptors (arrows in B). Abbreviations: BL basolateral complex of the amygdala, Ce central nucleus of the amygdale, LA lateral nucleus of the amygdala, OT optic tract.

In vitro experiments: connectivity of ITC neurons

During patch recordings in coronal slices of the amygdala, a total of 30 ITC cells were labeled with neurobiotin and recovered: 19 were ITCd cells and 11 were ITCv neurons. The physiological properties of these ITC cells matched the descriptions found in previous reports (Royer et al., 1999; Royer and Pare, 2002; Royer and Pare, 2003; Marowsky et al., 2005; Geracitano et al., 2007), including a very negative membrane potential (-86.7 ± 1.2 mV), a high input resistance (552.0 ± 35.2 MΩ), action potentials of intermediate durations (1.1 ± 0.05 msec at half amplitude), and limited spike frequency adaptation during prolonged depolarizing current pulses (34.2 ± 3.9% increase in interspike interval duration from the first to the last interval in current pulses eliciting 6 to 10 spikes).

Figure 3.2 shows representative examples of morphologically identified ITCd (Figure 3.2A) and ITCv (Figure 3.2B,C) neurons at low (panels 1) or high magnifications (panels 2-4). Irrespective of their position, ITC cells displayed a moderate to high density of dendritic spines (Figure 3.2A4,B4) and contributed varicose axons (Figure 3.2A3,B3) that ramified in various ways (see below). The appearance of their dendritic trees matched the shape of the clusters where their somata were located. Indeed, ITC cells located in the larger dorsal clusters tended to have radial and multipolar dendritic trees (Figure 3.2A2) whereas those located in the thinner ventral clusters cells typically had flattened and bipolar dendritic arborizations (Figure 3.2B2).

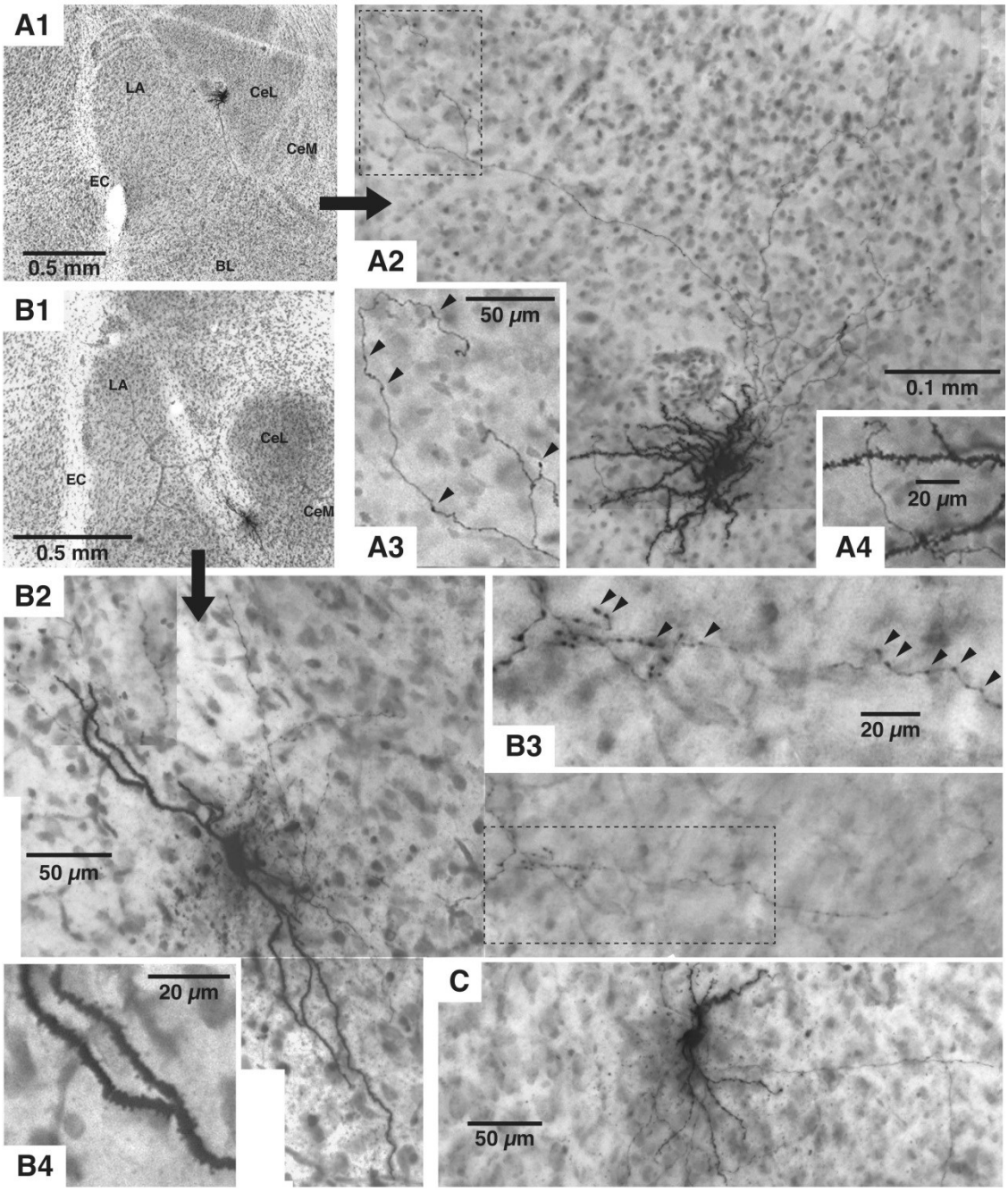

Figure 3.2 Morphological properties of ITC neurons. Whole-cell patch recordings of ITC cells were obtained in brain slices kept in vitro. ITC cells were labeled with neurobiotin present in the pipette solution. (**A-C**) Three different ITC cells. Panels **1** are low power photomicrographs showing the position of the cells on coronal sections counterstained with cresyl violet. Panels **2-4** are higher power photomicrographs of the same ITC cells. The dendritic trees of ITC cells ranged from stellate (**A2**) to flattened (**B2**). They had varicose axons (**A3, B3**) that contributed two or more collaterals. ITC cells displayed a moderate to high density of dendritic spines (**A4, B4**).

Although the electroresponsive properties of ITCd and ITCv cells were statistically indistinguishable (*t*-tests, $p>0.05$), marked differences in their projection patterns were observed. See Figure 3.3 for representative examples of ITCd (Figure 3.3A1-4) or ITCv (Figure 3.3B1-4) neurons. As a group, ITCd neurons projected to three sites: CeL (Figure 3.3A1-4), the amygdalostriatal transition area (ASt; Figure 3.3A2,A4) and to other ITCv cell clusters located more ventrally (Figure 3.3A2,A3). There were no significant differences in the incidence of projections to the three sites (Fisher Exact Probability Test, $p = 0.5$; CeL 58% or 11 of 19; ASt 53% or 10 of 19; ITCv 37% or 7 of 19) and many ITCd cells (58% or 11 of 19) projected to more than one of these three sites. However, the latter percentage is probably an underestimate because several axonal branches were seen to exit the plane of the slice close to the parent somata.

In contrast with ITCd cells, no ITCv neurons projected to ASt or CeL (Figure 3.3B1-4). Instead, they projected to CeM (45% or 5 of 11; Figure 3.3B1,2). In addition, 73% of ITCv cells (or 8 of 11) contributed one or more axonal branches toward ITCmain neurons (Figure 3B3,4). In this case too, the above probably underestimates the extent of the axonal arborization of ITCv cells as many axonal branches were seen to exit the plane of the slice close to the parent somata.

In summary, the general principles emerging from the above are that ITC cells located at the BL-Ce border project to Ce and to other ITC cells located more ventrally. The main difference between ITCd and ITCv cells resides in the

particular sector of Ce they target: CeL in the case of ITCd cells and CeM in the case of ITCv neurons.

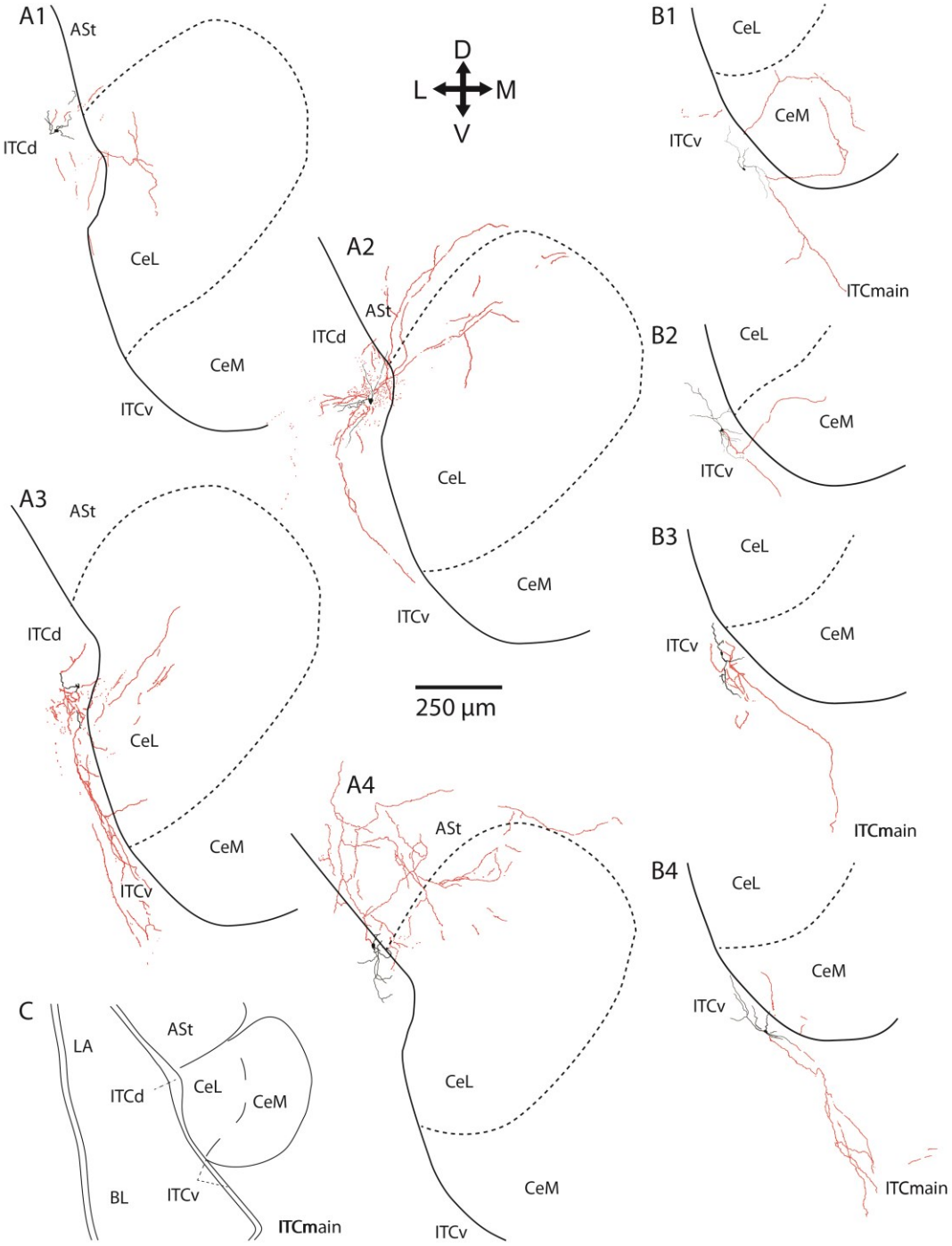

Figure 3.3 Axonal projection patterns of ITC cells located in the cluster adjacent to CeL (ITCd, **A**) or to CeM (ITCv, **B**). All the depicted cells were recorded in vitro. The scheme in **C** shows a general view of the amygdala nuclei depicted in **A** and **B**. The orientation of the sections is indicated by the cross in the top center of the figure where L, M, D, and V, stand for lateral, medial, dorsal, and ventral, respectively. **Red**, axons; **Black**, dendritic segments. (**A**) ITCd cells contributed axon collaterals to one or more of the following sites: CeL (**A1-4**), the amygdalostriatal transition area (ASt; **A2,4**), or to ITCv cells (**A2,3**). ITCv cells contributed axon collaterals to CeM (**B1,2,4**) and/or to the large ITCmain cluster (**B1,3,4**).

Synaptic responsiveness and spontaneous activity of ITC cells in vivo

Since the goal of the in vivo experiments was to determine whether ITC neurons could be distinguished from other types of amygdala neurons on the basis of their extracellularly recorded activity, we first describe the behavior of cells in the amygdala nuclei adjacent to ITC cells: BL and Ce. We will then compare the activity of these cells to that of ITC neurons. Below, Figure 3.4 summarizes the responsiveness of BL, Ce, and ITC neurons to brainstem and IL stimuli. Representative examples of unit responses to the same stimuli are provided in Figures 3.5 and 3.8.

Following histological reconstructions of 29 electrode tracks (Figure 3.4A), we determined that a total of 71 and 158 spontaneously active and/or anti- or orthodromically responsive neurons were recorded in BL and Ce, respectively.

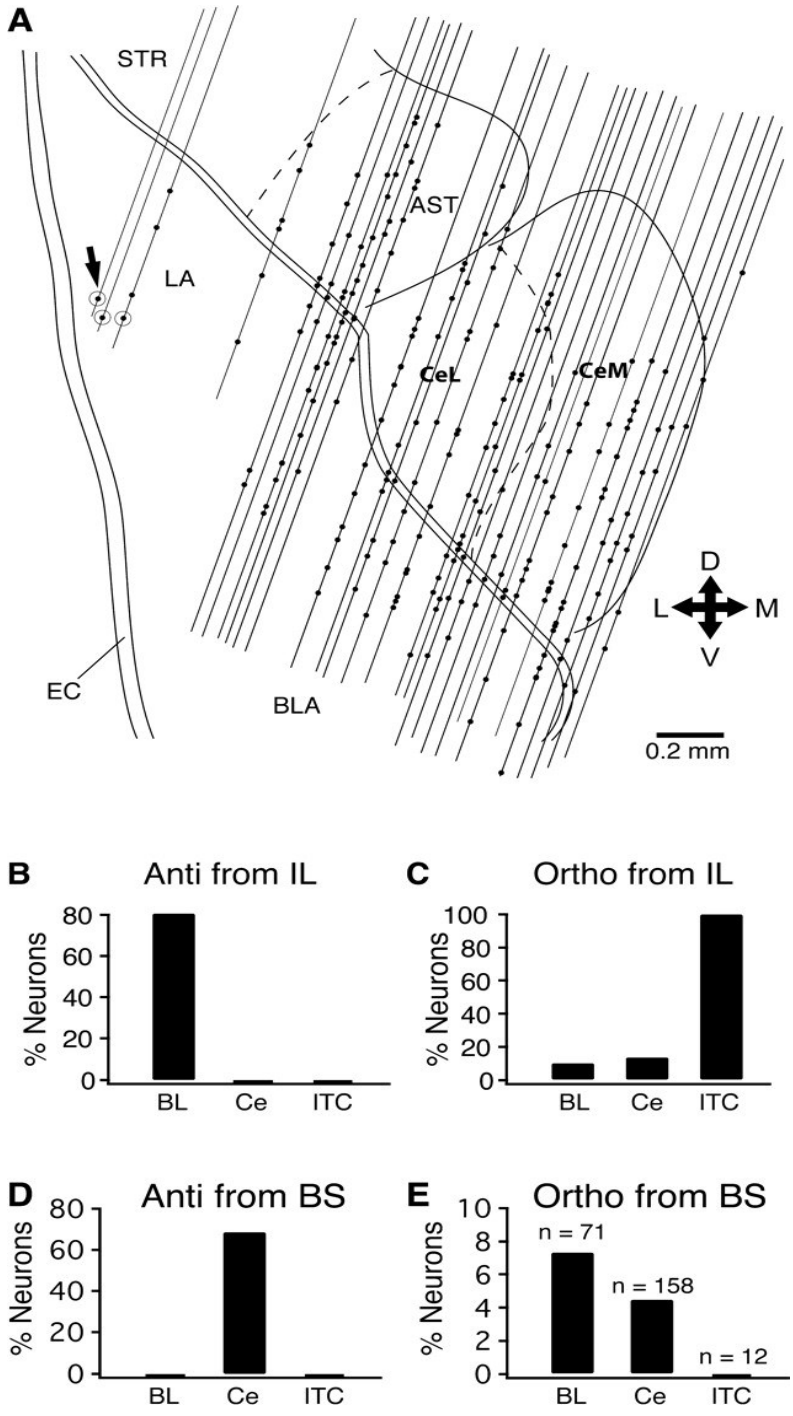

Figure 3.4 Contrasting responsiveness of BL, Ce, and ITC cells to electrical stimuli delivered in the infralimbic (IL) cortex and brainstem (BS). Single-unit recordings of amygdala neurons were obtained with high-impedance micropipettes in urethane-anesthetized rats. (**A**) Scheme showing 29 electrode tracks with dots indicating the position of recorded cells. In all cases, an amygdala neuron was juxtacellularly labeled

with neurobiotin, and its position used to infer the location of all recorded cells. In three of these tracks (arrow and circles), the labeled cells were located in LA. In the remaining tracks, we attempted to label cells near the Ce-BL border. The 19 cases where the recovered cells were within ≤ 0.2 mm of the Ce-BL border are depicted in Figure 3.7B. (**B-D**) Proportion of responsive BL, Ce, and ITC cells to electrical stimuli delivered in IL (**B**,**C**) or brainstem (**D**,**E**). Antidromic responses in **B** and **D**. Orthodromic responses in **C** and **E**.

BL neurons

It should be noted that a minority of the cells described in this section were recorded in the lateral nucleus (LA, n = 17). For simplicity, we pooled these LA neurons with BL cells because their spontaneous activity and responsiveness did not differ appreciably from that seen in BL cells. Consistent with earlier studies (Jacobs and McGinty, 1971; Paré and Gaudreau, 1996; Rosenkranz and Grace, 1999; Likhtik et al., 2006), BL cells generally exhibited low spontaneous discharge rates with as many as 69% of them firing ≤ 0.1 Hz (or 49 of 71). Among the BL cells with significant background activity (31% or 22 of 71), some neurons firing at rates as high as 7 Hz.

To determine whether this variability was related to the identity of the cells, we compared the firing rates of BL neurons that could be physiologically-identified as projection cells by antidromic invasion from IL vs. those of the unidentified units, a proportion of which likely corresponds to interneurons. Indeed, a minority of BL cells are local-circuit neurons (McDonald, 1992), many of which are intrinsically more excitable than projection cells (Sah et al., 2003; Pape and Pare, 2010). In keeping with this, firing rates were significantly higher in the sub-group of unidentified cells (2.86 ± 0.59 Hz, n = 14) than in projection neurons (0.23 ± 0.07 Hz, n = 57, t-test, p = 0.0011).

Consistent with previous reports (Likhtik et al., 2005), IL stimuli elicited antidromic responses in a high proportion of BL cells (80% or 57 of 71; latency of 14.9 ± 0.7 ms; Figure 3.4B; Figure 3.5A). A much lower proportion of BL cells were orthodromically activated by IL stimuli (10% or 7 of 71, Figure 3.4C). In most of these orthodromically responsive BL cells (4 of 7), IL stimuli elicited single spikes (Figure 3.5B1). See Figure 3.5C for an exception to this general rule. Here, it should be noted that when we stimulated IL, it is likely that current diffused from the stimulation site and activated neuronal processes in neighboring cortical fields (such as the prelimbic area) or coursing through or close to IL en route to other cortical regions. This effect could have artificially increased the proportion of antidromically responsive BL cells.

No BL neurons were antidromically responsive to brainstem stimuli (Figure 3.4D**)**. However, a few BL cells were orthodromically activated by brainstem stimuli (7% of cells or 5 of 71; latency, 5.8 ± 0.5 ms; Figure 3.4E, Figure 3.5E).

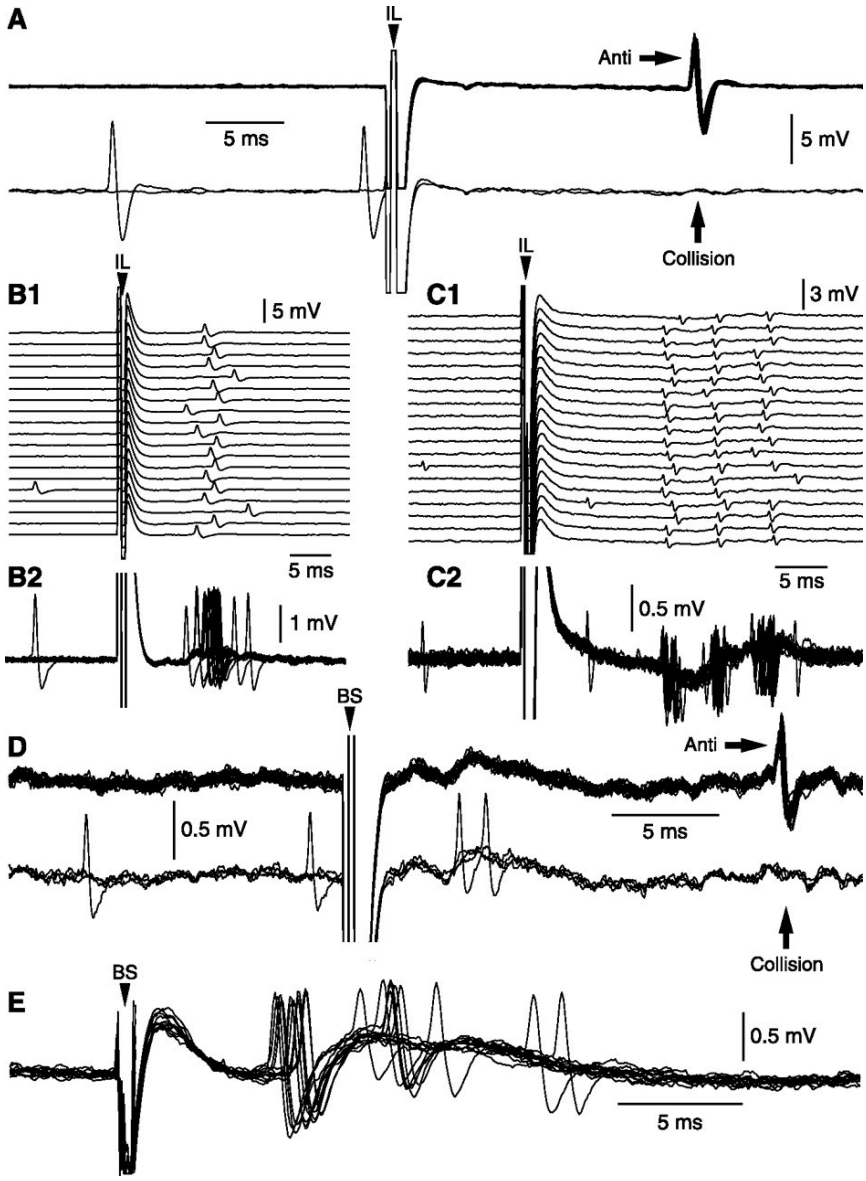

Figure 3.5 Examples of unit responses elicited by electrical stimuli delivered in IL (**A-C**) or brainstem (**D,E**). (**A**) In a high proportion of BL neurons (but never in Ce cells), IL stimulation elicited antidromic response characterized by fixed latency (top) and collision with spontaneous action potentials (bottom). In a few BL cells, IL stimulation evoked orthodromic responses consisting of single spikes (**B**) or, very rarely, spike bursts (**C**). The latter response pattern was only seen in three LA cells (their position is marked by an **arrow** in Figure 3.4A). (**D**) In a high proportion of Ce neurons (but never in BL cells), BS stimuli elicited antidromic responses characterized by a fixed latency (top) and collision with spontaneous action potentials (bottom). (**E**) BS stimuli elicited orthodromic responses in a few rare LA cells.

Ce neurons

As was seen in BL, the spontaneous firing rates of Ce neurons were extremely low, with the majority of cells (77 % or 122 of 158) firing ≤ 0.1 Hz. In response to brainstem stimuli, a high proportion of Ce cells generated antidromic spikes (67% or 106 of 158, latency, 19.2 ± 1.2 ms; Figure 3.4D, 3.5D) and a minority, orthodromic responses (Figure 3.4E; 4% or 7 of 158, latency of 9.9 ± 0.7 ms). As in BL, Ce projection neurons (identified as such by antidromic invasion from brainstem) fired at significantly lower rates than the unidentified cells (projection cells, 0.07 ± 0.04 Hz, n = 106; unidentified, 2.10 ± 0.65 Hz, n = 52; t-test, p = 0.007). In contrast to BL however, no Ce neurons were backfired from IL (Figure 3.4B**)** although a few unidentified cells (15% or 24 out of 158; Figure 3.4C) displayed long-latency (18.4 ± 1.2 ms) orthodromic responses that always consisted of single spikes. Finally, it should be mentioned that IL stimulation produced a dramatic reduction in the firing rate of all the spontaneously active Ce projection cells we encountered Figure 3.6, as previously reported (Quirk et al., 2003).

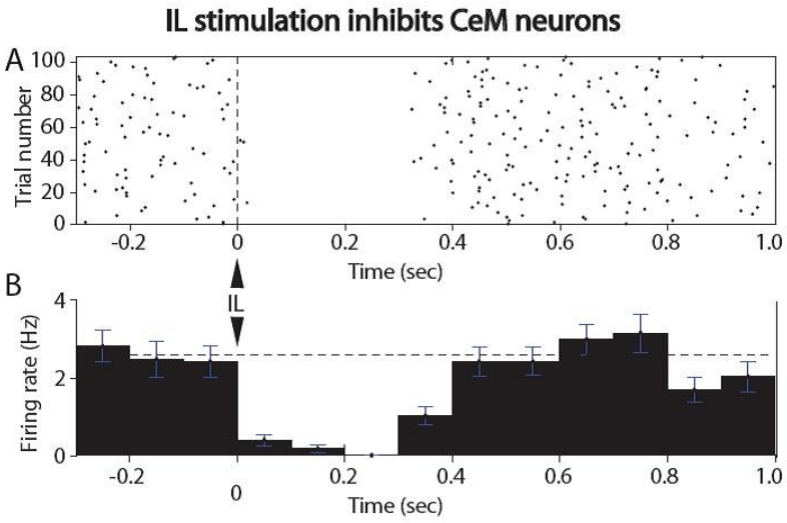

Figure 3.6 In spontaneously active CeM neurons that could be backfired from the BS, IL stimuli elicit a marked inhibition of baseline activity. (**A**) Raster plot with trial number on the Y-axis and time on the X-axis for a representative cell. (**B**) Peri-stimulus histogram of unit activity (100 ms bins; average ± s.e.m. of 4 cells). Dashed line indicates average pre-stimulus firing rate.

ITC cells

Because of the small size of ITC cell clusters, post-hoc histological reconstructions of electrode tracks marked with electrolytic lesions do not provide sufficient resolution to determine whether a given recorded cell is indeed an ITC cell. To circumvent this difficulty, the following approach was used. Micropipettes containing 1.5% neurobiotin were aimed to Ce and gradually lowered, applying brainstem and IL stimuli at regular intervals along the electrode track. Because Ce and BL neurons have differential projections to the brainstem and IL, at some point during most tracks, we observed an abrupt transition in the stimulation sites effective in backfiring recorded neurons (from brainstem to IL stimuli; Figure 3.7A). The region located between the last Ce cell antidromically responsive to brainstem stimuli and the first BL cell backfired from IL therefore corresponded to

the Ce-BL border where ITC cells are known to be located. Thus, the electrode was then retracted to the position of the last antidromically responsive Ce cell and moved 20-40 µm laterally or medially, while still in the brain. After a 20 min delay, the pipette was moved ventrally again and the first juxtacellularly-recorded neuron that was spontaneously active and/or orthodromically responsive was labeled with neurobiotin. In other cases, the pattern of antidromic responsiveness only allowed estimation of the ventral border of Ce or dorsal border of BL. In such cases, the pipette was again retracted to the estimated position of the BL-Ce border and we then used the same approach as described above.

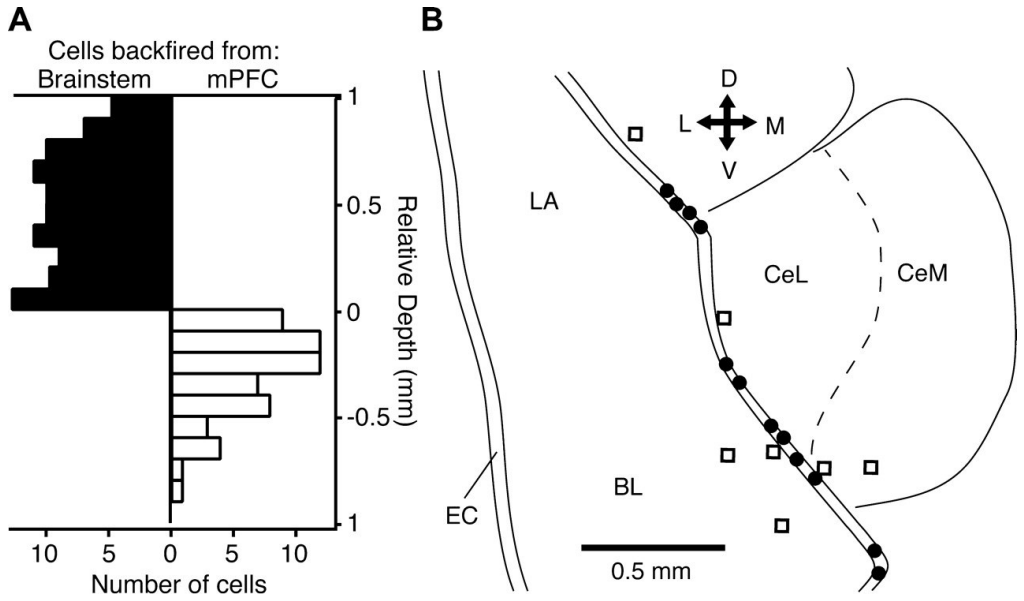

Figure 3.7 The position of the BLA-Ce border can be identified based on the contrasting pattern of antidromic responsiveness of Ce and BLA neurons to brainstem and IL stimuli, respectively. (**A**) Number of cells backfired from the brainstem (black bars) or IL (white bars) (x-axis) plotted as a function of depth (y-axis) relative to the BLA-Ce border in 29 microelectrode tracks. (**B**) Position of 19 neurons juxtacellularly labeled with neurobiotin in, or at proximity of (≤ 0.2 mm), the BLA-Ce border as identified during the experiment using physiological criteria. Filled circles represent positively identified ITC cells (n=12) whereas empty squares represent Ce or BLA neurons.

The position of the Ce-BL border could be estimated based on the pattern of antidromic responsiveness of Ce and/or BL neurons in 47 out of 150 rats. In 26 out of these 47 rats, a neurobiotin-labeled cell was successfully recovered. Of these, 19 were located immediately adjacent to (n=7, Figure 3.7B, empty squares) or within ITC cell clusters (n =12, Figure 3.7B, filled circles). Except for notable variations in spontaneous firing rates (range 0 to 1.8 Hz, 0.36 ± 0.17 Hz), ITC cells exhibited remarkably stereotyped features, some of which unambiguously distinguished them from BL and Ce neurons. Indeed, none of these ITC cells could be backfired from IL (Figure 3.4B) or brainstem (Figure 3.4D) and all were orthodromically responsive to IL stimuli (Figure 3.4C). In all ITC cells where we tested the impact of ipsi- and contralateral IL stimuli (n = 2), orthodromic discharges could be evoked from both hemispheres.

Figure 3.8A contrasts the properties of IL-evoked orthodromic responses in morphologically-identified ITC cells vs. BL and Ce neurons. In most ITC cells (75% or 9 of 12), IL shocks evoked high-frequency orthodromic spike bursts. The proportion of cells generating two or more orthodromic spikes in response to IL stimulation was significantly higher in ITC cells than BL (4%) or Ce (0%) neurons (Fisher exact probability test, $p < 0.0001$; Figure 3.8A1). Here, it should be mentioned that these response patterns were obtained with IL stimuli of 1 mA (0.1 ms). However, we routinely tested higher stimulation intensities (up to 1.5 mA) and could never make BL or Ce neurons change their response pattern from single spikes to spike bursts. Moreover, for those cells generating more than one spike in response to IL stimuli, the number of spikes per bursts was significantly

higher in ITC cells (t-test, p = 0.03; Figure 3.8A2). Last, the peak instantaneous firing frequency during IL-evoked spikes bursts was significantly higher in ITC cells (t-test p = 0.00013; Figure 3.8A3). However, there were no significant differences between the latency of IL-evoked responses between ITC and BL neurons (Figure 3.8A4).

Figure 3.8B-D depicts three examples of morphologically-identified ITC cells (panels 1), their responses to IL stimulation (panels 2), and their morphological properties (Figure 3.8E). As seen in the in vitro experiments, the shape of their dendritic trees generally matched the shape of the clusters where their somata were located with ITC cells located in ITCd clusters having radial and multipolar dendritic trees (Figure 3.8B1) whereas those located in ITCv clusters had flattened and usually bipolar dendritic arborizations (Figure 3.8C1). These cells also had spiny dendrites (insets in Figure 3.8E1,E2). Their axonal projections were also consistent with those seen in the in vitro experiments (Figure 3.8E3,4). The incidence of IL-evoked bursting was similar in ITCd (Figure 3.8B2) and ITCv cells (Figure 3.8C2, D2). The latency of IL-evoked responses typically ranged between 10 and 14 ms (Figure 3.8B2, D2). The case illustrated in Figure 3.8C2 was exceptional in this respect.

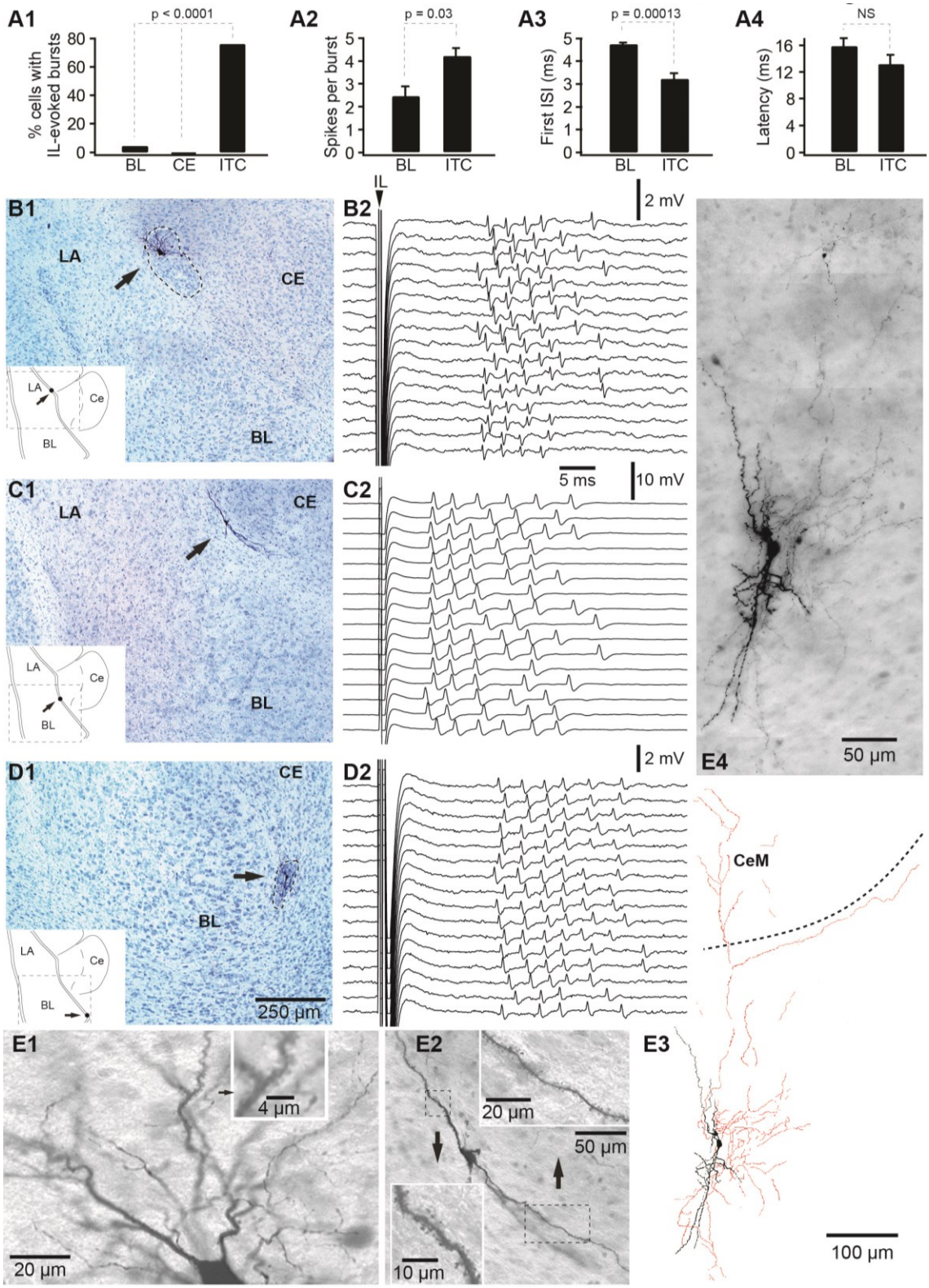
A1
p < 0.0001
% cells with IL-evoked bursts
BL
CE
ITC
A2
p = 0.03
Spikes per burst
BL
ITC
A3
p = 0.00013
First ISI (ms)
BL
ITC
A4
NS
Latency (ms)
BL
ITC
B1
LA
CE
BL
Ce
B2
IL
2 mV
5 ms
C1
LA
CE
BL
Ce
C2
10 mV
2 mV
D1
CE
BL
LA
Ce
250 µm
D2
E4
50 µm
CeM
E1
4 µm
20 µm
E2
20 µm
50 µm
10 µm
E3
100 µm

Figure 3.8 ITC cells can be identified during extracellular recordings on the basis of their unusual IL responsiveness. Using the contrasting pattern of antidromic responsiveness of Ce and BL neurons to BS and IL stimuli, the location of the Ce-BL border was identified. Then, juxtacellular recordings of border cells were obtained. After examining their responsiveness to IL and BS stimuli, the cells were labeled with neurobiotin. The bar graphs in **A** compare the proportion of morphologically- and/or histologically-identified ITC, Ce, and BL neurons responding to IL stimuli with high-frequency spike bursts (**A1**), the number of spikes in these bursts (**A2**), the first inter-spike interval (ISI) duration in these bursts (**A3**), and their latency (**A4**). Panels **B-D** show examples of morphologically-identified ITC cells (**1**) and their responses to IL stimuli (**2**). Higher power micrographs of the cells shown in panels **B-D** are provided in panels **E1,2,4**. A drawing of the cell in **D1**, and **E4** is shown in **E3**.

Can ITC neurons be distinguished from BL and CE cells using spike shapes, firing patterns, or rates?

The above suggests that a majority of ITC cells can be unambiguously distinguished from BL and Ce neurons on the basis of their responsiveness to IL stimuli. However, routinely testing the infralimbic responsiveness of amygdala cells in behaving animals constitutes a significant technical complication. Thus, it would be useful if ITC cells could be distinguished from other types of amygdala neurons using other, more easily accessible measures such as spike shape or firing patterns. To test this possibility, we therefore compared ITC to BL and Ce neurons along all available extracellularly recorded parameters.

Unfortunately, as shown in Figure 3.9, ITC cells proved indistinguishable from other amygdala neurons using these more accessible properties. For instance, whether we considered the overall duration (Figure 3.9A) or rising slope (Figure 3.9B) of action potentials, distributions in the three nuclei overlapped extensively. Similarly, firing rate (Figure 3.9C) and interspike interval (ISI) distributions could not be used to distinguish BL, Ce, and ITC cells. The latter

variable proved especially indiscriminating because a vast majority of cells at the three sites exhibited extremely sparse spike trains (Figure 3.9D) that consisted of isolated single spikes (generally < 2% of ISIs below 100 ms).

Last, we also tried to distinguish ITC, Ce, and BL cells by taking into account the entire spike shape using principal component analysis. Whether we considered all Ce and BL cells, or restricted out attention to identified projection cells at these two sites, ITC cells could not be discriminated from Ce and BL neurons with this method either.

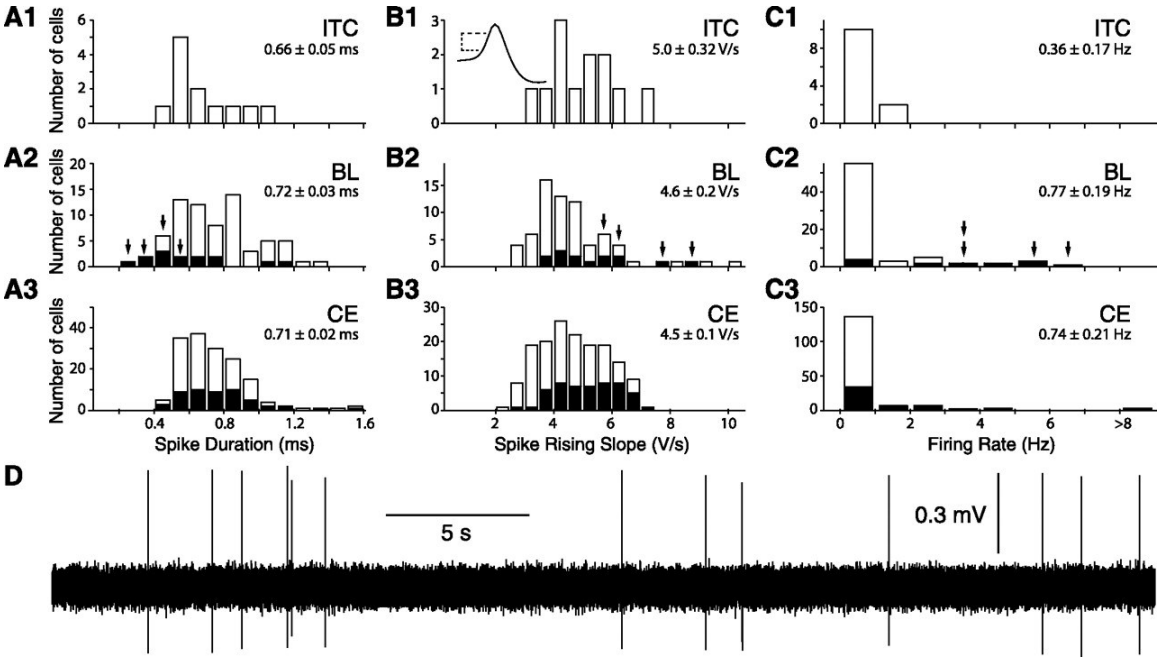

Figure 3.9 Overlapping distributions of action potential properties and firing rates in ITC, BL, and Ce neurons. All graphs are frequency distributions but for three different variables: (**A**) spike duration; (**B**) rising slope of action potentials (inferred from intervals between 25 to 75% of peak amplitude; absolute values, normalized for amplitude); (**C**) firing rates. Panels **1-3** show data obtained in ITC (n = 12), BL (n = 71), and Ce (n = 158) neurons, respectively. In **A-C**, identified projection cells of BL and Ce are represented by empty bars whereas filled bars are used for the cells that could not be backfired. The four **arrows** in A2,B2,C2 indicate four morphologically-identified aspiny neurons. These

presumed local-circuit cells had shorter spikes with faster rise times and relatively high firing rates compared to the rest of the population. **Inset** in B1 shows how the spike rising slope was measured. Various methods were used to estimate action potential durations (as in Likhtik et al., 2006) but all failed to reveal differences between cells in the three nuclei. **D**, Spontaneous activity of a representative ITC cell. ITC firing rates were very low. The firing rate of this cell was around 0.3 Hz.

3.3 Discussion

ITC amygdala neurons are thought to play a critical role in the extinction of conditioned fear. However, several factors hinder progress in studying ITC contributions to extinction. First, although extinction is usually studied in rats and mice, most ITC investigations were performed in guinea pigs or cats. Thus, it is unclear whether their connectivity is similar across species. Second, we lack criteria to identify ITC cells on the basis of their discharge pattern. As a result, key predictions of ITC extinction models remain untested. Among these, ITC cells were predicted to be strongly excited by infralimbic inputs, explaining why infralimbic inhibition interferes with extinction.

To study the connectivity of ITC cells, we labeled them with neurobiotin during patch-recordings in slices of the rat amygdala. This revealed that ITC cells project topographically to the central nucleus and to other ITC clusters located more ventrally.

To study the infralimbic responsiveness of ITC cells, we performed juxtacellular recording and labeling of amygdala cells with neurobiotin in anesthetized rats. All ITC cells were orthodromically responsive to infralimbic

stimuli and their responses usually consisted of high-frequency (~350 Hz) trains of 4-6 spikes, a response pattern never seen in neighboring amygdala nuclei.

Overall, our results suggest that the connectivity of ITC cells is conserved across species and that ITC cells are strongly responsive to infralimbic stimuli, as predicted by extinction models.

CHAPTER 4

SUPRESSION OF AMYGDALA SIGNALING DURING FORAGING IN A HAZARDOUS ENVIROMENT

4.1 Introduction

Survival requires reconciling opposite behavioral tendencies. For example, rodents have evolved defensive behavioral strategies that minimize the likelihood of encounters with predators (e.g. staying in small and dark spaces) and maximize the chance of survival if they encounter a predator (e.g. freezing). However, in order to attain food, these defensive behavioral tendencies must be suppressed or overcome.

Consistent with prior studies implicating the amygdala in the control defensive behaviors (Blanchard and Blanchard, 1972; LeDoux, 2000), Choi and Kim (2010) obtained evidence that the amygdala regulates risk-taking in a semi-naturalistic foraging task. In this task, rats had to leave a safe nest-like area to retrieve food pellets positioned at various distances from a robot predator. The mechanical predator-like figure was programmed to surge forward when rats got closer to obtain the food. Intra-amygdala infusions of drugs that presumably

reduced (muscimol) or enhanced (picrotoxin) the firing rates of amygdala neurons respectively led to increases or decreases in risk-taking (Choi and Kim, 2010).

While these findings indicate that the amygdala regulates risky foraging decisions, how it does so is unclear. Are amygdala neurons suddenly inhibited when rats initiate foraging? Or do they continue to signal threat? The latter possibility implies a form of quantitative competition between neuronal systems that signal threat vs. drive food seeking. The former implies a qualitative system-level shift in the balance of activity between competing neuronal systems. To address this question, we recorded neurons in the basolateral nucleus of the amygdala (BL) neurons with multishank silicon probes in rats engaged in the foraging task.

4.2 Results

After recovery from electrode implantation surgery, six rats were gradually introduced to the foraging task. This task took place in an arena divided into two compartments by a door: a small dimly-lit nest and a much longer and brighter foraging arena (Figure 4.1A). After habituation to the nest (Figure 4.1A, left), rats were allowed to retrieve sweetened food pellets in the foraging arena in the absence of the Robogator (Figure 4.1A, middle). During this phase, on each of 60 trials, a food pellet was placed at various distances from the nest, beginning with 25 cm and increasing in steps of 25 cm after three successful trials, up to 150 cm. Once the rats retrieved the food at 150 cm, the distances were varied

randomly. Rats did not eat the food pellets in the foraging arena. Rather, they seized the pellet with their mouth and returned to the nest to consume it, at which point the doorway was shut. The next trial started ≥ 1 min later. On Day 4, another set of 100-120 trials was conducted with blocks of trials carried out in the presence of the Robogator (n = 10-20; Figure 4.1A, right) alternating with trial blocks in its absence (n = 10-15). This was repeated on Day 5. The Robogator was programmed to surge forward ~80 cm when approached by the rat. Examples of failed and successful trials are illustrated in Figure 4.1B and C, respectively.

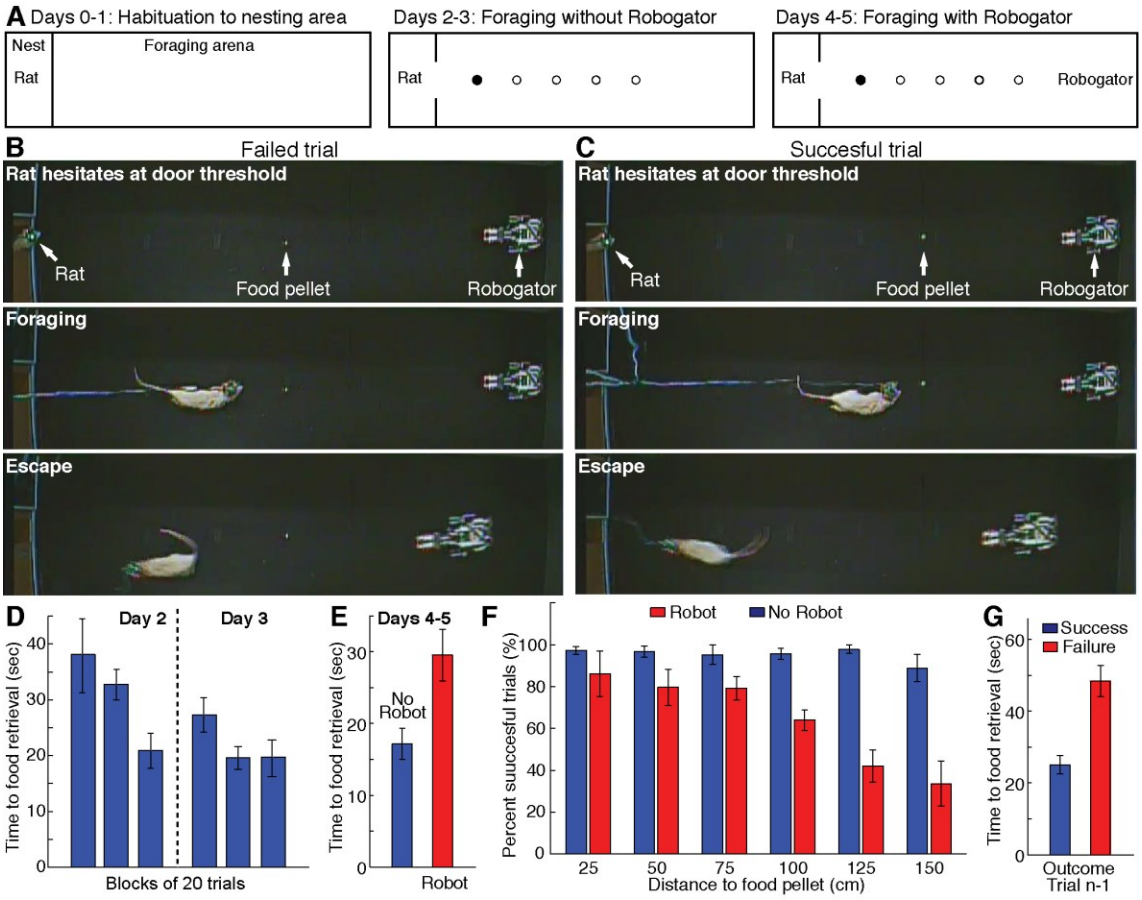

Figure 4.1 Experimental paradigm, apparatus, and behavioral results. (**A**) Apparatus. The behavioral apparatus consisted of a small dimly lit nesting area and a longer and brighter foraging arena. After 2 days of habituation to the nest (left), rats learned to retrieve food pellets in the foraging arena (middle) over a period of two days. One the fourth and fifth day, a mechanical predator (Robogator) was introduced (right). (**B**) Examples of trials with Robogator (left, failure; right, success). (**D-G**) Behavioral results. (**D**) Time from door opening to food retrieval (y-axis) in successive blocks of twenty trials on Days 2 and 3. Rapid and persistent reduction in time to food retrieval. (**E**) Time to food retrieval on alternating trial blocks with (red) or without (blue) the Robogator. Time to food retrieval is higher with Robogator present. (**F**) Proportion of successful trials (y-axis) as a function of distance to food pellet (x-axis) in trials with (red) or without (blue) Robogator. Lower proportion of successful trials in the presence of the Robogator, particularly for long distances. (**G**) Time to food retrieval (y-axis) is lower when the prior Robogator trial (trial n-1) was a success (blue) than a failure (red).

Behavior in the foraging task

We first provide a qualitative description of the rats' behavior in the foraging task and then quantify the impact of experience on their performance. In the early stages of training, shortly after door opening, rats approached the door threshold and stayed there for a time (hereafter termed "Waiting"). They then ventured into the foraging arena to retrieve the food pellet ("Foraging"). After obtaining the food, they abruptly turned around and ran back to the nest ("Escape") to consume it.

In the absence of the Robogator (Days 2-3), all rats quickly learned to retrieve the food pellets. A reliable index of progress on this task was the interval between door opening and retrieval of the food pellet (Figure 4.1D). Whereas it took rats nearly 40 sec during the first twenty-trial block (38 ± 7 s on average), the average duration of the retrieval interval eventually dropped to about 20 sec by the third trial block and remained low the next day (Figure 4.1D; 20 ± 4 sec

during the last trial block; ANOVA, $F = 10.6$, $P < 0.0001$; Tukey-Kramer, $p \leq 0.002$).

Introduction of the Robogator (Day 4) altered the rats' behavior in many ways. First, upon door opening and approach of the door threshold, rats often retreated back to the nest instead of initiating foraging (9.4 ± 2.1% of trials), a phenomenon rarely seen in the absence of Robogator (1.5 ± 0.5%, paired t-test, $p = 0.027$). Second, on those Robogator trials where rats initiated foraging, the duration of the food retrieval interval increased (Figure 4.1E; paired t-test, $p = 0.015$). Third, the proportion of successful trials was generally lower in the presence of the Robogator, particularly when the distance between the nest and food pellet was high (Figure 4.1F; Two-way ANOVA, Robogator vs. no Robogator, $F = 45$, $p < 0.0001$. Tukey-Kramer, $p \leq 0.0001$; Distance $F = 3.35$, $p = 0.007$) and there was a significant interaction between the two ($F = 4.73$, $p = 0.0006$). Last, performance on a given Robogator trial varied markedly depending on whether the prior trial had been successful or not (Figure 4.1G). Trials following successful ones (blue) were associated with significantly shorter times to food retrieval (Figure 4.1G, blue) than trials that followed failed attempts (Figure 4.1G, red; paired t-test, $p = 0.017$). Figure 4.2 contrasts the behavior of a representative rat on individual trials carried out in the absence (blue) and presence (red) of Robogator.

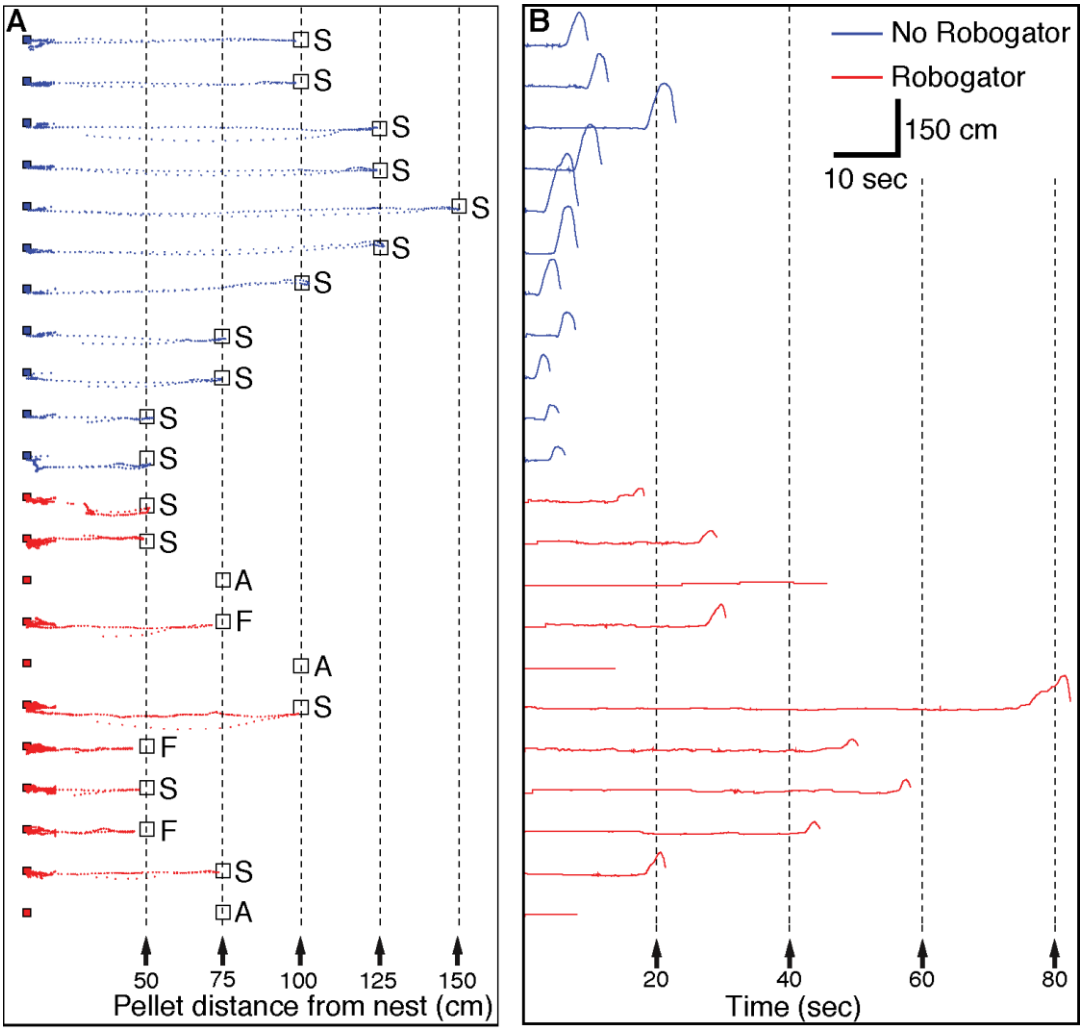

Figure 4.2 Behavior of a representative rat on individual trials carried out in the absence (blue) and presence (red) of Robogator. (**A**) The rat's position is marked by small dots. The distance between the dots is proportional to the rat's speed. From the nest (small colored squares), the rat moves toward the food pellets (empty squares on the right). In the absence of Robogator (top, blue), the rat succeeded (S) in retrieving the food pellet in all depicted trials. In the presence of Robogator, rats sometimes failed to initiate foraging (A for Abort), initiated foraging but failed to retrieve the food pellet (F), or succeeded. (**B**) Position (y-axis) as a function of time (x-axis) for the same trials as in a.

Activity of BLA neurons during the foraging task

We recorded a total of 705 BLA neurons during the foraging task with 233 cells recorded on Days 2-3 (in the absence of Robogator) and 472 cells on Days 4-5, when trial blocks with or without Robogator occurred. A representative example of 7 clusters obtained from one recording session is illustrated in Figure 4.3. All these clusters were extracted from a single representative shank.

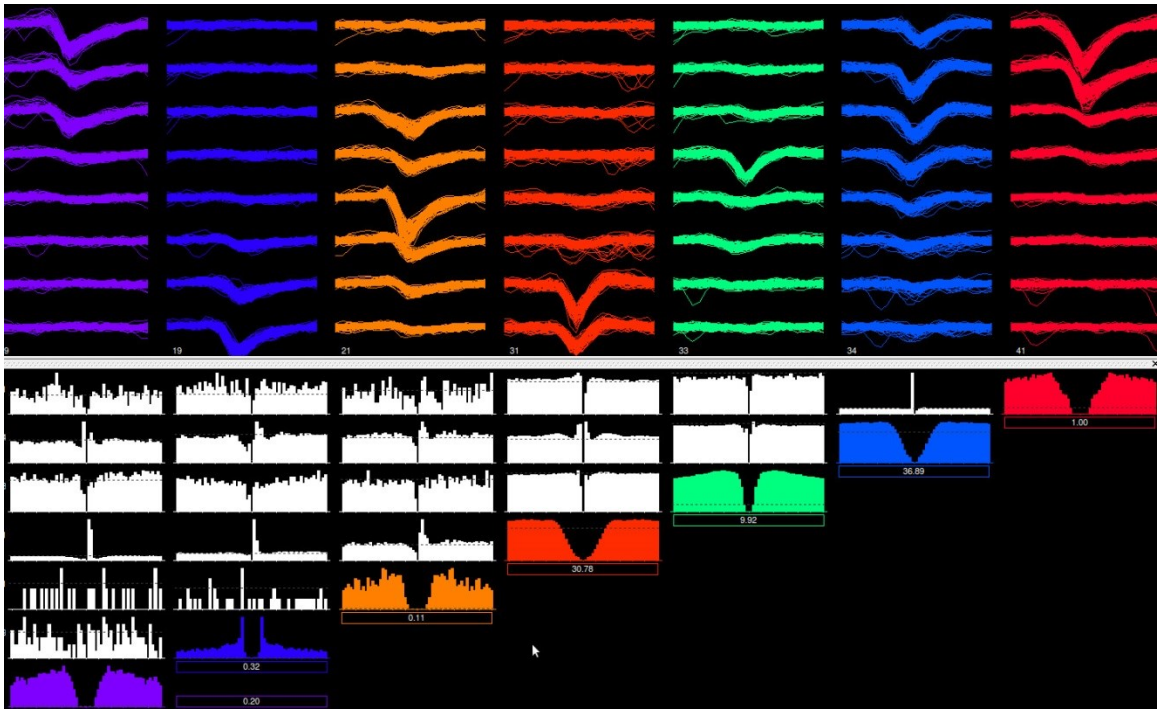

Figure 4.3 Representative examples clustering. After high-pass filtering, the data was thresholded to extract spikes. We then ran PCA on the spikes and the first three components were clustered using KlustaKwik. Spike clusters were then refined manually using Klusters. Top: seven clusters (from left to right). The eight group of traces arranged vertically show superimposed activity at the eight recording sites when the particular cell fired. The reliability of cluster separation was verified by inspecting autocorrelograms (colored histograms at botton) and crosscorrelograms (white histograms).

Consistent with earlier extracellular recording studies (Likhtik et al., 2006; Sosulina et al., 2006), BLA cells were classified as presumed projection cells (PNs; 88% or 618 cells; Figure 4.4A, blue) or interneurons (ITNs; 10 % or 71 cells, Figure 4.4A, red) on the basis of their firing rates in the nest (cutoff 6 Hz) and spike duration (spike through to peak of 0.6 ms). Some cells (2%) could not be classified (Figure 4.4A, gray) and are not considered further. Support for this classification was found in (1) the differential distribution of neurons antidromically responsive to electrical stimuli delivered in the medial prefrontal cortex (mPFC; Figure 4.4B) or nucleus accumbens (nAc): 19.5% of tested PNs (n = 287; Figure 4.4A, empty circles) compared to none of the presumed ITNs (n = 44; Fisher exact test, $p < 0.0007$).

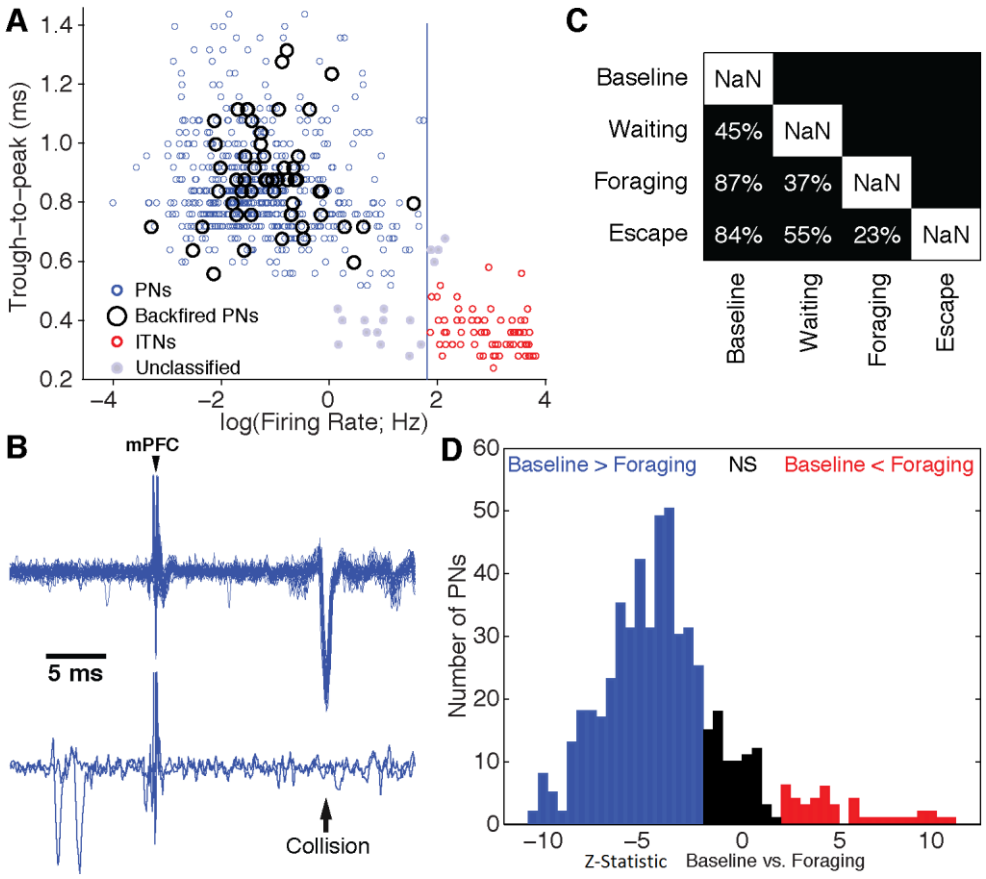

Figure 4.4 Criteria used for classification of BLA cells. (**A**) Spike duration (y-axis), here defined as interval between through to peak, as a function of firing rate (x-axis) among all recorded BLA cells. Neurons were classified as PNs (blue) when they had a long spike duration (≥ 0.55 ms) and low firing rate (≤ 6 Hz) and as ITNs (red) when they generated spikes shorter than 0.6 ms and fired at high rates (> 6 Hz). Supporting this classification, all neurons that were formally identified as PNs by antidromic invasion from a BLA projection field (empty black circles) overlapped with the blue clusters and none of them fell in the red cluster. (**B**) Example of PN backfired from mPFC (top, 25 superimposed responses; bottom two trials where the antidromic spike collided with a spontaneously occurring action potential). (**C**) Proportion of PNs that reached significance ($p \leq 0.05$) in post-hoc comparisons. (**D**) Frequency distribution of z-statistic for firing rate differences between baseline and foraging in PNs. Blue indicates cells with significantly higher firing rates during baseline than foraging. Red, indicates cells with significantly lower firing rates during baseline than foraging. Black, cells with non-significant (NS) differences between baseline and foraging.

To assess whether each recorded neuron showed significant task-related variations in activity, we computed a Kruskal-Wallis one-way ANOVA on its firing rate (threshold p of 0.05) during four distinct periods: (1) in the nest with the door closed ("baseline"), (2) during the waiting period at the door threshold ("waiting"), (3) during foraging, and (4) during escape (when rats turned around and ran toward the nest). Whether they were recorded in the absence or presence of Robogator, most BLA cells showed significant task-related activity. Moreover, as described below, their behavior in these two conditions was similar. Therefore, we first describe the activity of BLA cells in the foraging task irrespective of trial type and then carry out within-cell comparisons of activity in Robogator vs. no-Robogator trials.

Projection Cells

Overall, 89% of PNs cells showed significant firing rate variations in the foraging task. Figure 4.4C shows the proportion of cells with significant firing rate comparisons (Tukey-Kramer, threshold P of 0.05) between the various phases of the foraging task. The proportion was highest for firing rate differences between baseline and foraging (87%) or escape (84%), with the two being highly correlated ($r = 0.57$, $P < 0.0001$). Other comparisons yielded a markedly lower incidence of significant differences (23-55%). Since changes in firing rate from baseline to foraging were most sensitive in detecting significant task-related activity, we computed the distribution of z-statistic for this variable. As shown in Figure 4.4D, most PNs exhibited a significant decrease in firing rate from baseline to foraging (blue, 70% or 430 cells) and a minority showed the opposite (red, 7% or 42 cells). Hereafter, we will refer to these two groups of cells as Type 1 and Type 2 cells, respectively. Figures 4.5 and 4.6 show individual examples of these cells whereas Figure 4.7 shows their average behavior.

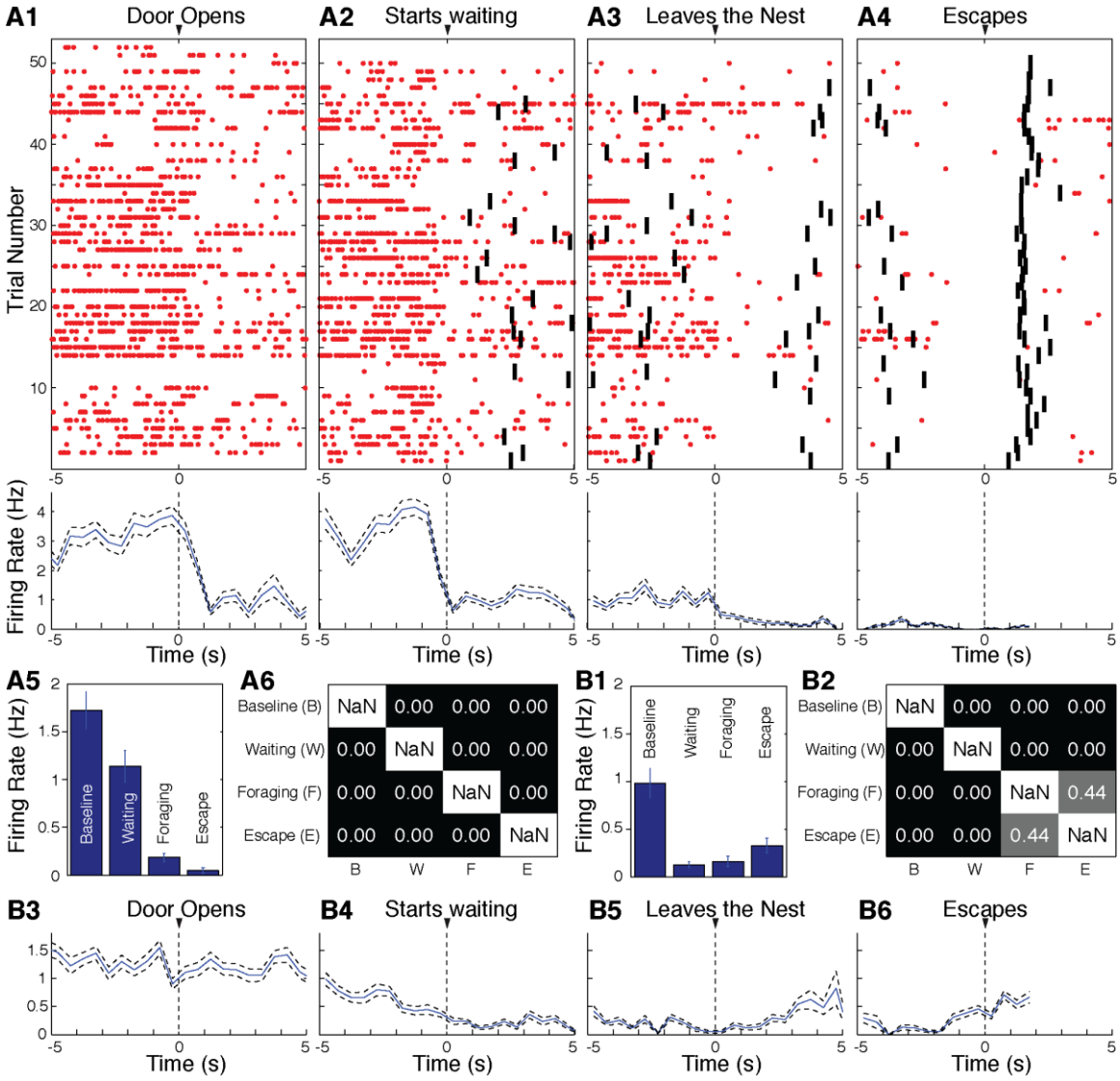

Figure 4.5 Examples of Type 1 PNs. (**A1-4**, top) Rasters showing spikes (red dots) generated within a ± 5 s window around salient task events: door opening (**A1**), onset of waiting (**A2**), onset of foraging (**A3**) and escape (**A4**). Y-axis indicates trials. Only successful trials are shown. Black bars indicate, for each trial, when the preceding and following task events occurred. (**A1-4**, bottom). Average firing rate (± SEM) for same trials as depicted in rasters above (0.5 s bins). (**A5**) Average firing rate (± SEM) during the various phases of the foraging task for same cell. (**A6**) Significance level for post-hoc comparisons of firing rates between the phases indicated (all p's marked 0.00 were <0.01). (**B1-2**) As in A5-6 but for different PN. (**B3-6**) As in A1-4, but for PN shown B1-2.

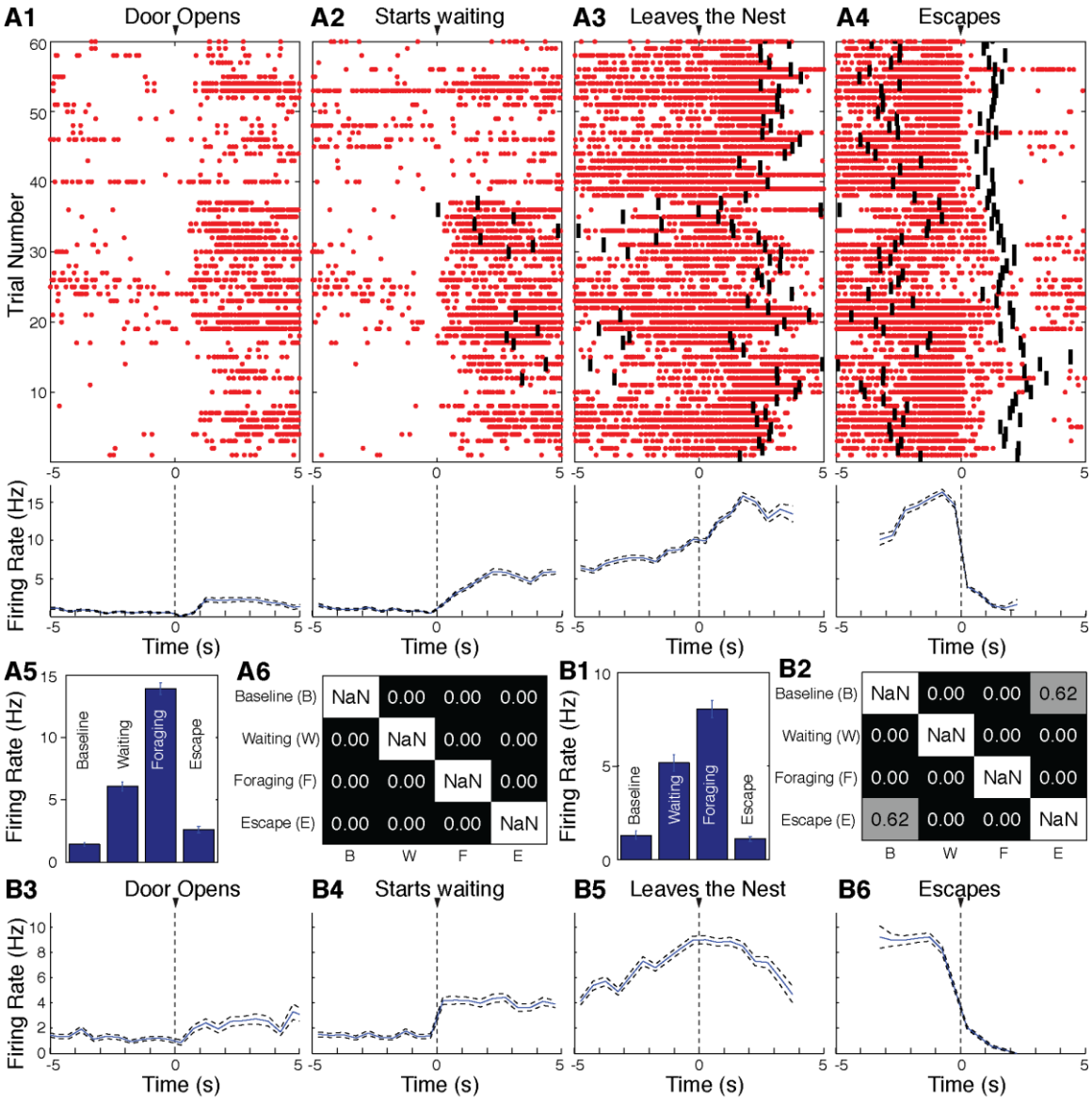

Figure 4.6 Examples of Type 2 PNs. (**A1-4**, top) Rasters showing spikes (red dots) generated within a ± 5 s window around salient task events: door opening (**A1**), onset of waiting (**A2**), onset of foraging (**A3**) and escape (**A4**). Y-axis indicates trials. Only successful trials are shown. Black bars indicate, for each trial, when the preceding and following task events occurred. (**A1-4**, bottom) Average firing rate (± SEM) for same trials as depicted in rasters above (0.5 s bins). (**A5**) Average firing rate (± SEM) during the various phases of the foraging task for same cell. (**A6**) Significance level for post-hoc comparisons of firing rates between the phases indicated (all p's marked 0.00 were <0.01). (**B1-2**) As in A5-6, but for different PN. (**B3-6**) As in A1-4, but for PN shown B1-2.

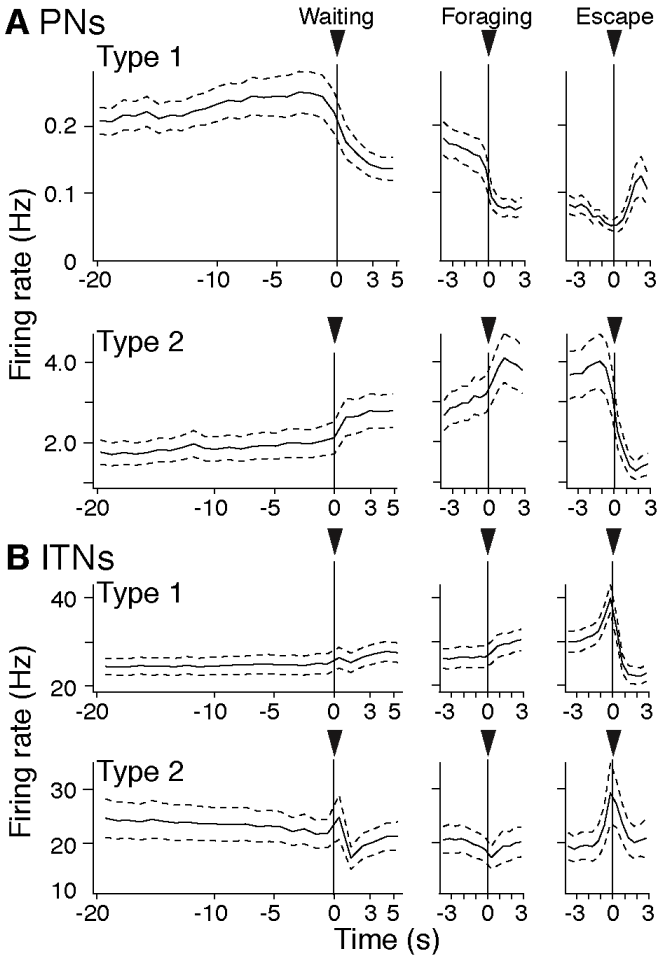

Figure 4.7 Population analyses. All graphs plot the average firing rate (thick lines) ± SEM (thin dashed lines) of different cell types in relation to the main task events (left, waiting at door threshold; middle, foraging initiation; right, escape). (**A**) PNs of Type 1 (top; n = 430) and Type 2 (bottom, n = 42). (**B**) ITNs of Type 1 (top, n = 44) and Type 2 (bottom, n = 14).

The predominant type of PNs (Type I) typically showed a firing rate reduction from baseline to the waiting period, as well as a further decrease upon foraging initiation and after food retrieval (Figures 4.5 and 4.7A, top). There was some heterogeneity among Type I cells, particularly with respect to their baseline

firing rates (0.03 to 3.26 Hz) and the task phase where their firing rates started to decrease (compared Figure 4.5A and 4.5B). Nevertheless, as a group, they exhibited little spontaneous activity during the baseline period (0.22 ± 0.03 Hz) and their firing rates were lowest during escape, when they were virtually silent (0.04 ± 0.01 Hz; Figure 4.7A, top).

By contrast, Type 2 PNs (Figures 4.6 and 4.7A, bottom) exhibited a slight and gradual increase in firing rate from baseline to the waiting period, continuing during foraging, and abruptly reversing to a reduction in firing rate after food retrieval. Last, we observed a heterogeneous group of neurons (Type 3, 13% or 80 cells) that generally lack sustained changes in firing rate during foraging, but instead displayed short-lived alterations in firing rate in relation to one or more of the transitions between different phases of the foraging task, most frequently upon food retrieval.

The incidence of antidromically responsive neurons was similar in the three groups of cells (Chi-Square test, $p = 0.36$; Table 1). Differences in the incidence of neurons responsive to mPFC or nAc stimuli did not reach significance (Chi-Square test, $p = 0.34$; Table 1).

	Tested Cells	Backfired Cells	Backfired from nAc	Backfired from mPFC	Backfired from nAc and mPFC
PNs Type 1	**218**	**48 (22%)**	**21 (10%)**	**22 (10%)**	**5 (2%)**
PNs Type 2	**14**	**2 (14%)**	**0 (0%)**	**2 (14%)**	**0 (0%)**
PNs Type 3	**36**	**4 (11%)**	**2 (6%)**	**1 (3%)**	**1 (3%)**
PN Not Significant	**19**	**2 (11%)**	**0 (0%)**	**2 (11%)**	**0 (0%)**
ITNs	**44**	**0 (0%)**	**0 (0%)**	**0 (0%)**	**0 (0%)**
Unclassified	**5**	**0 (0%)**	**0 (0%)**	**0 (0%)**	**0 (0%)**

Table 1. Incidence of antidromically invaded neurons among different types of BL cells.

Type 1 cells fired at significantly lower baseline rates (0.36 ± 0.02 Hz) than Type 2 (1.67 ± 0.24 Hz) and Type 3 PNs (0.64 ± 0.1 Hz; ANOVA, $F = 78$, $P < 0.0001$; Tukey-Kramer, Type 1 vs. 2, $p \leq 0.0001$; Type 1 vs. 3, $p = 0.0007$).

To shed light on the behavioral significance of the different activity patterns of Type 1 and 2 PNs, we examined how their firing rates varied depending on whether the prior trial was a failure or a success. The reader will

recall that following a failed Robogator trial, rats took longer to retrieve food pellets. This analysis revealed that Type 1 PNs fired at significantly higher rates following failed than successful trials during both the waiting (Figure 4.8A1) and foraging (Figure 4.8A2) phases (Wilcoxon signed-ranks tests: Waiting, $P < 0.0001$; Foraging, $P < 0.0001$). In contrast, no significant firing rate differences were seen in Type 2 cells (Wilcoxon signed-ranks tests: Waiting, $p = 0.09$; Foraging, $p = 0.29$).

Consistent with this, Type 1 PNs fired at significantly higher rates when, after approaching the door threshold, rats retreated back in the nest vs. initiated foraging (Figure 4.8B; Wilcoxon signed-ranks test, $p < 0.0001$). However, in this case, Type 2 cells showed the opposite behavior (Wilcoxon signed-ranks test, $p = 0.0006$). These results suggest that increased firing in Type 2 PNs is associated with approach/seeking of food pellets whereas higher activity levels in Type 1 PNs anticipate aborted foraging.

Last, we compared the firing rate of PNs in trials with vs. without Robogator during the waiting phase at the door threshold (Figure 4.8C1) and during foraging (Figure 4.8C2). Type 1 PNs fired at significantly higher rates during Robogator trials (Wilcoxon signed-ranks tests: Waiting, $p < 0.0001$; Foraging, $p < 0.0001$). In contrast, Type 2 PNs fired at similar rates in the two trial types (Wilcoxon signed-ranks tests: Waiting, $p = 0.6$; Foraging, $p = 0.43$; Table 2).

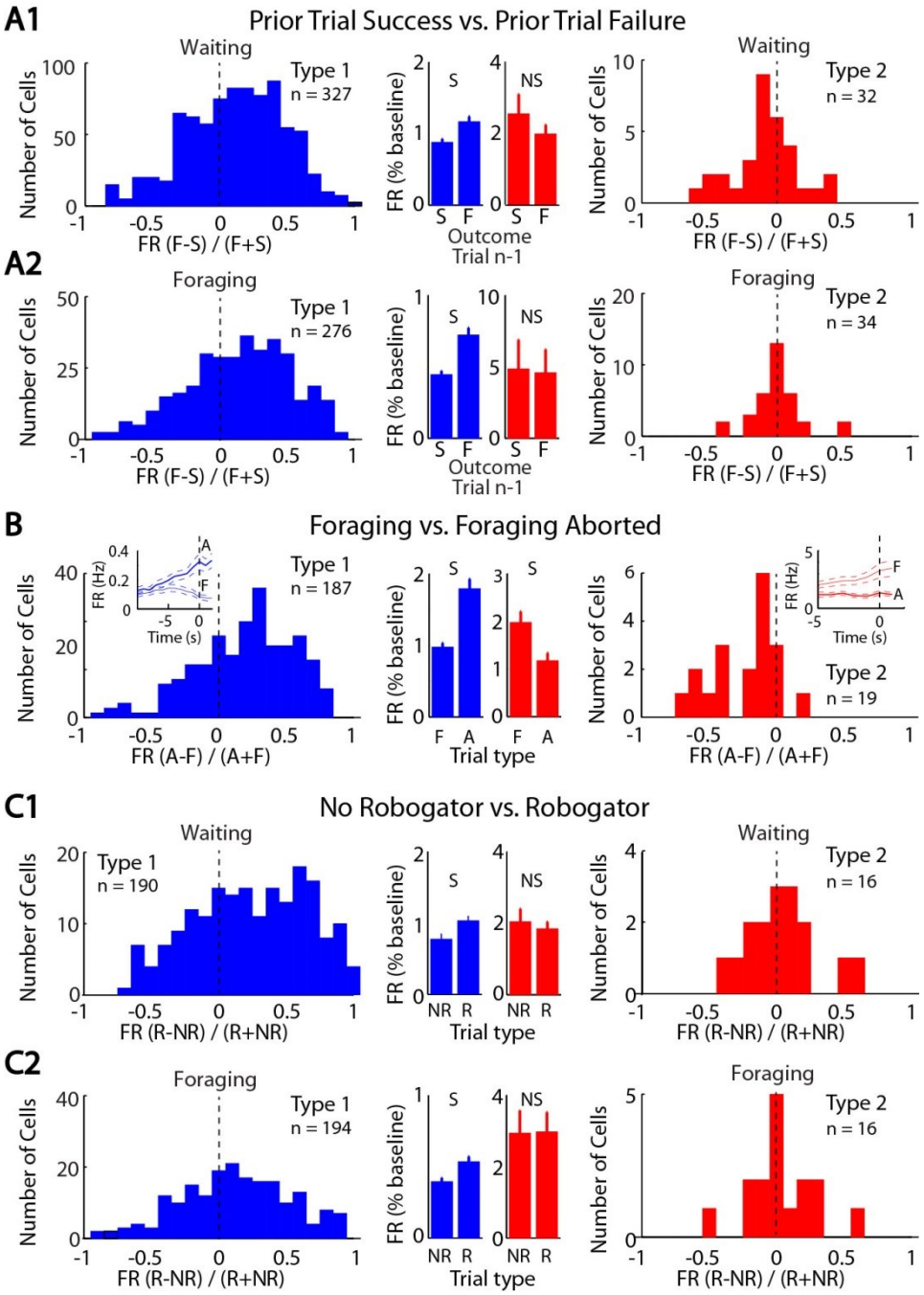

Figure 4.8 Comparison between firing rates of Type 1 and 2 PNs as a function of trial type. (**A-C**) Comparison of firing rates as a function of trial type in Type 1 (blue, left) and Type 2 (red, right). Firing rate comparisons are (**A**) depending on whether the prior Robogator trial was a failure (F) or success (S) during waiting (**A1**) or foraging (**A2**), (**B**) depending on whether waiting at door threshold is followed by retreat back to the nest (A) or foraging (F), (**C**) depending on whether the Robogator was present (R) or not (NR) during waiting (**C1**) and foraging (**C2**). **Insets in B** plot firing rate as a function of time

with respect to foraging (thin line) vs. retreat in the nest (thick line). Other abbreviations, S, significant at 0.05 level; NS, not significant.

	PNs Type1	**PNs Type 2**
Prior Trial Success vs. Failure		
Waiting	**N = 327 p < 0.0001** **ΔFR = 32.9 ± 6.5%**	**N =32 p = 0.09** **ΔFR = -22.8 ± 17.8%**
Foraging	**N = 276 p < 0.0001** **ΔFR = 62.3 ± 9.0%**	**N = 34 p = 0.29** **ΔFR = -5.7 ± 9.9%**
Foraging vs. Aborted Foraging	**N = 187 p < 0.0001** **ΔFR = 83.0 ± 11.6%**	**N = 19 p = 0.0006** **ΔFR = -40.5 ± 13.1%**
No Robogator vs. Robogator		
Waiting	**N = 190 p < 0.0001** **ΔFR = 33.2 ± 9.1%**	**N = 16 p = 0.60** **ΔFR = -9.30 ± 12.3%**
Foraging	**N = 194 p < 0.0001** **ΔFR = 35.4 ± 8.5%**	**N = 16 p = 0.43** **ΔFR = 1.0 ± 9.6%**

Table 2. Comparison between firing rates (FRs) of Type 1 and 2 PNs as a function of trial type (same analyses as in Figure 4.8).

We performed a number of control analyses to verify whether the effects described above were due to inter-dependence between the variables examined. For instance, comparisons of firing rates during the waiting phase on aborted trials vs. foraging were restricted to cases where the prior trial had been successful. Also, to test whether the impact of the Robogator was related to the higher proportion of failed trials or the longer duration of the waiting phase, we repeated the analyses after controlling for prior trial type (only success) or Waiting period duration. As detailed in Table 3, results qualitatively identical to those shown in Figure 4.8 were obtained: all significant differences remained significant.

	PNs Type1	PNs Type 2
Prior Trial Success vs. Failure (control for period duration)		
Waiting	**N = 307 p < 0.0001 ΔFR = 31.6 ± 7.1%**	**N = 32 p = 0.33 ΔFR = -7.0 ± 17.2%**
Foraging	**N = 264 p < 0.0001 ΔFR = 59.8 ± 8.9%**	**N = 34 p = 0.04 ΔFR = -12.2 ± 10.1%**
Foraging vs. Aborted Foraging (restricted to successful prior trial)	**N = 117 p < 0.0001 ΔFR = 136.1 ± 24.8%**	**N = 13 p = 0.01 ΔFR = -26.8 ± 15.9%**
Foraging vs. Aborted Foraging (restricted to failed prior trial)	**N = 145 p < 0.0001 ΔFR = 70.5 ± 18.3%**	**N = 13 p = 0.02 ΔFR = -19.1 ±10.7 %**
No Robogator vs. Robogator (control for period duration and restricted to successful prior trial)		
Waiting	**N = 174 p = 0.03 ΔFR = 20.9 ± 11.7%**	**N = 16 p = 0.95 ΔFR = -0.4 ± 10.6%**
Foraging	**N = 189 p = 0.04 ΔFR = 32.9 ± 8.7%**	**n=16 p=0.5 ΔFR = -0.9 ±10.1%**

Table 3. Comparison between firing rates (FRs) of Type 1 and 2 PNs as a function of trial type. Analyses shown in figure 4.8 were repeated after controlling for duration of the examined period and nature of the prior trial (success or failure). Because not all types of trial restrictions occurred for all cells, the number of cells included in the various analyses vary. Cells were included if at least five trials were available. To control for period duration, the beginning of the longer period was ignored.

Interneurons

Of the 71 presumed ITNs we recorded, 96% showed significant variations in firing rate during the foraging task (assessed as for PNs; Figure 4.9A). Despite this high proportion, these variations were minor, relative to their high baseline firing rates (< 10%), except for when rats approached the food pellet and escaped.

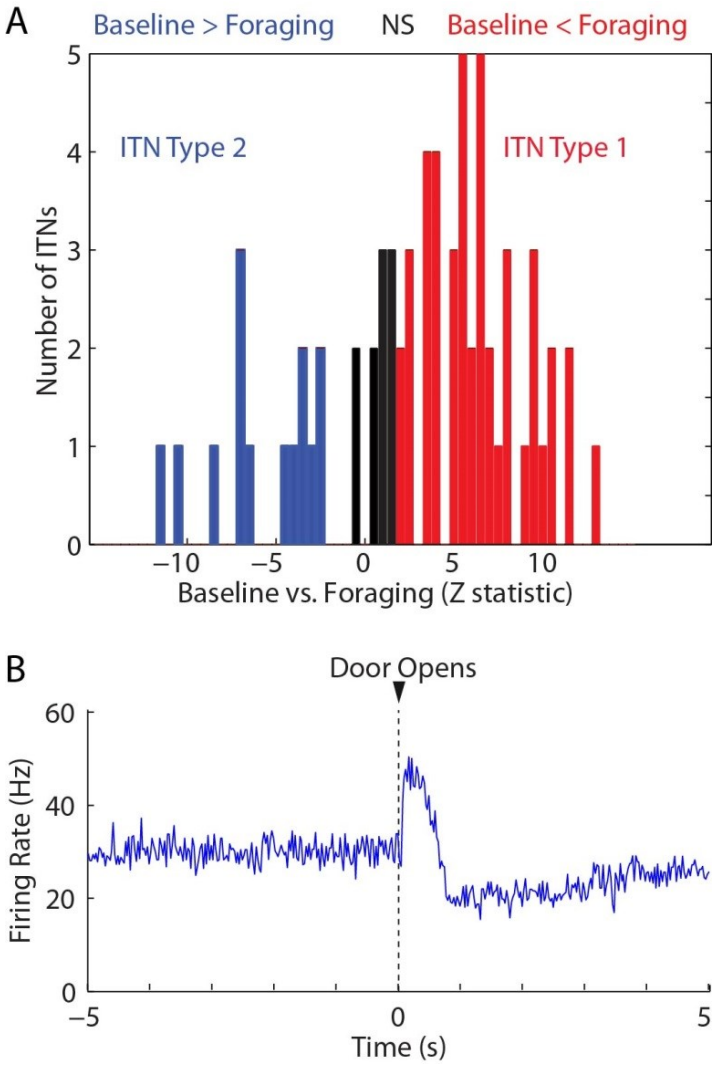

Figure 4.9 Activity of significantly modulated presumed ITNs during the foraging task. (**A**) Frequency distribution of z-statistic for firing rate differences

between baseline and foraging in presumed ITNs. Blue indicates cells with significantly higher firing rates during baseline than foraging. Red, indicates cells with significantly lower firing rates during baseline than foraging. Black, cells with non-significant (NS) differences between baseline and foraging. (**B**) Short-latency increase in firing rate in response to door opening. Peri-event histogram of neuronal discharges (25 ms bins) computed around the time of door opening in a Type-2 ITN.

Figure 4.7B (grouped data) and Figure 4.10 (individual examples) contrast the activity of the two main ITN types we recorded. The majority of ITNs (44; Figure 4.7B, top and 4.10A) displayed a slight increase in firing rate upon approach of the door threshold, a further progressive increase during foraging, followed by a steep increase as they approached the food. Upon escape, their firing rates rapidly returned toward baseline values. In contrast, most of the remaining ITNs (14 cells; Figure 4.7B, bottom and Figure 4.10B) displayed a minor firing rate reduction during waiting and foraging. Their activity in relation to approach of the food and escape was similar to the first ITN class. In addition, 27 and 36% of Type 1 and 2 ITNs (respectively) showed a phasic increase in firing rate when the door opened (Figure 4.9B). This phenomenon accounts for the bump in firing rates seen at time 0 in Figure 4.7B (left graph) and Figure 4.10B3.

In contrast with PNs (Figure 4.8), ITNs displayed little or no differences in activity as a function of trial type. For instance, their firing rates during the waiting period on trials where rats initiated foraging vs. retreated back into the nest did not differ significantly (p's ≥ 0.17). On Robogator vs. no Robogator trials, no difference was detected during the waiting period, only during foraging for the first type of ITNs. But even in this case, the difference, albeit statistically

significant (Wilcoxon signed-ranks test, p = 0.04), was very small (4.1 ± 1.5% lower with Robogator). Similarly, when we compared firing rates on trials following failed vs. successful trials, firing rate differences during the waiting period did not reach significance for the first type of ITN, only the second (9.2 ± 3.1% higher after a failed trial, p = 0.005). They did for the first type of ITNs during foraging, but again the effect was very small (1.3 ± 2.1% lower after failed trials, p = 0.03; see Table 4).

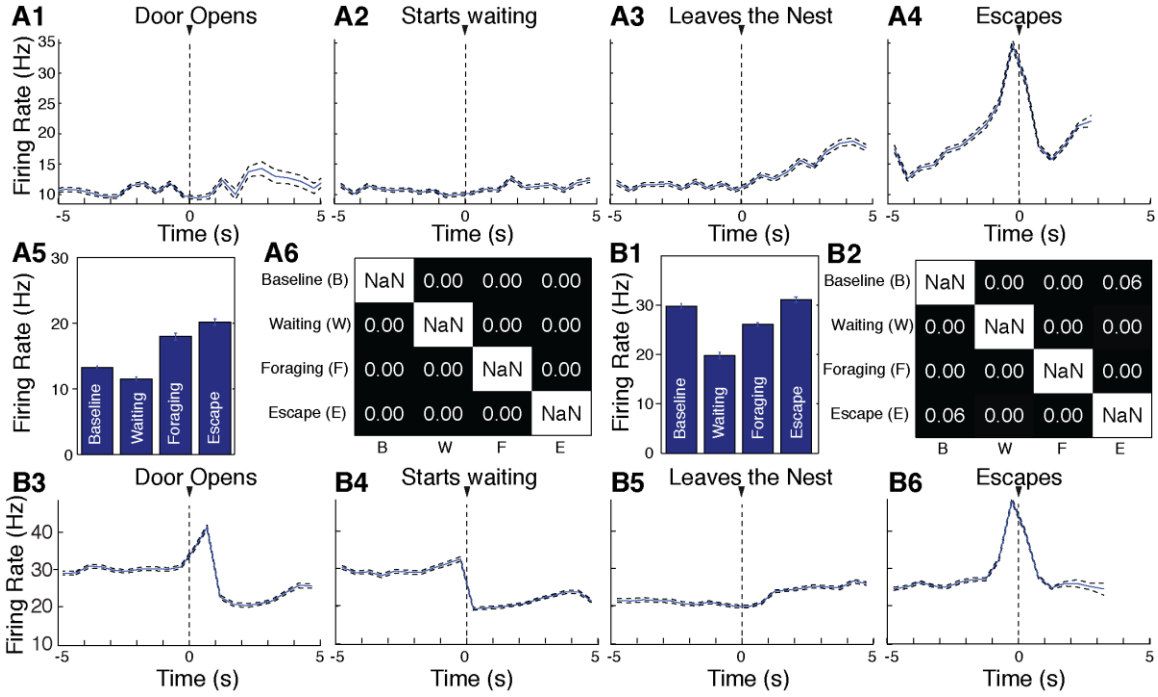

Figure 4.10 Activity of presumed ITNs during the foraging task. Examples of Type 1 (**A**) and 2 (**B**) ITNs. (**A1-4, B3-6**) Average firing rate (± SEM; y-axis) around different events (± 5s) in the foraging task (indicated above each graph) and based on 60 successful trials (0.5 sec bins). (**A5, B1**) Average (± SEM) of firing rate integrated over the entire duration of the various task phases. (**A6**, **B2**) Significance level for post-hoc comparisons of firing rates between the phases indicated (all p's marked 0.00 were <0.01).

	ITN Type 1	ITN Type 2
Prior Trial Success vs. Failure		
Waiting	**N = 31 p = 0.98** **ΔFR = 1.2 ± 1.9%**	**N = 10 p = 0.005** **ΔFR = 9.2 ± 3.1%**
Foraging	**N = 33 p = 0.03** **ΔFR = -1.3 ± 2.1%**	**N = 10 p = 0.16** **ΔFR = 7.11 ± 3.3%**
Foraging vs. Aborted Foraging	**N = 16 p = 0.17** **ΔFR = -1.8 ± 3.3%**	**N = 6 p = 0.22** **ΔFR = 8.5 ± 5.4%**
No Robogator vs. Robogator		
Waiting	**N = 23 p = 0.69** **ΔFR = 1.3 ± 3%**	**N = 9 p = 0.42** **ΔFR= 4.5 ±2.9%**
Foraging	**N = 23 p = 0.04** **ΔFR = -4.1 ± 1.5%**	**N = 9 p = 0.91** **ΔFR = 5.4 ± 4.9%**

Table 4. Comparison between firing rates (FRs) of Type 1 and 2 ITNs as a function of trial type. Same analyses as in Figure 4.8 but for ITNs.

For histological verification of all the silicon probe tracks in all 6 rats see Figure 4.11.

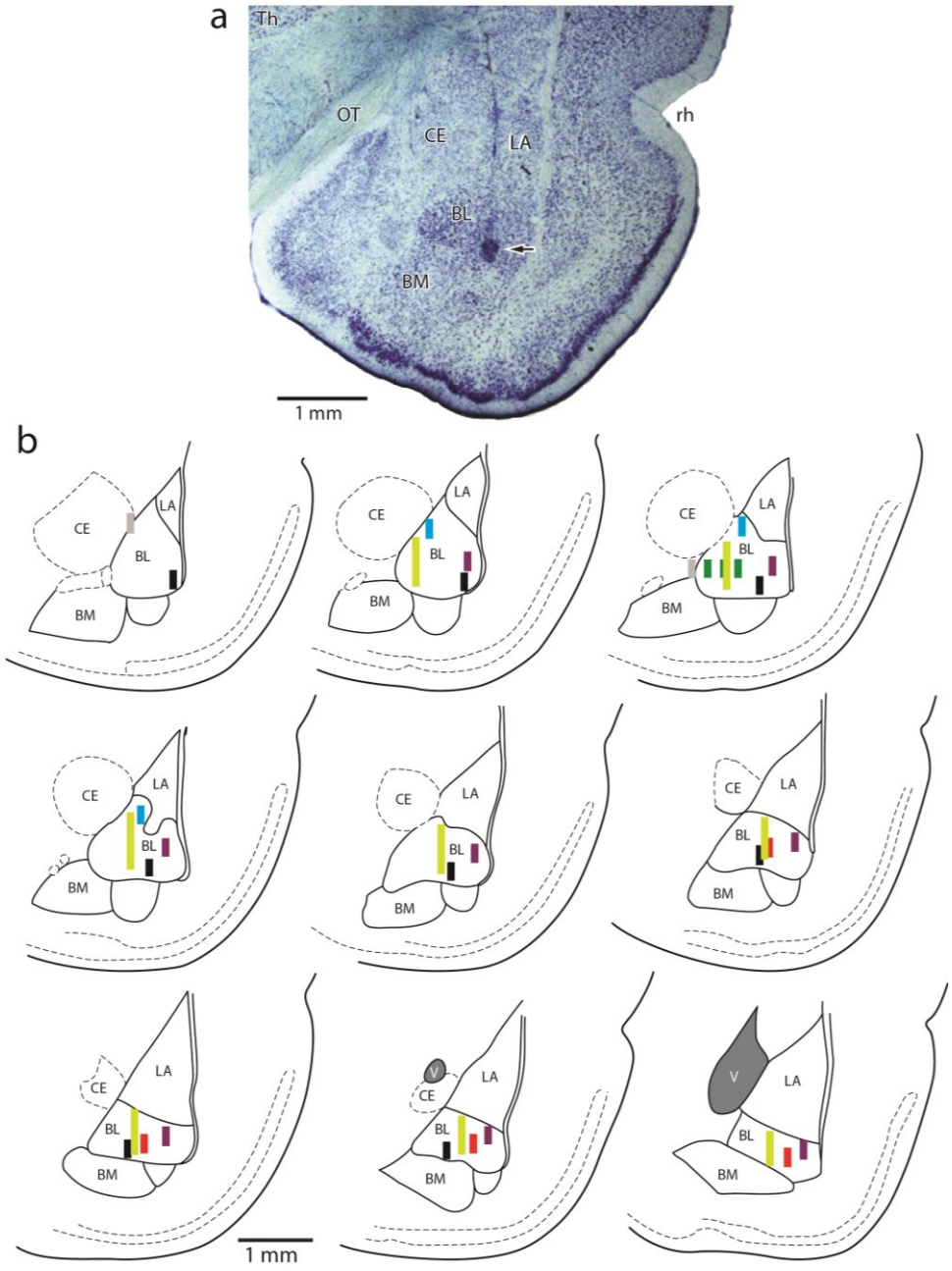

Figure 4.11 Histological verification of recording sites. (**a**) Coronal section of the amygdala showing location of silicon probe in the BL nucleus and electrolytic lesion (arrow) marking the deepest recording site. (**b**) Schemes showing location and trajectory of silicon probes on nine coronal sections arranged from rostral (top left) to caudal (bottom right). Different colors are used for different rats. Gray indicates recording sites we did not consider because they were not inside the BL nucleus. Abbreviations: CE, central nucleus of the amygdala; BM, basomedial nucleus of the amygdala, LA, lateral nucleus of the amygdala; OT, optic tract; Th, thalamus; rh, rhinal sulcus.

4.3 Discussion

In the wild, animals must weigh the need to attain food against the risk of predation. We used a semi-naturalistic foraging task to examine how the basolateral amygdala (BLA) participates in this process. In this task, rats are confronted with a mechanical predator (Robogator) when they leave their nest to obtain food. Because prior studies showed that BLA plays a critical role in fear expression, we expected BLA neurons to increase their firing rate as they approached the Robogator to retrieve food pellets. Instead, the vast majority of projection cells became nearly silent upon initiation of foraging. Yet, they fired at significantly higher rates when rats retrieved food in the presence compared to absence of the Robogator. Moreover, higher levels of activity in these cells were associated with aborted foraging. Together, these results suggest that foraging initiation is associated with a sudden system-level shift whereby signaling by the amygdala is suppressed.

CHAPTER 5

FACTORS UNDERLYING BL ACTIVITY

IN THE FORAGING TASK

5.1 Introduction

In the previous chapter, we recorded BL amygdala neurons in rats trained to leave their nest to retrieve food pellets in an elongated arena where they were confronted with a predator. Two types of principal cells were distinguished. Increased firing rates in the prevalent type (Type-1) anticipated aborted foraging and retreat to the nest. In contrast, augmented activity in Type-2 cells anticipated foraging. Upon initiation of foraging, Type-1 neurons showed a firing rate reduction, and Type-2 cells the opposite.

These findings indicate that BL contains two main types of PNs that exhibit opposite activity profiles in the foraging task. However, the semi-naturalistic character of the foraging task complicates analysis of the factors that drive neuronal activity. Is the presence of the predator, the reward, both, or none required? In other words, what factors determine the activity of BL cells? In addition, the foraging task features uncontrolled behavioral variables such as the rats' movements, particularly their speed. Therefore, to shed light on the impact of these various factors, we compared the activity of BL cells in two additional

tasks that did not include explicit threats (shuttle task, open field task) or rewards (open field task). The shuttle task was conducted on three rats that also performed the foraging task. This allowed us to compare the activity of the same cells in both tasks. In contrast, the open field task was conducted with naïve rats to ensure they would not expect rewards. Because we needed to determine the identity of the cells (Type1 vs. Type2), we first analyzed the spontaneous activity of Type1 and 2 cells in search of features we could use in the open field to infer their identity.

5.2 Results

State-dependent variations in the firing rates of Type-1 and 2 cells

Type-1 and 2 cells exhibited significant differences in firing rates and a dissimilar activity modulation by behavioral states (quiet waking, QW; slow-wave sleep; SWS; Figure 5.1a). In particular, Type-1 cells fired at significantly lower rates than Type-2 cells in QW (Type-1, 0.35±0.02 Hz; Type-2, 1.58±0.26 Hz; unpaired t-test, $P<0.0001$) and SWS (Type-1, 0.52±0.02 Hz; Type-2, 1.47±0.15 Hz; unpaired t-test, $P<0.0001$). Also, whereas the firing rate of Type-1 cells was significantly higher in SWS than QW (220±12% higher, paired t-test, $P<0.0001$), Type-2 cells showed inconsistent activity modulation by behavioral states, resulting in an insignificant average modulation (paired t-test, $P=0.9$). Of note, the likelihood that a particular PN would belong to the Type-1 or Type-2 class varied inversely with firing rate in both QW and SWS (Figure 5.1c). Figure 5.1b shows

the firing rates of 33 Type-1 and 3 Type-2 cells simultaneously recorded during spontaneous alternations between QW and SWS.

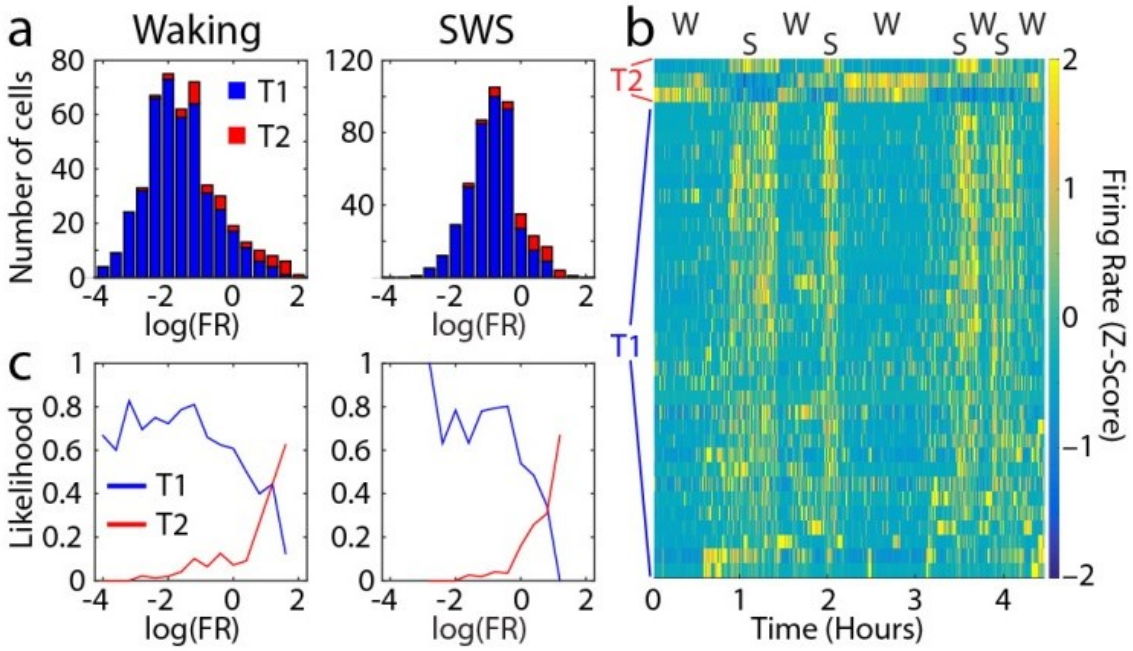

Figure 5.1 Activity variations of Type-1 and 2 PNs during QW, SWS. (**a**) Frequency distribution of firing rates among Type-1 (blue) and 2 (red) PNs in QW (left) and SWS (right). (**b**) Firing rate of 36 simultaneously recorded PNs during spontaneous alternations between QW and SWS. (**c**) The likelihood that a PN belongs to the Type-1 (blue) or 2 (red) classes plotted as a function of firing rate.

Food-seeking shuttle task

In this task (Figure 5.2), rats ran back and forth across a central arena to retrieve food pellets placed in two enclosures (hereafter termed “nests”) located at opposite ends of the central arena. Ambient light levels were uniformly low to minimize perceived threat. Recordings began after two daily 3-h sessions of

habituation to the apparatus. Three of the rats used for the foraging task also performed the shuttle task, allowing us to compare the activity of the same Type-1 (n=186) and Type-2 (n=14) cells in the two tasks.

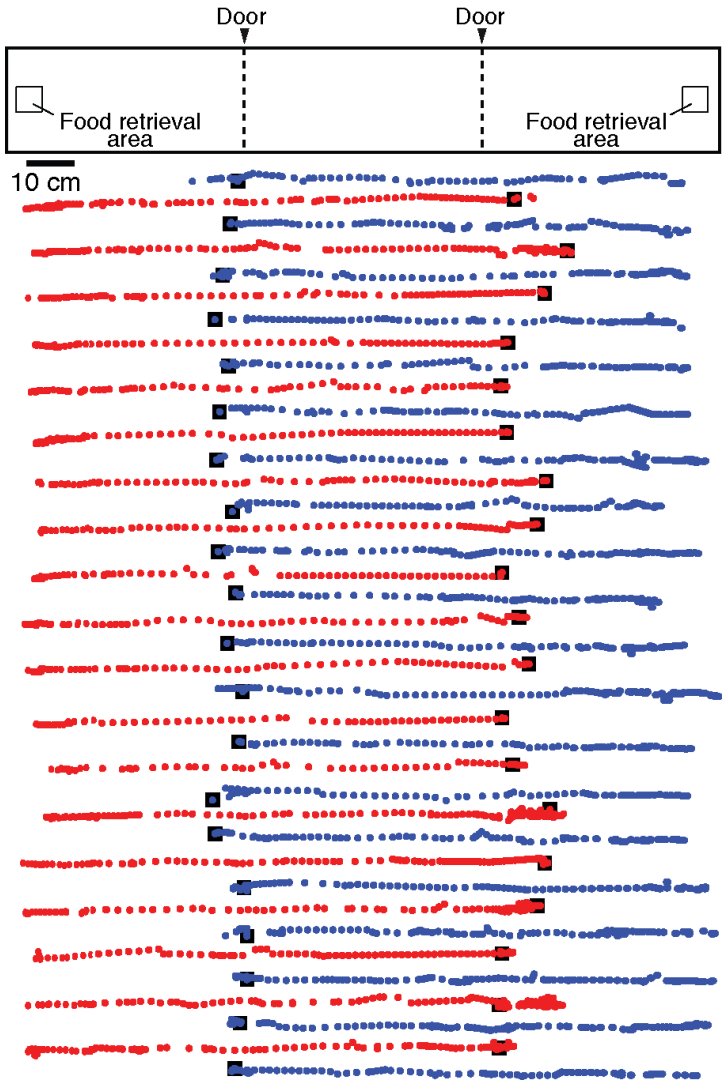

Figure 5.2 Shuttle task. (Top) Apparatus used for the shuttle task. (Bottom) Examples of shuttle trials. The rat's position is marked by dots. The distance between the dots is proportional to the rat's speed. Left to right (red) and right to left (blue) trials.

Behaviorally, the main difference between the two tasks was the absence of signs of apprehension in the shuttle task. Upon door opening, rats immediately entered the central compartment and ran to the other nest to retrieve the food pellet. This is in contrast with the foraging task where the rats waited at the door threshold for 15.9 ± 0.7 s before leaving the nest. Also, in contrast with the foraging task, rats never skipped a trial in the shuttle task. Surprisingly, variations in the activity of Type-1 cells in the foraging and shuttle tasks were nearly identical (Figure 5.3a,b). Although Type-2 cells started shuttle trials at a lower average firing rate than during Robogator trials, they also showed an increase in discharge rate upon door opening.

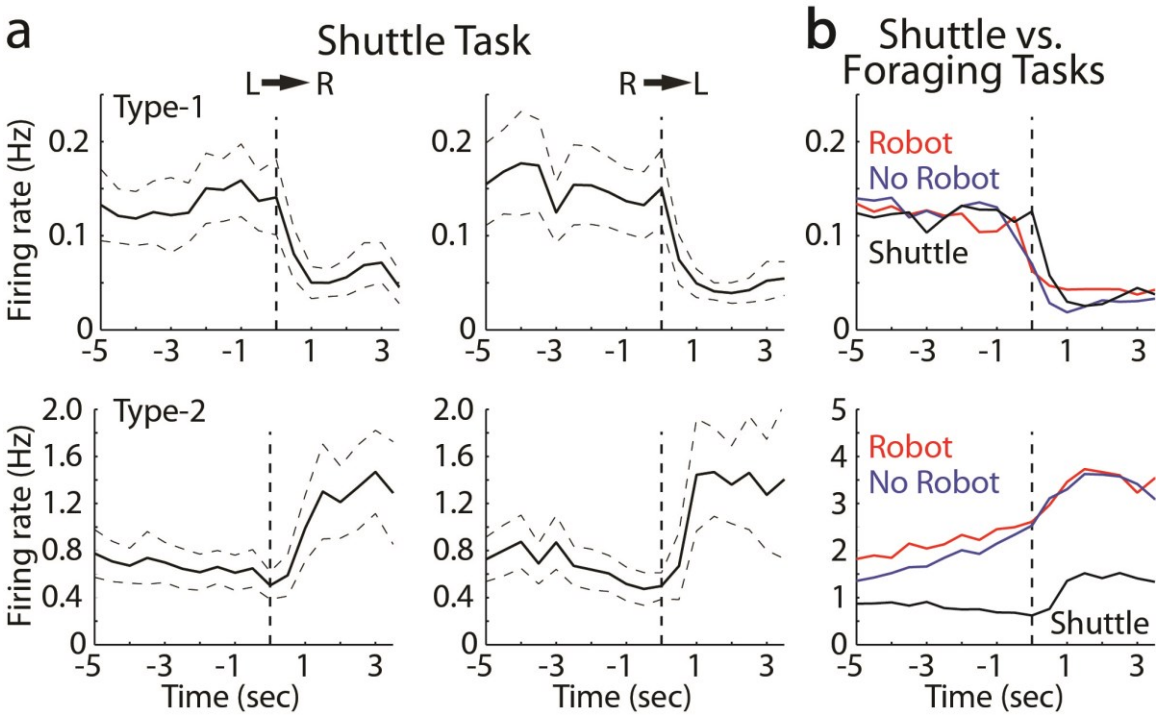

Figure 5.3 Variations in the activity of Type-1 and 2 PNs during the foraging and shuttle tasks. (**a**) Firing rate of Type-1 (top) or 2 (bottom) during shuttle task

(left, left to right trials; right, right to left trials). (**b**) Activity of PNs during the foraging task in the presence or absence of the Robogator and during the shuttle task.

Open field Exploration

Since the above suggests that the inverse activity patterns of Type-1 and 2 cells are not dependent on predator threat, we next considered the influence of rewards by recording BL neurons while rats explored a large open field, devoid of explicit rewards. Again, to minimize threat, this test was performed under low ambient light levels. Also, to ensure that the rats would not expect food in the open field, these tests were conducted in two naïve rats that had no prior experience with the foraging or shuttle tasks and were habituated to the open field for two daily 3-h sessions before the recordings began.

By definition, spontaneous exploration occurs irrespective of external events under investigator control. Thus, we could only relate neuronal activity to the rats' movements and position in the open field. Thus, we first examined whether there was a relationship between firing rates and movement speed. We reasoned that if the inverse activity modulation of Type-1 and 2 cells in the Robogator and shuttle tasks were related to movement as opposed to being driven by rewards, we should observe two subsets of neurons that display decreasing vs. increasing activity with movement speed and different spontaneous firing rates, as seen in the previous tasks. Consistent with this prediction, we found that 67% of PNs (n=355) showed significant variations in firing rates as a function of movement speed (Figure 5.4a, left; 53 and 14%

decreasing and increasing with speed, respectively). Critically, the likelihood that a particular PN would show diminishing (blue, presumed Type-1) vs. augmenting (red, presumed Type-2) activity with increases in movement speed varied inversely with firing rate in QW (Figure 5.4a, right).

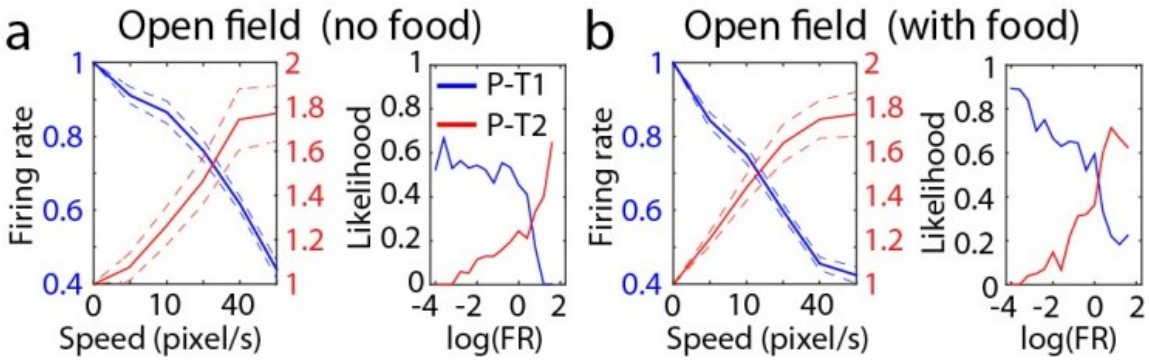

Figure 5.4 Activity variations of presumed Type-1 and 2 PNs during open field task. (**a**) Left: firing rate during open field exploration plotted as a function of movement speed (blue and red: cells with significant negative or positive correlation to speed, respectively). Right: The likelihood that the firing rate of a PN is negatively (blue) or positively (red) correlated with speed plotted as a function of overall QW firing rate. (**b**) Same as **a**, except that the rats were motivated with pellets dropped at random spots.

When, after completion of the above tests, food pellets were dropped at random spots in the open field to motivate movement, an even higher proportion of PNs showed a significant relation to movement speed (Figure 5.4b**;** n=209; 90% with significant modulation; 67 and 23% decreasing and increasing with speed, respectively). However, note that the higher proportion of significant cells is not due to the rewards but to the fact that rats ran more, increasing the statistical power of the tests. Indeed, when we artificially restricted the number of movements analyzed to mimic the spontaneous exploration, the proportion of significant cells was comparable to the above. Last, to ensure that the relation

with movement was not dependent on differences in firing rates as a function of the rats' position in the center vs. periphery of the open field (Likthik et al., 2014), we repeated the above analyses separately for movements starting and ending in these two sectors. Qualitatively identical results were obtained.

Relation between firing rates and movement in the foraging and shuttle tasks

The strong correlation between PN activity and movement velocity in the open field led us to examine whether this relationship also accounted for firing rate variations in the foraging and shuttle tasks. Complicating this analysis however, were the markedly different amounts of times available for analysis in the open field (~20 or 90 minutes) vs. the Robogator (~15 minutes) and shuttle (~3 minutes) tasks, reducing statistical power for the latter two tasks. Nevertheless, there was a strong bias for the firing rate of Type-1 and 2 cells to respectively show a negative and positive relation to movement velocity in the foraging and shuttle tasks (Figure 5.5a).

Although there is a strong correlation between speed and firing rates in all three tasks, it might be objected that PNs, particularly Type-1 cells, display changes in firing rates that anticipate movement by several seconds during the waiting period in the foraging task. In other words, dissociations between PN activity and movement occurred during the waiting period, when rats are immobile. A first dissociation is the differential activity of PNs during the waiting period on trials where rats, after approaching the door, retreated back in the nest vs. initiated foraging. Anticipating movement by several seconds, the firing rates

of Type-1 PNs increased when rats retreated back in the nest rather than initiating foraging; Type-2 cells showed the opposite (Figure 4.8B, insets). Second, on trials where rats initiated foraging, both cell types showed firing rate changes in the absence of movement (Figure 4.7A). This was seen even when we compared trials where rats initiated foraging after a ≥5 s waiting period (Figure 5.5b, blue) vs. those rare trials (≤4%) where rats initiated foraging immediately (Figure 5.5b, red).

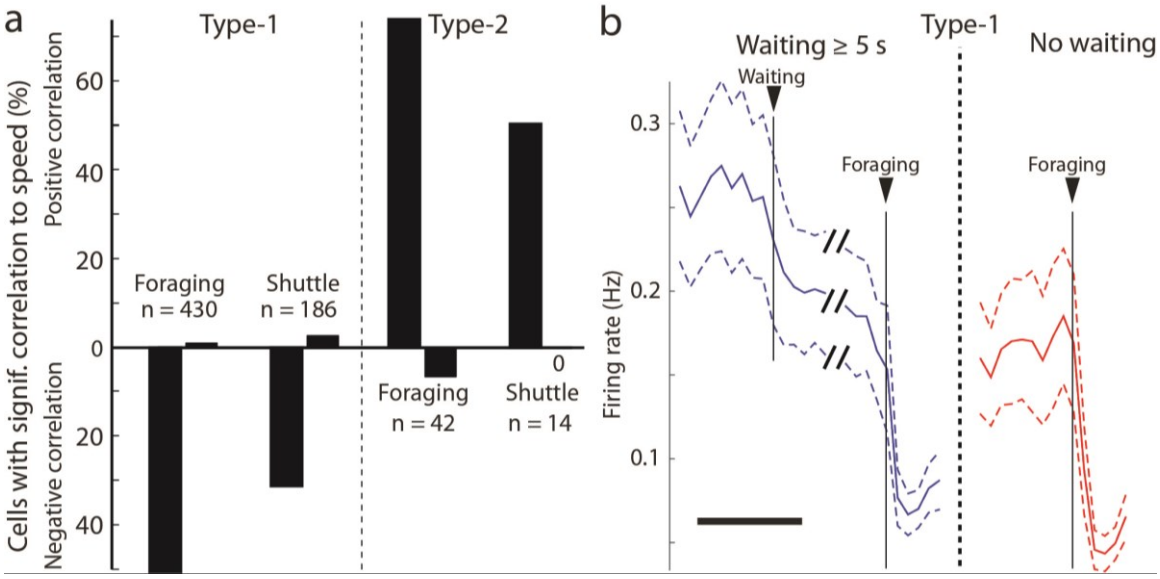

Figure 5.5 Relation between the firing rate of PNs and movement speed in the Robogator and shuttle tasks. (**a**) Proportion of Type-1 (left) and 2 (right) PNs whose firing rate shows a significant negative (bottom) or positive (top) correlation to movement speed. (**b**) Firing rates of Type-1 PNs on Robogator trials with long (≥5 s, blue) or (red) no waiting periods.

Another important consideration is whether Type-1 and 2 cells exhibit the same relation to movement speed irrespective of motion direction and Robogator proximity. To address this, we computed the FR of Type-1 and 2 cells (Figure 5.6a,b) as a function of position (x-axis) and speed (y-axis), with the latter separating forward (toward the food, top) and backward (toward the nest, bottom) movements. In these conditions, the FR of Type-1 cells exhibited a similar negative relation to movement speed irrespective of direction (Figure 5.6a). However, when we excluded the escape phase to separately consider trials where rats hesitated as they approached food (first moving forward, then backward, then forward again), an interesting phenomenon was observed: the FR of Type-1 cells showed decreased activity when the rats approached the food, but increased activity when rats moved backward (Figure 5.6c). In contrast, Type-2 cells showed a positive relation to movement in the forward direction and the opposite upon retreat, irrespective of whether we considered the entire foraging trials (foraging and retreat; Figure 5.6b), or only the foraging phase (Figure 5.6d).

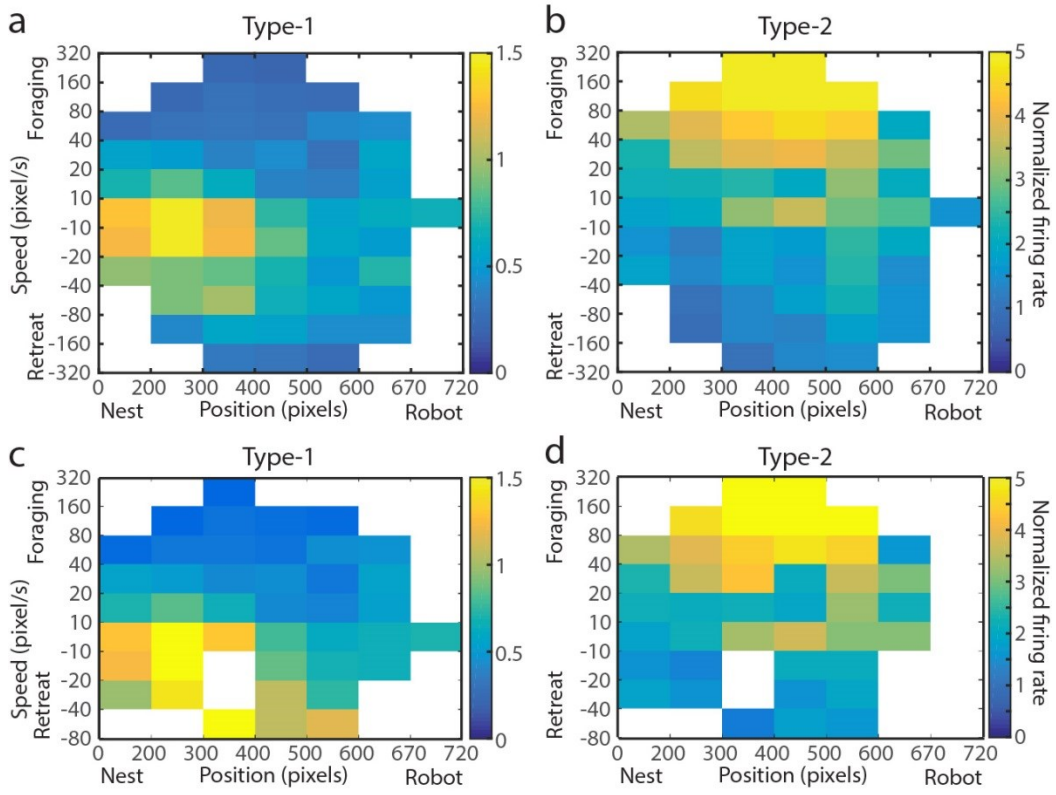

Figure 5.6 Relation between the firing rate of PNs and movement speed and position in the Robogator tasks. (**a**) Color-coded firing rates of Type-1 PNs plotted as a function of movement speed (y-axis) and position (x-axis). (**b**) Color-coded firing rates of Type-2 PNs plotted as a function of movement speed (y-axis) and position (x-axis). (**c**) Same analysis as panel **a**, with exception that the final escape phase was excluded. (**d**) Same analysis as panel **b**, with exception that the final escape phase was excluded. In **a-d**, rectangles are only shown if: (1) rats spent ≥4 sec at the given position and velocity; (2) data from ≥ 50% of the cells had to be available for that position and speed.

5.3 Discussion

In chapter 4, we recorded BL amygdala neurons in rats performing a semi-naturalistic foraging task. Upon foraging initiation, the prevalent type of principal cells (Type-1) showed a firing rate reduction, and Type-2 principal cells the

opposite. This pattern was reversed when rats aborted foraging. In this chapter, surprisingly, the two cell types maintained their opposite activity profile in two control tasks devoid of explicit threats or rewards. While the common behavioral correlate across the three tasks was movement speed, in the foraging task BL activity was also modulated by task engagement, threat proximity and reward availability. These findings lead us to conclude that BL activity should not only be conceived in terms of encoding threats and rewards. Instead, we propose that BL activity is best understood as reflecting a continuous evaluative process where internal states, reward availability, and threat determine whether rats will engage in a situation. As a result, in conditions where threat levels and reward availability are identical, BL output can be low or high, depending on whether rats engage with a situation or not. I will elaborate on this view in the general discussion (chapter 6).

CHAPTER 6

GENERAL DISCUSSION AND FUTURE DIRECTIONS

In this section, I will discuss the significance of my findings. I will first provide a general discussion regarding the experiments on the connectivity and infralimbic control of ITC cells (chapter 3). In particular, I will discuss the significance of these findings for the expression and extinction of classically conditioned fear responses. Then, I will discuss the implications of my observations in the foraging (chapter 4) and control tasks (chapter 5) for the role of the amygdala in the suppression of innate fear responses.

6.1 Connectivity and infralimbic control of ITC cells

Based on tracing and physiological studies (Pare and Smith, 1993a; Royer et al.,1999; Royer et al., 2000b), it was proposed that ITC cells are in an ideal position to gate the transfer of BL inputs about conditioned stimuli (CS) to fear output CeM neurons (Royer and Pare, 2002). It was further proposed that this gating constituted a likely mechanism for the extinction of conditioned fear (Royer and Pare, 2002). Although subsequent lesion and pharmaco-behavioral studies

in rats (Likhtik et al., 2008) and mice (Jungling et al., 2008) supported this extinction model, it has since proven difficult to further our understanding of ITC contributions to extinction because we lacked criteria to identify them in extracellular recordings. As a result, it has been impossible to test key predictions of ITC extinction models. For instance, it was predicted that ITC cells are strongly excited by IL inputs (Pare et al., 2004), explaining why IL inhibition interferes with the acquisition of extinction (Sierra-Mercado et al., 2006) and prevents the potentiation of BL inputs to ITC cells during extinction (Amano et al., 2010). Another difficulty stemmed from the fact that the ITC model of extinction is based on connectivity data obtained in guinea pigs and cats whereas behavioral studies of extinction are typically conducted in rats and mice. In chapter 3 of this thesis I aimed to address these gaps in our knowledge.

Projections of ITC cells in different species

To compare the pattern of findings obtained in guinea pigs and cats to the results obtained here in rats, one must take into account the differing orientation of the amygdala in these species. In the rat amygdala, Ce is medial to BL whereas in cats and guinea pigs, Ce is dorsal to BL. Thus, the dorsoventral axis of the rat amygdala corresponds to the lateromedial axis of the cat and guinea pigs amygdala. As a result, laterally vs. medially located ITC cell clusters in cats and guinea pigs respectively correspond to ITCd and ITCv clusters in rats.

In previous studies in cats and guinea pigs, it was reported that ITC cells project to Ce (Pare and Smith, 1993a; Royer et al., 1999) and to other ITC cells

(Royer et al., 2000b). Using labeling of single ITC cells with neurobiotin in slices of the guinea pig amygdala (Royer et al., 1999; Royer et al., 2000b), it was observed that ITC projections to Ce are topographically organized such that laterally located ITC cells (ITCd of rats) project to CeL and ASt whereas medially located ITC cells (ITCv of rats) project to CeM. In addition, ITC projections to other ITC cells were directionally polarized in that they only targeted more medially-located ITC cells (more ventrally located ITC cells in rats).

Thus, once the differing orientation of the amygdala in the two species is taken into account, the results obtained in guinea pigs and rats seem identical since we found that ITCd cells projected to CeL but not CeM whereas the opposite was seen in ITCv neurons. In addition, consistent with findings in guinea pigs, ITCd cells project toward more ventrally located ITCv clusters, whereas ITCv does not project to ITCd. Therefore, it appears that the connectivity of ITC cells is well preserved across species. In keeping with this, the results obtained in mice by Geracitano et al. (2007) are consistent with our observations in rats.

Distinctive responsiveness of ITC cells to IL inputs

Because several lines of evidence implicated ITC cells and IL in extinction of conditioned fear responses, it was natural to assume that the two sets of findings were causally related. In support of this, tracing studies revealed that IL sends a dense projection to ITC cells (Cassell and Wright, 1986; McDonald et al., 1996) and that IL disinhibition with picrotoxin increases the number of Fos

immunoreactive ITC neurons (Berretta et al., 2005). In behavioral studies, it was observed that CS presentation in the extinction training context induces Fos expression in IL and ITC neurons (Knapska and Maren, 2009) and that manipulations that facilitate extinction in extinction-deficient mice have the same effect (Whittle et al., 2010). Furthermore, electrical stimulation of IL facilitates extinction (Milad and Quirk, 2002), and causes an inhibition of CeM responses to BL inputs (Quirk et al., 2003; Figure 3.6) even though IL has no direct projections to CeM (Cassell and Wright, 1986; McDonald et al., 1996). This prompted the suggestion that IL stimulation caused a strong activation of ITC cells, thereby resulting in the feedforward inhibition of CeM cells.

The results obtained in chapter 3 support this suggestion. IL stimuli elicited orthodromic spikes in all tested ITC cells. In 75% of them, we observed that IL stimuli evoked high-frequency (up to 350 Hz) trains of 4-6 action potentials. This pattern of responsiveness was never seen in Ce or BL neurons. In LA, we did see a few cells generating more than one spike in response to IL stimuli. However, these spike bursts were comprised of significantly fewer spikes, were characterized by significantly lower intra-burst frequencies, and were only seen in cells that were far from the Ce-BL border, in the lateral third of LA. As a result, conventional methods for histological reconstructions of electrode tracks would allow investigators to determine that these cells are not ITC neurons. However, because the present experiments were conducted under urethane anesthesia, it is possible that the IL responsiveness and firing pattern of ITC cells is different in awake behaving animals. Although this possibility cannot be

excluded at the present time, since anesthetics generally depress neuronal excitability, we would expect ITC cells to display even stronger IL responses and higher spontaneous firing rates in behaving animals. Consistent with this notion, a previous study in unanesthetized cats (Collins and Pare, 1999) reported that ITC cells had much higher spontaneous firing rates than observed here. Therefore, we propose that the distinctive responses of ITC cells to IL inputs constitute a reliable criterion to identify them in behaving animals. As a result, it will now be possible to test whether the behavior of ITC cells can explain extinction, renewal, and reinstatement of conditioned fear responses.

Multiple superimposed layers of inhibition between the input and output stations of the amygdala

Fear conditioning:

Although the above focused on the role of ITC cells in extinction, our findings have significant implications for the mechanisms supporting the acquisition and expression of conditioned fear. Indeed, by virtue of the fact that ITCd and ITCv cells are respectively adjacent to LA and BL, one can expect that LA outputs constitute a major determinant of ITCd activity whereas BL outputs should prevalently affect ITCv neurons. And in fact, such a topographic arrangement was seen in guinea pigs (Royer et al., 1999). Thus, taking into account the differing orientation of the amygdala in rats in guinea pigs, this would mean that LA neurons target ITCd cells that in turn inhibit CeL neurons whereas BL would drive ITCv cells, resulting in the inhibition of CeM neurons.

Superimposed on these topographic relations between the BL, ITC cell clusters, and Ce, are two additional layers of inhibition. First, there are inhibitory projections from ITCd to ITCv cells, as well as from CeL to CeM (Lopez De Armentia and Sah, 2004; Petrovich and Swanson, 1997). Since the ultimate determinant of fear expression is CeM activity (Koo et al., 2004), it is important to consider how these multiple superimposed layers of inhibition affect CeM outputs. We first consider CeL to CeM interactions and then ITC activity.

CeL to CeM pathway: It was proposed that release of CeM neurons from inhibitory inputs arising in CeL plays a major role in the expression of conditioned fear (Ehrlich et al., 2009). First, pre-training inhibition of Ce or CeL only with muscimol (Wilensky et al., 2006; Ciocchi et al., 2010) as well as selective silencing of a subset of CeL neurons expressing PKC-δ^+ (Haubensak et al., 2010) prevented the acquisition of conditioned fear, suggesting that conditioning leads to synaptic plasticity in CeL. Moreover, one day after fear conditioning in mice, CS presentations was found to inhibit PKC-δ^+ CeL neurons (termed CeL-Off cells) (Ciocchi et al., 2010; Haubensak et al., 2010) whereas a different subset of PKC-δ^- negative CeL cells showed positive response to the CS (termed CeL-On cells). The presence of reciprocal inhibitory connections between CeL-On and CeL-Off neurons led to the proposal that when the CS is presented, the excitation of CeL-On cells causes the inhibition of CeL-Off neurons resulting in the disinhibition of CeM fear output neurons (Figure 6.1A; Ciocchi et al., 2010; Haubensak et al., 2010). At odds with this model however, Ciocchi et al. found that the incidence of CeL-On and CeL-Off neurons was

similar and both were found to project to CeM (Ciocchi et al., 2010; Haubensak et al., 2010). However, a more recent study found that SOM- but not SOM+ CeL neurons project to CeM projection cells (Li et al., 2013). Furthermore, the vast majority of SOM+ neurons correspond to PKC-δ^- and CeL-On neurons while most SOM- neurons correspond to PKC-δ^+ and CeL-Off neurons (Li et al., 2013). There are two possible explanations for this discrepancy regarding the projections of PKC-δ and SOM cells: First, Ciocchi et al., (2010) tested projections from CeL-On and CeL-Off cells to CeM cells in a very small sample of cells, reducing statistical power of their results. The second explanation is that although there is much overlap between SOM+ and PKC-δ^- cells, it is possible that SOM is a better marker than PKC-δ for predicting whether CeL cells will develop excitatory or inhibitory responses to the CS.

In sum, when the CS is not presented, CeM projection cells are under tonic inhibition that originates from CeL-Off cells (Ciocchi et al.,2010; Li et al., 2013). However, following fear conditioning, CeM cells are disinhibited by suppression of CeL-Off cells (Figure 6.1A; Ciocchi et al., 2010; Li et al., 2013).

ITC pathway: Similar to the CeL-CeM pathway, I speculate that ITCv cells also contribute tonic inhibitory inputs to CeM cells. Indeed, in chapter 3 we showed that ITCv neurons send axonal projections to CeM. Thus, following fear conditioning, CeM cells would be disinhibited when ITCd cells suppress ITCv neurons (Figure 6.1A).

While the above indicates that CeM cells are under tonic inhibition arising from CeL-Off and ITCv cells, in order to understand how CeL-Off and ITCv cells

regulate fear expression, one has to take into account the interactions of these cells with several structures involved in fear learning (Figure 6.1).

As I mentioned in the introduction, BL and mPFC are reciprocally connected and consist of two sub-circuits: a fear circuit and an extinction circuit (Senn et al., 2014). Indeed, BL-fear neurons project to PL, an area involved in fear learning (Sotres-Bayon and Quirk, 2010; Senn et al., 2014). In contrast, BL-extinction neurons project to IL, an area involved in fear extinction (Sotres-Bayon and Quirk, 2010; Senn et al., 2014). My hypothesis is that IL exclusively projects to BL extinction neurons, whereas PL projects back to BL fear neurons. In addition, I speculate that BL fear neurons excite CeM projection cells as well as ITCd cells, whereas BL extinction neurons excite ITCv cells (Figure 6.1A).

Thus, fear conditioning would be associated with an overall shift in favor of the fear circuit (activation of PL and BL fear neurons; suppression of BL extinction neurons). This would result in the activation of ITCd cells (Figure 6.1A). In turn, the activation of ITCd cells would cause the suppression of CeL-Off cells and excitation of CeL-On cells, leading to disinhibition of CeM projection neurons (Figure 6.1A; Ciocchi et al., 2010; Li et al., 2013). Finally, activation of ITCd cells would also cause the inhibition of ITCv neurons, with the final result of disinhibiting CeM neurons (Figure 6.1A).

This model is based on the three following assumptions: (1) ITCd cells are excited following fear conditioning. In support of this, fear conditioning is associated with the elevation of the Zif268 protein in the ITCd cluster, but not the ITCv cluster (Busti et al., 2011); (2) ITCd cells inhibit ITCv cells following fear

conditioning. In support of this, in chapter 3 I showed that ITCd cells send axonal projections to ITCv; (3) ITCd cells inhibit CeL-Off cells, but not CeL-On cells.

In support of the third assumption, there is indirect evidence that ITCd cells indeed inhibit CeL-Off but not CeL-On cells. In a study in rats (Duvarci et al., 2011), the CS responsiveness of CeL neurons was compared during habituation, at the end of training, and during a recall test the next day. During habituation and at the end of training, around 10% of CeL cells showed positive or negative responses to the CS. Thus, low and high fear states were associated with a similar profile of CS responsiveness in CeL. During the recall test the next day, the incidence of CeL-Off cells nearly tripled with no change in that of CeL-On neurons. If CeL-On cells are responsible for the inhibition of CeL-Off neurons, how could the incidence of CeL-Off cells increase from training to recall when that of CeL-On neurons does not change? One possibility is that CeL-On to CeL-Off synapses are potentiated as a result of fear conditioning. Another, and in my opinion, more parsimonious possibility is that a different inhibitory input, extrinsic to CeL, is involved. For instance, CS presentations might cause the glutamatergic activation of ITCd cells (Figure 6.1A; Busti et al., 2011), leading to the inhibition of CeL-Off with the final result of disinhibiting CeM neurons.

Extinction of fear conditioning:

As mentioned earlier, BL contains fear neurons, extinction neurons and extinction-resistant neurons. Fear neurons acquire positive responses to the CS as a result of fear conditioning, but lose their responsiveness following extinction

training. In contrast, extinction neurons become CS responsive only following extinction training (Herry et al., 2008). Extinction-resistant neurons are similar to fear neurons, except that they do not lose their CS responsiveness following fear extinction.

CeM projection cells lose their CS responsiveness following fear extinction, while BL cells, a major excitatory input to CeM, continue to respond to the CS (extinction-resistant cells). This suggests that an inhibitory pathway prevents the activation of CeM projection cells following fear extinction. Two candidate structures for this role are CeL and ITCv.

CeL to CeM pathway: Duvarci et al. (2011) showed that during the fear recall test, the incidence of CeL-Off cells nearly tripled with no change in the incidence of CeL-On cells. In contrast, the incidence of CeL-Off and CeL-On neurons returned to baseline (habituation level) after extinction training (Duvarci et al., 2011). These results suggest that, following fear extinction, the amount of inhibition that originates from CeL-Off neurons returns to baseline levels. Thus, CeL-Off cells likely do not mediate extinction.

ITC pathway: There is a significant increase in the number of Zif268 positive cells after extinction retrieval in the ITCv but not the ITCd cluster (Busti et al., 2011). I speculate that this activation of ITCv cells results in a suppression of CeM projection neurons, and causes a reduction in the expression of fear. Supporting this speculation, in chapter 3, I showed that ITCv cells send axonal projections toward CeM (Figure 6.1B). Figure 6.1B summarized the neuronal interactions hypothesized to support fear extinction.

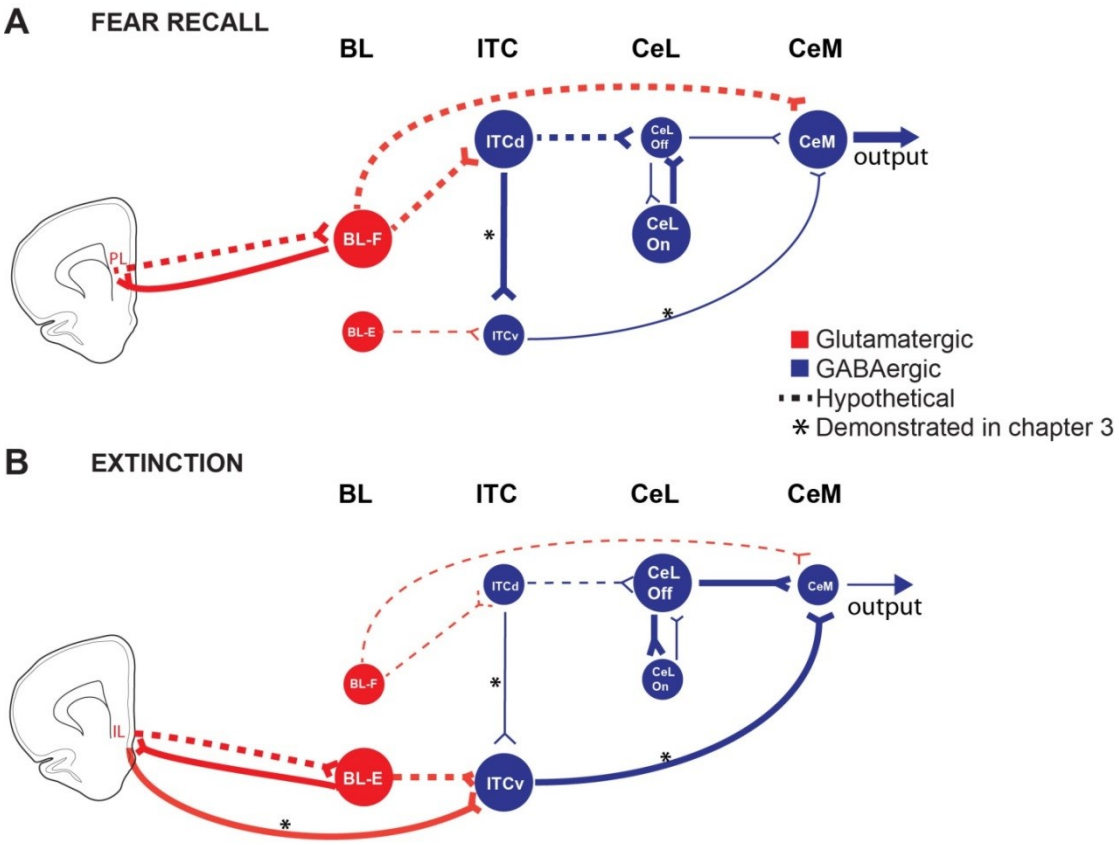

Figure 6.1 Interactions supporting fear expression and extinction. These models include well established pathways (solid lines) and hypothetical ones (dash lines). Thick lines and thin lines represent connections that are more or less active, respectively. Large and small circles represent higher or lower neural activity, respectively. Blue and red lines represent GABAergic or Glutamatergic connection, respectively. Astrocytes represent connections that have been establishes in chapter 3. (**A-B**) PL cells are excited during fear recall while IL cells are excited during extinction recall (Sotres-Bayon and Quirk, 2010). BL-Fear cells are excited during fear recall (Herry et al., 2008; Amano et al., 2011) and project to PL (Senn et al., 2014) whereas BL-Extinction cells are excited during extinction recall (Herry et al., 2008; Amano et al., 2011) and project to IL (Senn et al., 2014). ITCd cells are excited during fear recall as seen indirectly using expression of Zif268 protein whereas ITCv cells are excited during extinction recall (Busti et al., 2011). Suppression of CeL-Off cells increases during fear recall (Ciocchi et al., 2010) and this suppression returns to baseline during extinction training (Duvarci et al., 2011). CeL-Off and CeL-On cells are reciprocally connected (Ciocchi et al., 2010; Li et al., 2013) and CeL-Off cells project to CeM cells (Li et al., 2013). Lastly, CeM cells are excited during fear expression and return to baseline during extinction training (Duvarci et al., 2011). Abbreviations, BL-E, BL extinction cells; BL-F, BL fear cells.

6.2 Suppression of amygdala signaling during foraging in a hazardous environment and during control tasks devoid of explicit threats or rewards

Prior classical and operant conditioning studies have implicated the basolateral amygdaloid complex (BLA) in the development of conditioned responses to stimuli (CSs) that predict aversive (Anglada-Figuero and Quirk, 2005; Amano et al., 2011) or rewarding outcomes (Setlow et al., 2002; Everitt et al., 2003; Ambroggi et al., 2008). Consistent with this, as a result of conditioning, many BLA neurons acquire robust excitatory, inhibitory, or mixed responses to negatively or positively valenced CSs (Rorick-Kehn and Steinmetz, 2005; Belova et al., 2008; Herry et al., 2008; Shabel and Janak, 2009; Amano et al., 2011).

However, by design in conditioning studies, positively or negatively valenced CSs are presented in isolation or at different times. This is in contrast with natural conditions where animals are simultaneously presented with potential risks and rewards (e.g. predators, food) that are associated with opposite response tendencies (e.g. behavioral inhibition and freezing vs. approach and food seeking). As a result, there is little information on how BLA activity contributes to help animals weigh the need to attain food against the associated increase in the risk of predation.

Recently, Choi and Kim (2010) introduced a task that reproduces natural foraging conditions. In this task, rats are confronted with a mechanical predator (Robogator) when they leave their nest to obtain food pellets. Intra-amygdala infusions of drugs that reduced or enhanced the firing rates of amygdala neurons

respectively led to increases or decreases in risk-taking (Choi and Kim, 2010). While these findings indicate that the amygdala regulates risky foraging decisions, how it does so is unclear.

To address this question, we studied BL activity in a semi-naturalistic foraging task as well as control tasks devoid of explicit threats or rewards. In these various conditions, threat proximity and reward availability did not consistently predict BL activity. Instead, BL activity was strongly correlated with movement speed as well as task engagement and was a function of the rats' decisions on a particular trial. Thus, we propose that BL activity should not only be conceived in terms of encoding threats and rewards. Rather, we propose that it is best understood as reflecting a continuous evaluative process where internal states, reward availability, and threat determine whether rats will engage in a situation. Consequently, in conditions where threat levels and reward availability are identical, BL output can be low or high, depending on whether rats engage with a situation or not.

Relation to prior work on threat and reward signaling by the amygdala

Early lesion studies (Kluver and Bucy, 1937; Weiskrantz, 1956; Blanchard and Blanchard, 1972) led to the view that the amygdala plays a key role in the control of defensive behaviors. This notion was reinforced by subsequent studies implicating the amygdala in the acquisition and expression of classically conditioned fear. For instance, it was commonly reported that fear conditioning leads to the emergence of amygdala cells with potentiated responses to

conditioned stimuli (CSs) predicting aversive outcomes (Maren and Quirk, 2004). Overall, this work suggested that amygdala neurons signal threat and trigger defensive behaviors. Extrapolated to the foraging task, this suggests that the rats' cautious behavior depends on threat signaling by amygdala neurons. In apparent agreement with this inference, local infusions of drugs that enhanced or reduced threat signaling by amygdala neurons diminished or increased risk-taking, respectively (Choi and Kim, 2010). Yet, our recordings revealed a different situation.

We distinguished two types of principal BL neurons based on their activity in the foraging task. Increased FRs in the prevalent type (Type-1) anticipated aborted foraging and retreat into the nest. In contrast, augmented activity in Type-2 cells anticipated foraging. Thus, Type-1 cells seem to correspond to the threat-signaling neurons expected from prior work. Surprisingly however, upon initiation of foraging, these cells showed a near complete firing suppression, despite the increasing proximity of the predator. In other words, Type-1 cells do not signal threat during foraging. Thus, amygdala inactivation does not increase risk-taking because it suppresses threat signaling, but because it reproduces the state of Type-1 cell suppression that occurs during foraging.

Since rats continue to forage when the amygdala is inactivated (Choi and Kim, 2010), the drive to seek food does not require the amygdala. Yet, many studies have implicated the amygdala in reward seeking (Setlow et al., 2002; Everitt et al., 2003; Ambroggi et al., 2008). A critical question emerging from these studies is whether the same or different pools of amygdala neurons are

involved in the processing of threats and rewards. In monkeys, different populations of BLA neurons signal positively or negatively valenced CSs (Belova et al., 2008). In contrast, a study using a mixed appetitive-aversive learning paradigm in rats emphasized the similar behavior of BLA neurons in response to CSs predicting rewarding or aversive outcomes (Shabel and Janak, 2009). Related to this, Roesch and colleagues (Roesch et al., 2010) reported that rat BLA neurons signal unexpected deviations in reward outcomes, whether positive or negative. Further complicating this picture, Genud-Gabai et al. (2013) reported a mixture of excitation and inhibition with aversive, neutral, and positively valenced CSs in monkeys.

Together, these findings suggest that the amygdala contains multiple populations of cells somehow related to processing of negative, neutral, or positively valenced CSs. This raises the question of what factors drive the inverse activity fluctuations of Type-1 and 2 cells in the foraging task: predator threat or food availability. To shed light on this question, we examined their activity in two control tasks (chapter 5) devoid of explicit threats or rewards. Despite the absence of explicit threats in both control tasks, Type-1 cells exhibited the same activity fluctuations as in the foraging task: whether rats moved to secure food pellets (shuttle task) or spontaneously for no apparent reason in the open field, their FRs diminished as the rats' velocity increased (Figure 5.4a and Figure 5.5a). Similarly, the FR of Type-2 cells in the two control tasks showed a strong relation to movement speed, except that it was in the opposite direction (Figure 5.4a and Figure 5.5a).

To our knowledge, there are no precedents in the literature for the motor correlates we observed. Unfortunately, prior conditioning studies were performed in head-restrained animals or in small chambers, reducing the possibility of observing this relation. Another obstacle to the detection of this relationship is the low FRs of PNs. Unless long activity periods are considered, most of these slowly firing cells are discarded at the clustering stage.

Origin of the inverse activity fluctuations displayed by Type-1 and 2 PNs

Our results add to a growing body of evidence suggesting there are at least two PN types in BL. In fear conditioning studies (Herry et al., 2008; Amano et al., 2011), two main types were distinguished based on CS responsiveness. Most cells developed increased responses to the CS that were either abolished by or persisted despite extinction training. A second cell class displayed inhibitory CS responses after conditioning, which reversed to excitatory responses following extinction training. Similarly, two PN types were distinguished based on their opposite pattern of activity in relation to a spontaneously occurring **s**low **o**scillation in vitro (SOs; Rainnie, 1999; Chung and Moore, 2009). SOs are generated in BL: they persist after its isolation from the rest of the slice (Popescu and Pare, 2011). In most PNs (~85%), SOs appear as large, long-lasting, and synchronized GABA-A IPSPs (Rainnie, 1999; Chung and Moore, 2009). Yet, non-NMDA glutamate receptor antagonists abolish SOs, implying that they arise from the interplay between glutamatergic and GABAergic BL neurons (Chung

and Moore, 2009; Popescu and Pare, 2011). In support of this idea, a second subset of PNs (15%) fire shortly before IPSP onset and drive interneuronal firing (Popescu and Pare, 2011).

Together with our findings, these results suggest that BL contains at least two PN types that form distinct extrinsic connections (Senn et al., 2014), and entertain contrasting relations with different BL interneuronal subtypes (Duvarci and Pare, 2014), resulting in reciprocal activity fluctuations. Because BL projects to the medial part of the central amygdala (CeM) and SOs have no correlate in CeM neurons (Popescu and Pare, 2011), it is likely that the rare PN type (Type-2) does not project to CeM whereas the predominant one (Type-1) does. The significance of this inference stems from the fact that most amygdala projections to the periaqueductal gray (PAG), controlling behavioral freezing, originate from CeM (Hopkins and Holstege, 1978). Therefore, suppressed firing in Type-1 PNs would cause a disfacilitation of PAG-projecting CeM neurons, thereby reducing freezing, a prerequisite for foraging initiation. At present, the factors that drive the inverse activity fluctuations of Type-1 and 2 PNs are unclear. We speculate that they are driven by an extrinsic signal, possibly originating in the pre- or orbitofrontal cortices.

Significance of the inverse activity fluctuations displayed by Type-1 and 2 PNs

So far, concepts about amygdala function have centered on the processing of threat and rewards. Yet, the fact that Type-1 and 2 cells show the

same inverse activity pattern in the absence of explicit rewards and threats suggests that amygdala activity is indirectly related to these variables. Based on the strong correlations with movement and task engagement we observed, we propose that the level of amygdala activity relates to a more basic behavioral process: approach vs. behavioral inhibition (Figure 6.2). We envision an approach/avoidance continuum where the rats' decisions are determined by the exact or anticipated reward/threat contingencies as well as their internal state, influenced by prior experience with the same or similar situations. BL activity levels would be related to the rats' position along this continuum at any given time (Figure 6.2). Consistent with this, we found that approach is associated with reduced activity levels in Type-1 cells and avoidance, with higher FRs. For instance, Type-1 cells show a stronger suppression during foraging in the absence than presence of Robogator (Figure 4.8C). They are less active in anticipation of trials where rats initiate rather than abort foraging (Figure 4.8B insets), prior to trials when rats skip waiting (Figure 5.5b), and when rats move faster toward the food (Figure 5.6 c). Moreover, even in the control tasks, where reward or threat were absent, the rats engagement with the situation, as reflected in their speed, negatively correlated with the FR of Type-1 cells whereas Type-2 cells showed the opposite relationship. Assuming, as reasoned above, that Type-1 and 2 cells are differentially connected with CeM, suppression of Type-1 cells would be required for animals to engage with a situation. Otherwise, Type-1 cells would, via CeM, generate freezing (behavioral inhibition). An important challenge

for future experiments will be to determine how this behavioral dichotomy relates to the acquisition of conditioned fear or reward-seeking behaviors.

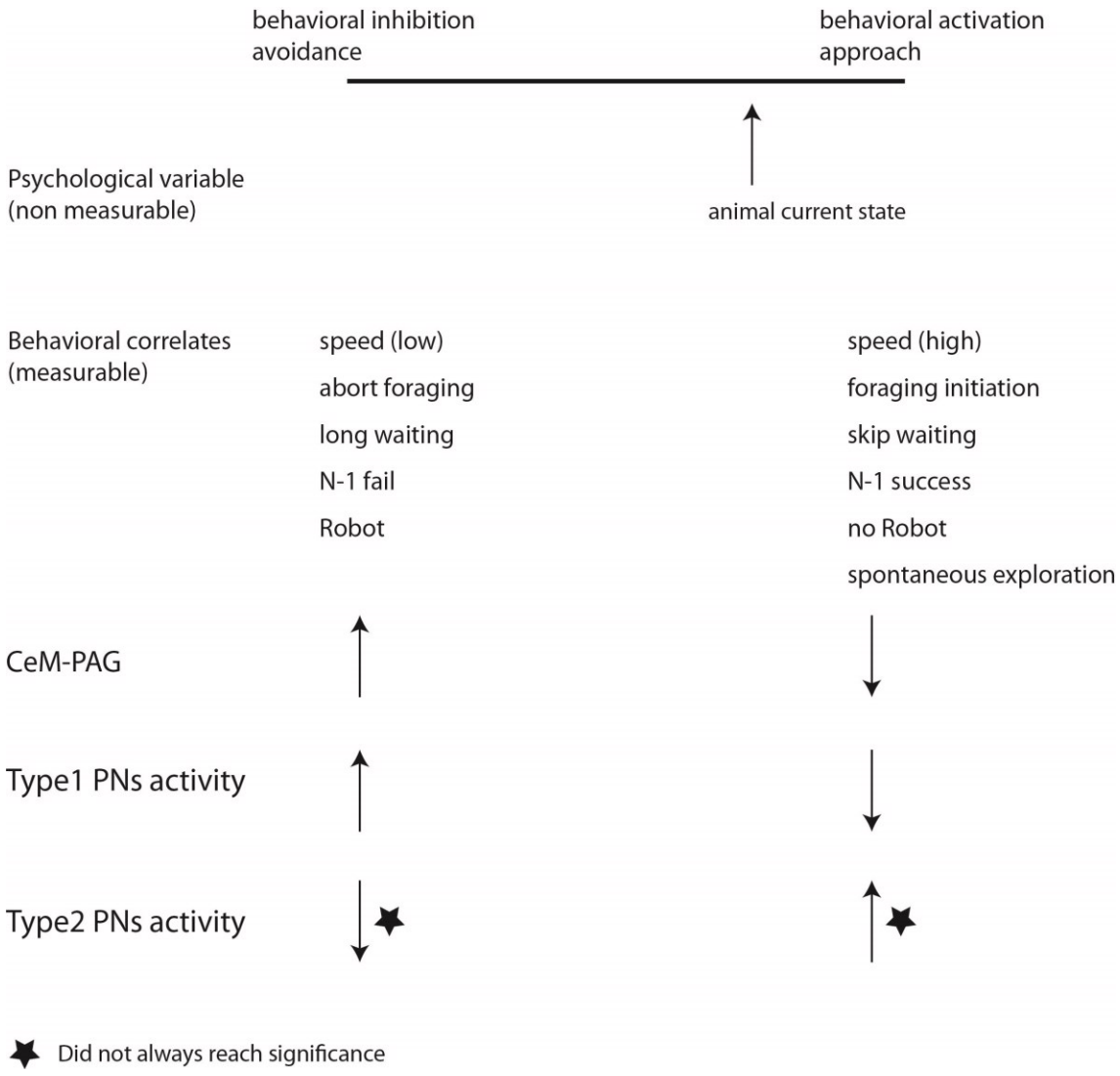

Figure 6.2 BL activity levels correlate with the animal's current position along behavioral-inhibition/approach continuum. Behavioral correlates associated with avoidance include: long waiting, aborted foraging, and low speed toward the food. These behaviors coincided with increased activity of Type-1 cells. In contrast, behavioral correlates associated with approach include: skipping waiting, foraging initiation, and high speed toward the food. These behaviors coincided with suppression of Type-1 cells. Of note, when the rats were hesitant, movement speed away from the robogator was associated with increased FR of Type-1 cells.

Learned fear versus innate fear suppression

Our results diverge starkly from past investigations of amygdala activity in relation to conditioned fear. While previous reports generally found that fear eliciting CSs evoke increases in activity in the lateral and basolateral amygdala (Duvarci and Pare, 2014), we instead observed a dramatic reduction in firing. There are a number of differences between the foraging task and classical Pavlovian fear conditioning that may account for these discrepancies. The most obvious difference is the training situation, with all prior studies utilizing a classical Pavlovian conditioning paradigm with brief unconditioned stimuli, while the foraging task embedded the aversive stimulus within a semi-naturalistic foraging task. The latter task requires a fundamentally different behavioral repertoire from the subject: they must overcome an innate freezing response to acquire sustenance, and evade an anticipated predator. Furthermore, Pavlovian fear is learned whereas fear of a predator is not. Another important difference is that in the foraging task, the animal can control the level of exposure to the fear object (predator) while in classical fear conditioning the animal cannot avoid it. Thus, the difference in amygdala unit activity between the Pavlovian and foraging tasks might reflect the distinct defensive strategies employed by the subject. Underscoring the importance of this point is the growing realization that defensive behavior is a more tractable object of investigation than the traditional notion of a fear state, which cannot be objectively assessed in non-human subjects (LeDoux, 2014). Consequently, the suppression we observed may reflect another operating mode of the amygdala as a promoter of defensive

behavior, a mode that is important for the kinds of risky behaviors animals routinely engage in.

REFERENCES

Aarts E, Verhage M, Veenvliet JV, Dolan CV, van der Sluis S (2014) A solution to dependency: using multilevel analysis to accommodate nested data. Nat Neurosci 17:491-496.

Amano T, Unal CT, Paré D (2010) Synaptic correlates of fear extinction in the amygdala. Nat Neurosci 13:489-494.

Amano T, Duvarci S, Popa D, Paré D (2011) The fear circuit revisited: contributions of the basal amygdala nuclei to conditioned fear. J Neurosci 31:15481-15489.

Amaral DG (2002) The primate amygdala and the neurobiology of social behavior: implications for understanding social anxiety. Biol Psychiatry 51:11-17.

Ambroggi F, Ishikawa A, Fields HL, Nicola SM (2008) Basolateral amygdala neurons facilitate reward-seeking behavior by exciting nucleus accumbens neurons. Neuron 59:648-661.

Amir A, Amano T, Paré D (2011) Physiological identification and infralimbic responsiveness of rat intercalated amygdala neurons. J Neurophysiol 6:3054-66

Amorapanth P, LeDoux JE, Nader K (2000) Different lateral amygdala outputs mediate reactions and actions elicited by a fear-arousing stimulus. Nat Neurosci 3:74-79.

Anderson AK, Phelps EA (2002) Is the human amygdala critical for the subjective experience of emotion? Evidence of intact dispositional affect in patients with amygdala lesions. J Cogn Neurosci 14:709-720.

Anglada-Figueroa D, Quirk GJ (2005) Lesions of the basal amygdala block expression of conditioned fear but not extinction. J Neurosci 25:9680-9685.

Barthó P, Hirase H, Monconduit L, Zugaro M, Harris KD, Buzsáki G (2004) Characterization of neocortical principal cells and interneurons by network interactions and extracellular features. J Neurophysiol 92:600-608.

Bechara A, Tranel D, Damasio H, Adolphs R, Rockland C, Damasio AR (1995) Double dissociation of conditioning and declarative knowledge relative to the amygdala and hippocampus in humans. Science 269:1115-1118.

Behbehani MM (1995) Functional characteristics of the midbrain periaqueductal gray. Prog Neurobiol 46:575-605.

Belova MA, Paton JJ, Salzman CD (2008) Moment-to-moment tracking of state value in the amygdala. J Neurosci 28:10023-10030.

Bernard JF, Peschanski M, Besson JM (1989) A possible spino (trigemino)-ponto-amygdaloid pathway for pain. Neurosci Lett 100:83-88.

Bernard JF, Alden M, Besson JM (1993) The organization of the efferent projections from the pontine parabrachial area to the amygdaloid complex: a Phaseolus vulgaris leucoagglutinin (PHA-L) study in the rat. J Comp Neurol 329:201-229.

Berretta S, Pantazopoulos H, Caldera M, Pantazopoulos P, Paré D (2005) Infralimbic cortex activation increases c-Fos expression in intercalated neurons of the amygdala. Neuroscience 132:943-953.

Blanchard DC, Blanchard RJ (1972) Innate and conditioned reactions to threat in rats with amygdaloid lesions. J Comp Physiol Psychol 81:281-290.

Blanchard RJ, Blanchard DC (1990) Anti-predator defense as models of fear and anxiety. In: Fear and Defense, P.F. Brain, R.J. Blanchard, D. Mainardi, eds. (Chur, Switzerland, Harwood Academic Publishers), pp. 89–108.

Blechert J, Michael T, Vriends N, Margraf J, Wilhelm FH (2007) Fear conditioning in posttraumatic stress disorder: evidence for delayed extinction of autonomic, experiential, and behavioural responses. Behav Res Ther 45:2019-2033.

Bordi F, LeDoux JE (1994) Response properties of single units in areas of rat auditory thalamus that project to the amygdala. I. Acoustic discharge patterns and frequency receptive fields. Exp Brain Res 98:261-274.

Bornemann B, Winkielman P, van der Meer E (2012) Can you feel what you do not see? Using internal feedback to detect briefly presented emotional stimuli. Int J Psychophysiol 85:116-124.

Bouton ME, Bolles RC (1979) Role of conditioned contextual stimuli in reinstatement of extinguished fear. J Exp Psychol Anim Behav Process 5:368-378.

Büchel C, Morris J, Dolan RJ, Friston KJ (1998) Brain systems mediating aversive conditioning: an event-related fMRI study. Neuron 20:947-957.

Busti D, Geracitano R, Whittle N, Dalezios Y, Mańko M, Kaufmann W, Sätzler K, Singewald N, Capogna M, Ferraguti F (2011) Different fear states engage distinct networks within the intercalated cell clusters of the amygdala. J Neurosci 31:5131-5144.

Butler RK, Sharko AC, Oliver EM, Brito-Vargas P, Kaigler KF, Fadel JR, Wilson MA (2011) Activation of phenotypically-distinct neuronal subpopulations of the rat amygdala following exposure to predator odor. Neuroscience 175:133-144.

Cassell MD, Wright DJ (1986) Topography of projections from the medial prefrontal cortex to the amygdala in the rat. Brain Res Bull 17:321-333.

Cassell MD, Gray TS, Kiss JZ (1986) Neuronal architecture in the rat central nucleus of the amygdala: a cytological, hodological, and immunocytochemical study. J Comp Neurol 246:478-499.

Cho JH, Deisseroth K, Bolshakov VY (2013) Synaptic encoding of fear extinction in mPFC-amygdala circuits. Neuron 80:1491-1507.

Choi JS, Kim JJ (2010) Amygdala regulates risk of predation in rats foraging in a dynamic fear environment. Proc Natl Acad Sci U S A 107:21773-21777.

Chung L, Moore SD (2009) Neuropeptides modulate compound postsynaptic potentials in basolateral amygdala. Neuroscience 164:1389-1397.

Ciocchi S, Herry C, Grenier F, Wolff SBE, Letzkus JJ, Vlachos I, Ehrlich I, Sprengel R, Deisseroth K, Stadler MB, Müller C, Lüthi A (2010) Encoding of conditioned fear in central amygdala inhibitory circuits. Nature 468:277-282.

Collins DR, Paré D (1999) Spontaneous and evoked activity of intercalated amygdala neurons. Eur J Neurosci 11:3441-3448.

Collins DR, Paré D (2000) Differential fear conditioning induces reciprocal changes in the sensory responses of lateral amygdala neurons to the CS(+) and CS(-). Learn Mem 7:97-103.

Davis M, Shi C (1999) The extended amygdala: are the central nucleus of the amygdala and the bed nucleus of the stria terminalis differentially involved in fear versus anxiety? Ann NY Acad Sci 877:281-291.

Davis M, Whalen PJ (2001) The amygdala: vigilance and emotion. Mol Psychiatr 6:13-34.

Davis M, Rainnie D, Cassell M (1994) Neurotransmission in the rat amygdala related to fear and anxiety. Trends Neurosci 17:208-214.

Day HE, Curran EJ, Watson SJ, Akil H (1999) Distinct neurochemical populations in the rat central nucleus of the amygdala and bed nucleus of the stria terminalis: evidence for their selective activation by interleukin-1beta. J Comp Neurol 413:113-128.

Dong HW, Swanson LW (2004) Organization of axonal projections from the anterolateral area of the bed nuclei of the stria terminalis. J Comp Neurol 468:277-298.

Dong HW, Swanson LW (2006) Projections from bed nuclei of the stria terminalis, dorsomedial nucleus: implications for cerebral hemisphere integration of neuroendocrine, autonomic, and drinking responses. J Comp Neurol 494:75-107.

Dong HW, Petrovich GD, Swanson LW (2000) Organization of projections from the juxtacapsular nucleus of the BST: a PHAL study in the rat. Brain Res 859:1-14.

Dumont EC, Martina M, Samson RD, Drolet G, Paré D (2002) Physiological properties of central amygdala neurons: species differences. Eur J Neurosci 15:545-552.

Duvarci S, Pare D (2014) Amygdala microcircuits controlling learned fear. Neuron 82:966-980.

Duvarci S, Popa D, Paré D (2011) Central amygdala activity during fear conditioning. J Neurosci 31:289-294.

Ehrlich I, Humeau Y, Grenier F, Ciocchi S, Herry C, Lüthi A (2009) Amygdala inhibitory circuits and the control of fear memory. Neuron 62:757-771.

Everitt BJ, Cardinal RN, Parkinson JA, Robbins TW (2003) Appetitive behavior: impact of amygdala-dependent mechanisms of emotional learning. Ann NY Acad Sci 985:233-250.

Faber ESL, Sah P (2002) Physiological role of calcium-activated potassium currents in the rat lateral amygdala. J Neurosci 22:1618-1628.

Faber ESL, Sah P (2003) Ca2+-activated K+ (BK) channel inactivation contributes to spike broadening during repetitive firing in the rat lateral amygdala. J Physiol 552:483-497.

Faber ESL, Callister RJ, Sah P (2001) Morphological and electrophysiological properties of principal neurons in the rat lateral amygdala in vitro. J Neurophysiol 85:714-723.

Fanselow MS, Kim JJ, Yipp J, De Oca B (1994) Differential effects of the N-methyl-D-aspartate antagonist DL-2-amino-5-phosphonovalerate on acquisition of fear of auditory and contextual cues. Behav Neurosci 108:235-240.

Feinstein JS (2013) Lesion studies of human emotion and feeling. Curr Opin Neurobiol 23:304-309.

Felix-Ortiz AC, Beyeler A, Seo C, Leppla CA, Wildes CP, Tye KM (2013) BLA to vHPC inputs modulate anxiety-related behaviors. Neuron 79:658-664.

Gauriau C, Bernard JF (2002) Pain pathways and parabrachial circuits in the rat. Exp Physiol 87:251-258.

Genud-Gabai R, Klavir O, Paz R (2013) Safety signals in the primate amygdala. J Neurosci 33:17986-17994.

Geracitano R, Kaufmann Wa, Szabo G, Ferraguti F, Capogna M (2007) Synaptic heterogeneity between mouse paracapsular intercalated neurons of the amygdala. J Physiol 585:117-134.

Goosens KA, Maren S (2003) Pretraining NMDA receptor blockade in the basolateral complex, but not the central nucleus, of the amygdala prevents savings of conditional fear. Behav Neurosci 117:738-750.

Hasselmo ME, Giocomo LM (2006) Cholinergic modulation of cortical function. J Mol Neurosci 30:133-135.

Haubensak W, Kunwar PS, Cai H, Ciocchi S, Wall NR, Ponnusamy R, Biag J, Dong H-W, Deisseroth K, Callaway EM, Fanselow MS, Lüthi A, Anderson DJ (2010) Genetic dissection of an amygdala microcircuit that gates conditioned fear. Nature 468:270-276.

Hazan L, Zugaro M, Buzsáki G (2006) Klusters, NeuroScope, NDManager: a free software suite for neurophysiological data processing and visualization. J Neurosci Methods 155:207-216.

Herry C, Trifilieff P, Micheau J, Lüthi A, Mons N (2006) Extinction of auditory fear conditioning requires MAPK/ERK activation in the basolateral amygdala. Eur J Neurosci 24:261-269.

Herry C, Ciocchi S, Senn V, Demmou L, Müller C, Lüthi A (2008) Switching on and off fear by distinct neuronal circuits. Nature 454:600-606.

Holahan MR, White NM (2002) Conditioned memory modulation, freezing, and avoidance as measures of amygdala-mediated conditioned fear. Neurobiol Learn Mem 77:250-275.

Hopkins DA, Holstege G (1978) Amygdaloid projections to the mesencephalon, pons and medulla oblongata in the cat. Exp Brain Res 32:529-547.

Horikawa K, Armstrong WE (1988) A versatile means of intracellular labeling: injection of biocytin and its detection with avidin conjugates. J Neurosci Methods 25:1-11.

Jacobs BL, McGinty DJ (1971) Amygdala unit activity during sleep and waking. Exp Neurol 33:1-15.

Jacobsen KX, Höistad M, Staines WA, Fuxe K (2006) The distribution of dopamine D1 receptor and mu-opioid receptor 1 receptor immunoreactivities in the amygdala and interstitial nucleus of the posterior limb of the anterior commissure: relationships to tyrosine hydroxylase and opioid peptide terminal syst. Neuroscience 141:2007-2018.

Jasnow AM, Ressler KJ, Hammack SE, Chhatwal JP, Rainnie DG (2009) Distinct subtypes of cholecystokinin (CCK)-containing interneurons of the basolateral amygdala identified using a CCK promoter-specific lentivirus. J Neurophysiol 101:1494-1506.

Jüngling K, Seidenbecher T, Sosulina L, Lesting J, Sangha S, Clark SD, Okamura N, Duangdao DM, Xu Y-L, Reinscheid RK, Pape HC (2008) Neuropeptide S-mediated control of fear expression and extinction: role of intercalated GABAergic neurons in the amygdala. Neuron 59:298-310.

Kalin NH, Shelton SE, Davidson RJ (2004) The role of the central nucleus of the amygdala in mediating fear and anxiety in the primate. J Neurosci 24:5506-5515.

Kalyuzhny AE, Arvidsson U, Wu W, Wessendorf MW (1996) mu-Opioid and delta-opioid receptors are expressed in brainstem antinociceptive circuits: studies using immunocytochemistry and retrograde tract-tracing. J Neurosci 16:6490-6503.

Kamal AM, Tömböl T (1975) Golgi studies on the amygdaloid nuclei of the cat. J Hirnforsch 16:175-201.

Kapp BS, Gallagher M, Underwood MD, McNall CL, Whitehorn D (1982) Cardiovascular responses elicited by electrical stimulation of the amygdala central nucleus in the rabbit. Brain Res 234:251-262.

Kemppainen S, Pitkänen A (2000) Distribution of parvalbumin, calretinin, and calbindin-D(28k) immunoreactivity in the rat amygdaloid complex and colocalization with gamma-aminobutyric acid. J Comp Neurol 426:441-467.

Kim J, Lee S, Park H, Song B, Hong I, Geum D, Shin K, Choi S (2007) Blockade of amygdala metabotropic glutamate receptor subtype 1 impairs fear extinction. Biochem Biophys Res Commun 355:188-193.

Kluver H, Bucy PC (1937) “Psychic blindness” and other symptoms following bilateral temporal lobectomy in rhesus monkeys. American J Physiol 119:352-353.

Knapska E, Maren S (2009) Reciprocal patterns of c-Fos expression in the medial prefrontal cortex and amygdala after extinction and renewal of conditioned fear. Learn Mem 16:486-493.

Koo JW, Han JS, Kim JJ (2004) Selective neurotoxic lesions of basolateral and central nuclei of the amygdala produce differential effects on fear conditioning. J Neurosci 24:7654-7662.

Krettek JE, Price JL (1977a) Projections from the amygdaloid complex and adjacent olfactory structures to the entorhinal cortex and to the subiculum in the rat and cat. J Comp Neurol 172:723-752.

Krettek JE, Price JL (1977b) Projections from the amygdaloid complex to the cerebral cortex and thalamus in the rat and cat. J Comp Neurol 172:687-722.

Krettek JE, Price JL (1978a) A description of the amygdaloid complex in the rat and cat with observations on intra-amygdaloid axonal connections. J Comp Neurol 178:255-280.

Krettek JE, Price JL (1978b) Amygdaloid projections to subcortical structures within the basal forebrain and brainstem in the rat and cat. J Comp Neurol 178:225-254.

LaBar KS, Gatenby JC, Gore JC, LeDoux JE, Phelps EA (1998) Human amygdala activation during conditioned fear acquisition and extinction: a mixed-trial fMRI study. Neuron 20:937-945.

Lang EJ, Paré D (1998) Synaptic responsiveness of interneurons of the cat lateral amygdaloid nucleus. Neuroscience 83:877-889.

Laurent V, Westbrook RF (2009) Inactivation of the infralimbic but not the prelimbic cortex impairs consolidation and retrieval of fear extinction. Learn Mem 16:520-529.

Lazarus RS, McCleary RA (1951) Autonomic discrimination without awareness: A study of subception. Psychol Rev 58:113-122.

LeDoux JE (2000) Emotion circuits in the brain. Annu Rev Neurosci 23:155-184.

LeDoux JE (2014) Coming to terms with fear. Proc Natl Acad Sci U S A 111:2871-2878.

LeDoux JE, Farb CR, Romanski LM (1991) Overlapping projections to the amygdala and striatum from auditory processing areas of the thalamus and cortex. Neurosci Lett 134:139-144.

LeDoux JE, Iwata J, Cicchetti P, Reis DJ (1988) Different projections of the central amygdaloid nucleus mediate autonomic and behavioral correlates of conditioned fear. J Neurosci 8:2517-2529.

LeDoux JE, Cicchetti P, Xagoraris A, Romanski LM (1990) The lateral amygdaloid nucleus: sensory interface of the amygdala in fear conditioning. J Neurosci 10:1062-1069.

Ledoux JE, Ruggiero DA, Forest R, Stornetta R, Reis DJ (1987) Topographic organization of convergent projections to the thalamus from the inferior colliculus and spinal cord in the rat. J Comp Neurol 264:123-146.

Li H, Penzo MA, Taniguchi H, Kopec CD, Huang ZJ, Li B (2013) Experience-dependent modification of a central amygdala fear circuit. Nat Neurosci 16:332-339.

Likhtik E, Pelletier JG, Paz R, Paré D (2005) Prefrontal control of the amygdala. J Neurosci 25:7429-7437.

Likhtik E, Pelletier JG, Popescu AT, Paré D (2006) Identification of basolateral amygdala projection cells and interneurons using extracellular recordings. J Neurophysiol 96:3257-3265.

Likhtik E, Popa D, Apergis-Schoute J, Fidacaro GA, Paré D (2008) Amygdala intercalated neurons are required for expression of fear extinction. Nature 454:642-645.

Likhtik E, Stujenske JM, Topiwala MA, Harris AZ, Gordon JA (2014) Prefrontal entrainment of amygdala activity signals safety in learned fear and innate anxiety. Nat Neurosci 17:106-113.

Linke R, Braune G, Schwegler H (2000) Differential projection of the posterior paralaminar thalamic nuclei to the amygdaloid complex in the rat. Exp Brain Res 134:520-532.

Lopez de Armentia M, Sah P (2004) Firing properties and connectivity of neurons in the rat lateral central nucleus of the amygdala. J Neurophysiol 92:1285-1294.

Lu KT, Walker DL, Davis M (2001) Mitogen-activated protein kinase cascade in the basolateral nucleus of amygdala is involved in extinction of fear-potentiated startle. J Neurosci 21:RC162.

Marcellino D, Frankowska M, Agnati L, Perez de la Mora M, Vargas-Barroso V, Fuxe K, Larriva-Sahd J (2012) Intercalated and paracapsular cell islands of the adult rat amygdala: a combined rapid-Golgi, ultrastructural, and immunohistochemical account. Neuroscience 226:324-347.

Maren S, Quirk GJ (2004) Neuronal signalling of fear memory. Nat Rev Neurosci 5:844-852.

Maren S, Yap SA, Goosens KA (2001) The amygdala is essential for the development of neuronal plasticity in the medial geniculate nucleus during auditory fear conditioning in rats. J Neurosci 21:1-6.

Marowsky A, Yanagawa Y, Obata K, Vogt KE (2005) A specialized subclass of interneurons mediates dopaminergic facilitation of amygdala function. Neuron 48:1025-1037.

Martina M, Royer S, Paré D (1999) Physiological properties of central medial and central lateral amygdala neurons. J Neurophysiol 82:1843-1854.

Martinez RC, Carvalho-Netto EF, Ribeiro-Barbosa ER, Baldo MVC, Canteras NS (2011) Amygdalar roles during exposure to a live predator and to a predator-associated context. Neuroscience 172:314-328.

McAllister WR, McAllister DE, Scoles MT, Hampton SR (1986) Persistence of fear-reducing behavior: relevance for the conditioning theory of neurosis. J Abnorm Psychol 95:365-372.

McDonald AJ (1982) Cytoarchitecture of the central amygdaloid nucleus of the rat. J Comp Neurol 208:401-418.

McDonald AJ (1991a) Topographical organization of amygdaloid projections to the caudatoputamen, nucleus accumbens, and related striatal-like areas of the rat brain. Neuroscience 44:15-33.

McDonald AJ (1991b) Organization of amygdaloid projections to the prefrontal cortex and associated striatum in the rat. Neuroscience 44:1-14.

McDonald AJ (1992) Projection neurons of the basolateral amygdala: a correlative Golgi and retrograde tract tracing study. Brain Res Bull 28:179-185.

McDonald AJ (1998) Cortical pathways to the mammalian amygdala. Prog Neurobiol 55:257-332.

McDonald AJ, Augustine JR (1993) Localization of GABA-like immunoreactivity in the monkey amygdala. Neuroscience 52:281-294.

McDonald AJ, Mascagni F (2001) Colocalization of calcium-binding proteins and GABA in neurons of the rat basolateral amygdala. Neuroscience 105:681-693.

McDonald AJ, Betette RL (2001) Parvalbumin-containing neurons in the rat basolateral amygdala: morphology and co-localization of Calbindin-D(28k). Neuroscience 102:413-425.

McDonald AJ, Mascagni F (2002) Immunohistochemical characterization of somatostatin containing interneurons in the rat basolateral amygdala. Brain Res 943:237-244.

Mcdonald AJ, Mascagni F, Guo L (1996) Projections of the medial and lateral prefrontal cortices to the amygdala: a Phaseolus vulgaris leucoagglutinin study in the rat. Neuroscience 71:55-75.

McDonald AJ, Shammah-Lagnado SJ, Shi C, Davis M (1999) Cortical afferents to the extended amygdala. Ann NY Acad Sci 877:309-338.

McKernan MG, Shinnick-Gallagher P (1997) Fear conditioning induces a lasting potentiation of synaptic currents in vitro. Nature 390:607-611.

Milad MR, Quirk GJ (2002) Neurons in medial prefrontal cortex signal memory for fear extinction. Nature 420:70-74.

Milad MR, Vidal-Gonzalez I, Quirk GJ (2004) Electrical stimulation of medial prefrontal cortex reduces conditioned fear in a temporally specific manner. Behav Neurosci 118:389-394.

Milad MR, Orr SP, Lasko NB, Chang Y, Rauch SL, Pitman RK (2008) Presence and acquired origin of reduced recall for fear extinction in PTSD: results of a twin study. J Psychiatr Res 42:515-520.

Millhouse OE (1986) The intercalated cells of the amygdala. J Comp Neurol 247:246-271.

Milner B, Squire LR, Kandel ER (1998) Cognitive neuroscience and the study of memory. Neuron 20:445-468.

Moga MM, Herbert H, Hurley KM, Yasui Y, Gray TS, Saper CB (1990) Organization of cortical, basal forebrain, and hypothalamic afferents to the parabrachial nucleus in the rat. J Comp Neurol 295:624-661.

Muller JF, Mascagni F, McDonald AJ (2007) Postsynaptic targets of somatostatin-containing interneurons in the rat basolateral amygdala. J Comp Neurol 500:513-529.

Myers KM, Davis M (2007) Mechanisms of fear extinction. Mol Psychiatr 12:120-150.

Nader K, Majidishad P, Amorapanth P, LeDoux JE (2001) Damage to the lateral and central, but not other, amygdaloid nuclei prevents the acquisition of auditory fear conditioning. Learn Mem 8:156-163.

Nili U, Goldberg H, Weizman A, Dudai Y (2010) Fear thou not: activity of frontal and temporal circuits in moments of real-life courage. Neuron 66:949-962.

Nitecka L, Ben-Ari Y (1987) Distribution of GABA-like immunoreactivity in the rat amygdaloid complex. J Comp Neurol 266:45-55.

Ohman A, Soares JJ (1994) "Unconscious anxiety": phobic responses to masked stimuli. J Abnorm Psychol 103:231-240.

Olsson A, Phelps EA (2004) Learned fear of "unseen" faces after Pavlovian, observational, and instructed fear. Psychol Sci 15:822-828.

Pape HC, Pare D (2010) Plastic synaptic networks of the amygdala for the acquisition, expression, and extinction of conditioned fear. Physiol Rev 90:419-463.

Pape HC, Paré D, Driesang RB (1998) Two types of intrinsic oscillations in neurons of the lateral and basolateral nuclei of the amygdala. J Neurophysiol 79:205-216.

Papez JW (1937) A proposed mechanism of emotion. Archives of Neurology and Psychiatry 38:725-743.

Paré D, Smith Y (1993a) The intercalated cell masses project to the central and medial nuclei of the amygdala in cats. Neuroscience 57:1077-1090.

Paré D, Smith Y (1993b) Distribution of GABA immunoreactivity in the amygdaloid complex of the cat. Neuroscience 57:1061-1076.

Paré D, Smith Y (1994) GABAergic projection from the intercalated cell masses of the amygdala to the basal forebrain in cats. J Comp Neurol 344:33-49.

Paré D, Gaudreau H (1996) Projection cells and interneurons of the lateral and basolateral amygdala: distinct firing patterns and differential relation to theta and delta rhythms in conscious cats. J Neurosci 16:3334-3350.

Paré D, Smith Y, Paré JF (1995a) Intra-amygdaloid projections of the basolateral and basomedial nuclei in the cat: Phaseolus vulgaris-leucoagglutinin anterograde tracing at the light and electron microscopic level. Neuroscience 69:567-583.

Paré D, Pape HC, Dong J (1995b) Bursting and oscillating neurons of the cat basolateral amygdaloid complex in vivo: electrophysiological properties and morphological features. J Neurophysiol 74:1179-1191.

Paré D, Quirk GJ, Ledoux JE (2004) New vistas on amygdala networks in conditioned fear. J Neurophysiol 92:1-9.

Petrovich GD, Swanson LW (1997) Projections from the lateral part of the central amygdalar nucleus to the postulated fear conditioning circuit. Brain Res 763:247-254.

Petrovich GD, Canteras NS, Swanson LW (2001) Combinatorial amygdalar inputs to hippocampal domains and hypothalamic behavior systems. Brain Res Brain Res Rev 38:247-289.

Phelps EA, LeDoux JE (2005) Contributions of the amygdala to emotion processing: from animal models to human behavior. Neuron 48:175-187.

Phelps EA, Delgado MR, Nearing KI, LeDoux JE (2004) Extinction learning in humans: role of the amygdala and vmPFC. Neuron 43:897-905.

Pinard CR, Mascagni F, McDonald AJ (2012) Medial prefrontal cortical innervation of the intercalated nuclear region of the amygdala. Neuroscience 205:112-124.

Pinto A, Sesack SR (2008) Ultrastructural analysis of prefrontal cortical inputs to the rat amygdala: spatial relationships to presumed dopamine axons and D1 and D2 receptors. Brain Struct Funct 213:159-175.

Pitkänen A, Amaral DG (1993) Distribution of calbindin-D28k immunoreactivity in the monkey temporal lobe: the amygdaloid complex. J Comp Neurol 331:199-224.

Pitkänen A, Savander V, LeDoux JE (1997) Organization of intra-amygdaloid circuitries in the rat: an emerging framework for understanding functions of the amygdala. Trends Neurosci 20:517-523.

Pitkänen A, Pikkarainen M, Nurminen N, Ylinen A (2000) Reciprocal connections between the amygdala and the hippocampal formation, perirhinal cortex, and postrhinal cortex in rat. Ann NY Acad Sci 911:369-391.

Popescu AT, Paré D (2011) Synaptic interactions underlying synchronized inhibition in the basal amygdala: evidence for existence of two types of projection cells. J Neurophysiol 105:687-696.

Quirk GJ (2002) Memory for extinction of conditioned fear is long-lasting and persists following spontaneous recovery. Learn Mem 9:402-407.

Quirk GJ, Mueller D (2008) Neural mechanisms of extinction learning and retrieval. Neuropsychopharmacology 33:56-72.

Quirk GJ, Repa C, LeDoux JE (1995) Fear conditioning enhances short-latency auditory responses of lateral amygdala neurons: parallel recordings in the freely behaving rat. Neuron 15:1029-1039.

Quirk GJ, Likhtik E, Pelletier JG, Paré D (2003) Stimulation of medial prefrontal cortex decreases the responsiveness of central amygdala output neurons. J Neurosci 23:8800-8807.

Rainnie DG (1999) Serotonergic modulation of neurotransmission in the rat basolateral amygdala. J Neurophysiol 82:69-85.

Rainnie DG, Asprodini EK, Shinnick-Gallagher P (1993) Intracellular recordings from morphologically identified neurons of the basolateral amygdala. J Neurophysiol 69:1350-1362.

Rainnie DG, Mania I, Mascagni F, McDonald AJ (2006) Physiological and morphological characterization of parvalbumin-containing interneurons of the rat basolateral amygdala. J Comp Neurol 498:142-161.

Rescorla RA, Heth CD (1975) Reinstatement of fear to an extinguished conditioned stimulus. J Exp Psychol Anim Behav Process 1:88-96.

Rizvi TA, Ennis M, Behbehani MM, Shipley MT (1991) Connections between the central nucleus of the amygdala and the midbrain periaqueductal gray: topography and reciprocity. J Comp Neurol 303:121-131.

Roesch MR, Calu DJ, Esber GR, Schoenbaum G (2010) Neural correlates of variations in event processing during learning in basolateral amygdala. J Neurosci 30:2464-2471.

Rorick-Kehn LM, Steinmetz JE (2005) Amygdalar unit activity during three learning tasks: eyeblink classical conditioning, Pavlovian fear conditioning, and signaled avoidance conditioning. Behav Neurosci 119:1254-1276.

Rosenkranz JA, Grace AA (1999) Modulation of basolateral amygdala neuronal firing and afferent drive by dopamine receptor activation in vivo. J Neurosci 19:11027-11039.

Royer S, Paré D (2002) Bidirectional synaptic plasticity in intercalated amygdala neurons and the extinction of conditioned fear responses. Neuroscience 115:455-462.

Royer S, Paré D (2003) Conservation of total synaptic weight through balanced synaptic depression and potentiation. Nature 422:518-522.

Royer S, Martina M, Paré D (1999) An inhibitory interface gates impulse traffic between the input and output stations of the amygdala. J Neurosci 19:10575-10583.

Royer S, Martina M, Pare D (2000a) Bistable behavior of inhibitory neurons controlling impulse traffic through the amygdala: role of a slowly deinactivating K+ current. J Neurosci 20:9034-9039.

Royer S, Martina M, Paré D (2000b) Polarized synaptic interactions between intercalated neurons of the amygdala. J Neurophysiol 83:3509-3518.

Sah P, Faber ESL, Lopez De Armentia M, Power J (2003) The amygdaloid complex: anatomy and physiology. Physiol Rev 83:803-834.

Savander V, Go CG, LeDoux JE, Pitkänen A (1995) Intrinsic connections of the rat amygdaloid complex: projections originating in the basal nucleus. J Comp Neurol 361:345-368.

Savander V, Miettinen R, LeDoux JE, Pitkänen A (1997) Lateral nucleus of the rat amygdala is reciprocally connected with basal and accessory basal nuclei: a light and electron microscopic study. Neuroscience 77:767-781.

Schiess MC, Callahan PM, Zheng H (1999) Characterization of the electrophysiological and morphological properties of rat central amygdala neurons in vitro. J Neurosci Res 58:663-673.

Senn V, Wolff SBE, Herry C, Grenier F, Ehrlich I, Gründemann J, Fadok JP, Müller C, Letzkus JJ, Lüthi A (2014) Long-range connectivity defines behavioral specificity of amygdala neurons. Neuron 81:428-437.

Setlow B, Gallagher M, Holland PC (2002) The basolateral complex of the amygdala is necessary for acquisition but not expression of CS motivational value in appetitive Pavlovian second-order conditioning. Eur J Neurosci 15:1841-1853.

Shabel SJ, Janak PH (2009) Substantial similarity in amygdala neuronal activity during conditioned appetitive and aversive emotional arousal. Proc Natl Acad Sci U S A 106:15031-15036.

Shammah-Lagnado SJ, Alheid GF, Heimer L (1999) Afferent connections of the interstitial nucleus of the posterior limb of the anterior commissure and adjacent amygdalostriatal transition area in the rat. Neuroscience 94:1097-1123.

Shi C, Davis M (2001) Visual pathways involved in fear conditioning measured with fear-potentiated startle: behavioral and anatomic studies. J Neurosci 21:9844-9855.

Shi CJ, Cassell MD (1998a) Cascade projections from somatosensory cortex to the rat basolateral amygdala via the parietal insular cortex. J Comp Neurol 399:469-491.

Shi CJ, Cassell MD (1998b) Cortical, thalamic, and amygdaloid connections of the anterior and posterior insular cortices. J Comp Neurol 399:440-468.

Sierra-Mercado D, Corcoran KA, Lebrón-Milad K, Quirk GJ (2006) Inactivation of the ventromedial prefrontal cortex reduces expression of conditioned fear and impairs subsequent recall of extinction. Eur J Neurosci 24:1751-1758.

Smith Y, Paré D (1994) Intra-amygdaloid projections of the lateral nucleus in the cat: PHA-L anterograde labeling combined with postembedding GABA and glutamate immunocytochemistry. J Comp Neurol 342:232-248.

Smith Y, Paré JF, Paré D (2000) Differential innervation of parvalbumin-immunoreactive interneurons of the basolateral amygdaloid complex by cortical and intrinsic inputs. J Comp Neurol 416:496-508.

Sosulina L, Meis S, Seifert G, Steinhäuser C, Pape HC (2006) Classification of projection neurons and interneurons in the rat lateral amygdala based upon cluster analysis. Mol Cell Neurosci 33:57-67.

Sotres-Bayon F, Quirk GJ (2010) Prefrontal control of fear: more than just extinction. Curr Opin Neurobiol 20:231-235.

Sotres-Bayon F, Bush DEA, LeDoux JE (2007) Acquisition of fear extinction requires activation of NR2B-containing NMDA receptors in the lateral amygdala. Neuropsychopharmacology 32:1929-1940.

Spampanato J, Polepalli J, Sah P (2011) Interneurons in the basolateral amygdala. Neuropharmacology 60:765-773.

Tsvetkov E, Carlezon WA, Benes FM, Kandel ER, Bolshakov VY (2002) Fear conditioning occludes LTP-induced presynaptic enhancement of synaptic transmission in the cortical pathway to the lateral amygdala. Neuron 34:289-300.

Tye KM, Prakash R, Kim SY, Fenno LE, Grosenick L, Zarabi H, Thompson KR, Gradinaru V, Ramakrishnan C, Deisseroth K (2011) Amygdala circuitry mediating reversible and bidirectional control of anxiety. Nature 471:358-362.

Unal G, Paré JF, Smith Y, Paré D (2014) Cortical inputs innervate calbindin-immunoreactive interneurons of the rat basolateral amygdaloid complex. J Comp Neurol 522:1915-1928.

Washburn MS, Moises HC (1992) Electrophysiological and morphological properties of rat basolateral amygdaloid neurons in vitro. J Neurosci 12:4066-4079.

Weiskrantz L (1956) Behavioral changes associated with ablation of the amygdaloid complex in monkeys. J Comp Physiol Psychol 49:381-391.

Whittle N, Hauschild M, Lubec G, Holmes A, Singewald N (2010) Rescue of impaired fear extinction and normalization of cortico-amygdala circuit dysfunction in a genetic mouse model by dietary zinc restriction. J Neurosci 30:13586-13596.

Wilensky AE, Schafe GE, LeDoux JE (1999) Functional inactivation of the amygdala before but not after auditory fear conditioning prevents memory formation. J Neurosci 19:1-5.

Wilensky AE, Schafe GE, Kristensen MP, LeDoux JE (2006) Rethinking the fear circuit: the central nucleus of the amygdala is required for the acquisition, consolidation, and expression of Pavlovian fear conditioning. J Neurosci 26:12387-12396.

Wilson MA, Mascagni F, McDonald AJ (2002) Sex differences in delta opioid receptor immunoreactivity in rat medial amygdala. Neurosci Lett 328:160-164.

Woodruff AR, Sah P (2007) Networks of parvalbumin-positive interneurons in the basolateral amygdala. J Neurosci 27:553-563.